Variability and trends of tropical cyclones over the western North Pacific for the last decades.

Dissertation zur Erlangung des Doktorgrades der Naturwissenschaften im Fachbereich Geowissenschaften der Universität Hamburg

vorgelegt von Monika Barcikowska

aus Malbork

Hamburg 2012

Als Dissertation angenommen vom Fachbereich Geowissenschaften der Universität Hamburg

auf Grund der Gutachten von Dr. F. Feser
und Prof. Dr. H. von Storch

Hamburg, den 03.12.2012

Prof. Dr. Dirk Gajewski
(Sprecher des Fachbereichs Geowissenschaften)

ABSTRACT

Tropical cyclones (TCs) have a tremendous impact on coastal populations. Very intense winds, torrential rain and storm surges, which are related to TCs, pose a serious threat for human health, life and economy. Therefore it is important to know the past evolution, as well as the upcoming state of TCs activity. The observation-based studies so far haven't reached consensus regarding TCs trends in the western North Pacific in the last decades. Therefore the main goal of this study is to construct and analyse the alternative, long-term and homogeneous TCs data set, using a dynamical downscaling approach. For this purpose, NCEP reanalysis was downscaled with a regional climate model (CCLM) for the period 1948-2011.

First, it was required to assess the reliability of the TCs climatology derived from observations of the last decades. Analysis of data sets revealed strong discrepancies in TCs activity trends, varying between decreasing and increasing trends. These discrepancies were mainly attributed to different operational practises and changing over time measurement techniques applied by meteorological agencies to estimate TC intensities. Data set provided by Japan Meteorological Agency was assessed as the most homogenous and, in comparison to other data set, the most reliable one for deriving TCs climate statistics.

The second part of the study investigates the potential of CCLM to construct an alternative long-term TCs climatology. It presents an assessment of model skill to simulate TCs climatology, with a focus on the influence of the spectral nudging technique. Analysis has shown that CCLM has high skill to resolve TCs meso-scale features from the large-scale reanalysis. However, the simulated TC intensities are lower than the observed. Nevertheless, spectral nudging has a positive impact on simulated mean atmospheric TC conditions - and consequently - TC climatology, which justifies its application for regional long - term simulations of the past decades.

The last part of the study presents and analyses the TCs climatology constructed for the western North Pacific for the period 1948-2011. Comparison with more recent observations (1978-2008) shows that the simulated TCs climatology:

- represents realistically many important features of the TCs activity variability at inter-annual and inter-decadal time scales,
- reproduces a realistic relationship between the large-scale atmospheric-oceanic fields, such as sea surface temperature and the Maximum Potential Intensity.

The constructed TC climatology shows an increase and a north-westward shift of intense TC tracks for the period 1948-2011. Such changes in the TCs activity are related to the large-scale environmental patterns, which show also a shift of favourable for TCs genesis thermodynamic conditions toward north-west.

ACKNOWLEDGEMENTS

First and foremost, I would like to thank my advisory panel: Frauke Feser, Hans von Storch and Stephan Bakan for their guidance through my PhD studies. I am grateful for their enthusiastic discussions, encouraging for an independent research and, on the other hand, restraining my never-ending ideas☺.

Secondly, I would like to thank all the members of our research group for a friendly and stimulating for progress environment. I am endlessly grateful to Lan and Bach. With your support I can survive every catastrophe I am causing ☺.

I would like to thank The School of Integrated Climate System Sciences (SICSS) for establishing the advisory panel, which was very helpful to get through the PhD processes.

The work is supported (in parts) through the Cluster of Excellence 'CliSAP', University of Hamburg, funded through the German Science Foundation (DFG-EXC177) and through the Helmholtz-Zentrum Geesthacht, Centre for Materials and Coastal Research.

Most importantly I thank my family for the constant love, support and understanding.

LIST OF ABBREVIATIONS

AMSR-E Advanced Microwave Scanning Radiometer of NASA's Earth Observing System

BTD Best Track Data

CCA Canonical Correlation Analysis

CCLM Cosmo-Climate Lokal Model

CFSR Climate Forecast System Reanalysis

CMA China Meteorological Administration

EOF Empirical Orthogonal Function

GCM Global Circulation Model

IBTrACS International Best Track Archive for Climate Stewardship

ITOP Impacts of Typhoons on the Ocean in the Pacific

JASO July, August, September, October

JMA Japan Meteorological Agency

JTWC Joint Typhoon Warning Center

MPI Maximum Potential Intensity

NCEP National Center for Environmental Prediction

NCAR National Center for Atmospheric Research

NOAA National Oceanic and Atmospheric Administration

QuikSCAT Quik Scatterometer

RCM Regional Climate Model

SFMR Stepped-Frequency Microwave Radiometer

SNT spectral nudging technique

SSHS Saffir-Simpson Hurricane Scale

SSM/I Special Sensor Microwave/Imager

SST sea surface temperature

TC tropical cyclone

TRMM Tropical Rainfall Measuring Mission

TMI Microwave Imager

TPARC THORPEX Pacific Asian Regional Campaign

WNP western North Pacific

TABLE OF CONTENTS

LIST OF ABBREVIATIONS 7

CHAPTER 1. INTRODUCTION 11

CHAPTER 2. MODEL, TROPICAL CYCLONE TRACKING AND DETECTION METHOD 16

2.1 CCLM model 17

2.2 Tropical cyclones detection and tracking method 18

CHAPTER 3. TROPICAL CYCLONE TRENDS DERIVED FROM OBSERVATIONS AND THEIR RELIABILITY 21

3.1 Introduction 21

3.2 Data and methods 22

3.2.1 Quantifying tropical cyclones trend differences derived from BTD sets 25

3.2.2 BTD-reference data comparison methods 27

3.3 Results and discussion 28

3.3.1 Trends of tropical cyclones activity in WNP for 1977-2008 given by observations .. 28

3.3.2 Impact of unification of conversion tables in BTD on climate statistics – discussion 32

3.3.3 Can the reasons for discrepancies between BTD and the discrepancies themselves be evaluated? Reliability of climate statistics derived from BTD sets 34

3.3.4 Additional contributors for BTD inconsistencies 39

3.3.5 Can the Current Intensity discrepancies between BTD sets be evaluated? A NOAA-BTD, aircraft-BTD comparison 40

3.3.6 Accuracy of intensity estimations given by BTD sets - discussion 43

3.4 Trends of tropical cyclones activity for the period 1978-2008 and the reliability of statistics derived from observations - summary 46

CHAPTER 4. CAPABILITY OF CCLM TO DYNAMICALLY DOWNSCALE TROPICAL CYCLONES 51

4.1 State of regional climate model's abilities to simulate tropical cyclones and related uncertainties 51

4.2 Experimental design, analysis methods, observational data 53

4.3. Representation of tropical cyclones features simulated with CCLM..... 54

4.3.1. Impact of spectral nudging on tropical cyclones frequency, track patterns and spatial density 54

4.3.2. Impact of spectral nudging on tropical cyclones intensity 58

4.3.3 Impact of spectral nudging on tropical cyclones climatology..... 63

4.3.4. Representation of the meso-scale features in TCs simulated by CCLM..... 67

4.4 Capability and limitations of CCLM to simulate tropical cyclones climatology using spectral nudging 70

CHAPTER 5. A LONG-TERM TROPICAL CYCLONES CLIMATOLOGY OVER THE PERIOD 1948-2011..... 73

5. 1 Introduction 73

5.2 Data and Methodology 74

5.3 Results 76

5.3.1 Tropical cyclones spatial and temporal variability for the western North Pacific in modelled and observational data 76

5.3.2 Tropical cyclones variability and associated environmental factors..... 81

5.3 Discussion of tropical cyclones variability and associated environmental factors 84

5.4 Trend analysis 1948-2011 86

5.4 Tropical cyclones variability and changes during the last decades – analysis and comparisons with observations 90

CHAPTER 6. SUMMARY AND CONCLUSIONS 92

REFERENCES: 96

Chapter 1. Introduction

Tropical cyclone (TC) activity is of obvious importance for societies. Especially coastal populations are directly exposed to its damaging impact on health, life and properties. Very intense winds, torrential rain and storm surges can cause extensive coastal flooding.

TC Bhola (1970), which formed over the Indian Ocean, is the deadliest tropical cyclone on record. It killed more than 300 000 people [Southern, 1979] causing a powerful storm surge in the densely populated region of the Ganges Delta in Bangladesh. Typhoon Nina (1975), which is up to now the deadliest TC in the Pacific Ocean, killed up to 100 000 people after causing a 100-year flood in China ([Anderson-Berry and Weyman, 2008]). Hurricane Katrina caused the death of at least 1800 people and the highest economical losses, estimated as $81.2 billion in property damage [Pielke et al., 2008].

Additionally, TCs may play an important role in the large-scale climate system. Recent studies ([Emanuel, 2001, Sriver and Huber, 2007, Pasquero and Emanuel, 2008, Hu and Meehl, 2009]) suggested that TCs can transfer huge amounts of heat into the ocean along its trajectories. Due to such processes global TC activity can affect the long-term oceanic meridional overturning circulation and the meridional heat transport.

TC climatology and physical mechanisms of TCs formation are still a subject of ongoing research. This issue was primarily raised by [Gray, 1968]. The author presented the large-scale environmental factors necessary for TC formation. These factors are: high sea surface temperature (SST), high moisture content in the lower troposphere, conditional convective instability, cyclonic vorticity and weak vertical shear of horizontal winds. Changes of these conditions during the last decades and its possible impact on TC activity have stimulated a number of theoretical, modelling, and empirical studies.

Application of remote sensing techniques after 1970s facilitated TC observations. These were compiled into the form of a historical TC database, which enabled researchers to re-examine TC activity in the last decades. [Webster et al., 2005] have shown an upward trend in the intense (category 4-5 on the Saffir-Simpson Hurrican Scale) TCs in all ocean basins. [Emanuel, 2005] demonstrated a clear upswing in the potential destructiveness of TCs in the North Atlantic (NA) for the last three decades, based on the total dissipation of power. Many studies (e.g. [Emanuel, 2006, Mann and Emanuel, 2006, Trenberth and Shea, 2006]) interpreted such an increase as part of a long-term upward trend caused by anthropogenically induced global warming, others (e.g., Goldenberg et al. 2001) - as a positive phase of a multidecadal cycle of natural variability. Rapidly changing TC activity was attributed mainly to increasing sea surface temperature over the North Atlantic basin ([Webster et al., 2005, Hoyos et al., 2006, Emanuel, 2005, Holland and Webster, 2007, Saunders and Lea, 2008]). Only few studies ([Landsea et al., 2004, Landsea, 2005, Landsea et al., 2006]) emphasized the uncertainty in determining factors controlling TC activity, provided by relatively short and contestable historical observations.

For the western North Pacific (WNP), where intense TCs occur most frequently of all ocean basins, three independent observational data sets (best track data, hereafter referred to as BTD) provide records of TC activity since at least the 1950s. However, results driven by those data sets are ambiguous and differ among each other. Comparing the three BTD sets, Ren et al. (2011) showed increasing TC tendencies for the BTD from the Joint Typhoon Warning Center (JTWC) of the U.S.A., but decreasing tendencies for the other two data sets (of the Japan Meteorological Agency (JMA) and the China Meteorological Administration (CMA)).

The reasons for such differences are associated with the Dvorak technique applied in the forecasting centers to estimate TC intensity. The Dvorak technique [Velden et al., 2006] has remarkable shortcomings. Firstly, it is based on subjective classifications of cloud patterns

visible in geostationary satellite imageries. The given classifications suffer from severe biases in estimated minimum central TC pressure ([Kossin and Velden, 2004]). Finally, an implementation of this technique with standards varying among the forecasting centers ([Kamahori et al., 2006, Wu et al., 2006, Song et al., 2010, Barcikowska et al., 2012]) possibly lead to discrepancies between TC trends derived from BTD sets.

Some studies (e.g. [Lander, 2008, Knaff and Sampson, 2006]) stated clearly that differences in estimated intensity among BTD sets are irreconcilable, and alternative data sets are necessary to derive unambiguous TC trends.

Dynamical simulations provide an alternative way to construct long, homogeneous TC time series, giving a possibility to derive TC statistics and to analyse TC climatology. This enables researchers to study the impact of global warming on TC activity. Coarse-resolution global circulation models (GCMs) have shown the capability to simulate TC-like vortices ([Manabe et al., 1970, Bengtsson et al., 1982, Bengtsson et al., 1995]) and under increasing greenhouse gases project mostly a global decrease in TC frequency ([Broccoli and Manabe, 1990, Bengtsson et al., 1995, Sugi et al., 2002, Sugi et al., 2009, Tsutsui, 2002]). Such results converge with the projections from high- resolution GCMs (~ 60 [km] and less) or regional climate models (RCMs).

High-resolution GCMs simulate more realistic intensities, and thus are more suitable to investigate intense TCs. Projections indicate an increase in global mean TC maximum wind speed, with the ratio (and sometimes even the sign of tendency) varying among individual basins. The upward trend is due to increasing frequency of intense TCs, with noticeable contribution from the western North Pacific ([Oouchi et al., 2006, Yoshimura and Sugi, 2005, Murakami et al., 2011a, Murakami et al., 2011b]). High-resolution GCM projections demand high computing capacity, therefore some of the studies applied time-slice experiments. This approach has also a considerable drawback, like reduced feasibility to distinguish between external greenhouse forcing signal and internal variability. Alternatively,

many studies apply downscaling methods using RCMs, focusing on regional climate long-term projections.

The conclusions drawn from experiments employing RCMs confirm previous findings, showing a decrease in TC frequency and an increase in TC intensity ([Knutson et al., 1998, Knutsona and Tuleya, 2004, Knutson et al., 2008, Walsh and Ryan, 2000, Walsh, 2004]). The projected changes are also supported by theoretical studies of potential intensity ([Emanuel, 1987, Emanuel, 1988, Bister and Emanuel, 1998, Holland, 1997]). Potential intensity is minimum sustainable central pressure and maximum sustainable wind speed of a developed TC. It depends mainly on the sea surface temperature and convective available potential energy. Consequently, an increase in sea surface temperature will have positive impact on maximum attainable TC intensity, as projected in future scenarios.

Atmospheric RCMs demonstrated high skill in simulating meso-scale features of TCs ([Feser and von Storch, 2008b, Walsh, 2004, Bender et al., 2010]). An experiment with a hurricane prediction model which downscaled TC intensity to a resolution of ~ 10 [km] [Bender et al., 2010] has shown the RCM's capability to simulate TC intensities of category 5.

On the other hand, RCM applications have some drawbacks, which should be regarded while interpreting RCMs results. Downscaled atmospheric fields may significantly deviate from the forcing fields, prescribed through the lateral boundary conditions. Many studies ([Kanamitsu et al., 2010, Leduc and Laprise, 2009, Nutter et al., 2004, Rapaic et al., 2011, Seth and Giorgi, 1998]), investigated the influence of lateral boundary conditions and suggested their critical importance for long-term simulations.

In order to simulate the mean TC climate correctly, the spectral nudging technique (SNT, [von Storch et al., 2000]) was applied. It improved large-scale circulation patterns and reduced significantly the sensitivity of simulated TC activity to the initial conditions. Spectral nudging was also applied by Knutson et al., 2007, who successfully downscaled TC

variability over the Atlantic for the recent three decades. Other ocean basins are lacking of such long-term simulations.

As the observation-based studies so far haven't reached consensus regarding TC trends in the western North Pacific in the last decades, the main goal of this study is to construct a long-term and homogeneous TC data set with a dynamical downscaling approach. Therefore the specific tasks for this work are:

Chapter 3:

- Assess the reliability of observational data sets (BTD) to derive climate statistics of TC activity over the WNP
- Derive trends of TC activity over the WNP region for the last decades.

Chapter 4:

- Assess the capability of an RCM (CCLM) to derive TC activity statistics. This specifically includes the impact of spectral nudging on a simulated TC climatology.

Chapter 5:

- Validate the simulated TC climatology with recent observations
- Derive a long-term climatology of TC activity over the WNP

A summary and conclusions for all given results can be found in Chapter 6.

This thesis includes results which were published in peer-review journals. All these results base entirely on my work. Chapter 3 bases on the manuscript:

M. Barcikowska, F. Feser, and H. von Storch; Usability of best track data in climate statistics in the western north pacific. *Monthly Weather Review*, 2012, **140**, 2818-2830.,

Chapter 4 comprises results, which contribute to the article:

F. Feser and M. Barcikowska; 2012, The Influence of Spectral Nudging on Typhoon Formation in Regional Climate Models. *Environmental. Research Letters*, 2010, ***7***, 014024.

These results are included in sections 4.3.1 and 4.3.2 and originate mostly from my work (about 90%). The analysis given in the article was extended and is presented in detail in sections 4.3.3 and 4.3.4. Chapter 5 bases on the manuscript entitled: “Changes in tropical cyclone activity for the western North Pacific during the last decades, derived from a regional climate model” and was submitted to *Journal of Climate.*

Chapter 2. Model, tropical cyclone tracking and detection method

2.1 CCLM model

The regional climate model used to simulate long-term TC climate is COSMO-CLM (CCLM, www.clm-community.eu; ([Rockel et al 2008; [Steppeler et al., 2003]). The model domain covers the western North Pacific and South-East Asia (Figure 2.1), with a horizontal resolution of 0.5° (~ 55 km) and 32 vertical levels. The model is non-hydrostatic and the Kain-Fritsch scheme ([Kain, 2004]) was used as a convective parameterization.

CCLM is driven by large-scale fields provided by global NCEP–NCAR reanalyses I ([Kalnay et al., 1996, Kistler, 2001], hereafter called NCEP, at a horizontal resolution of T62 (~ 210 km)) as boundary and initial conditions. Additionally, the spectral nudging technique [von Storch et al., 2000] hereafter referred to SNT) was applied to the whole model domain.

This method adds a nudging term to the large-scale solution of regional model. It nudges atmospheric fields toward the direction of the global forcing fields. Therefore it prevents the model from excessive altering the large-scale circulation forced by lateral boundaries. The nudging terms are added only to the large spatial scales, larger than ~ 660 [km]. SNT is applied only to the upper levels, above 850 hPa, and its strength increases with height, therefore it does not constrain the regional–scale processes influencing the model solution in the lower levels. For this study SNT was applied only for the horizontal wind components.

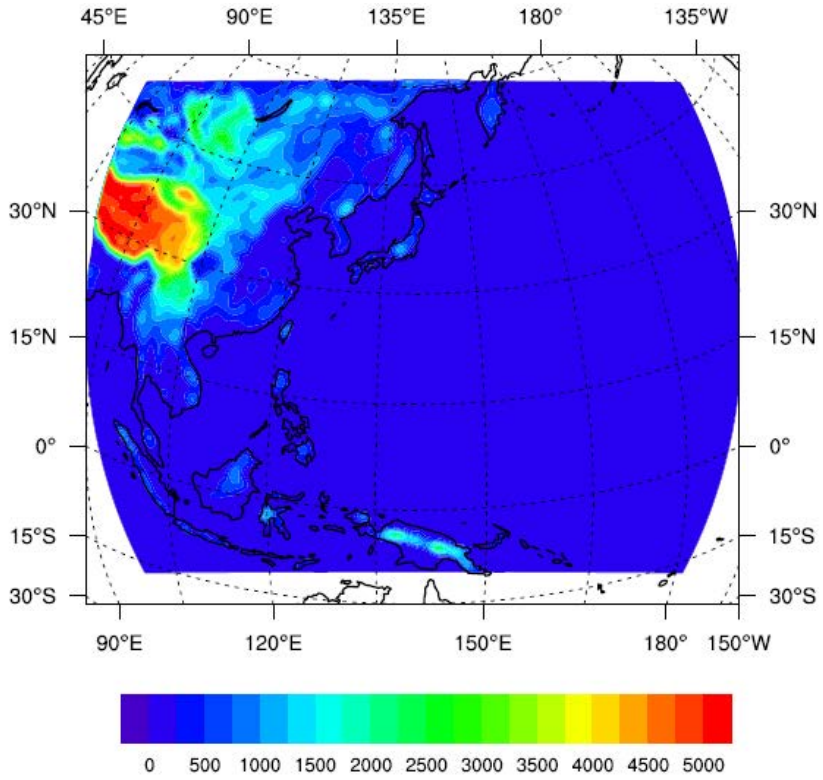

Figure 2.1 CCLM model domain and surface elevation (m) of the CCLM simulation for Southeast Asia and the western North Pacific with a grid distance of 0.5° latitude x 0.5° longitude.

2.2 Tropical cyclones detection and tracking method

TC tracks are extracted with a simple tracking algorithm ([Feser and von Storch, 2008a]). Primarily it searches potential TCs with local minimum sea level pressure and maximum wind speed. Localized points are connected with the closest ones in consecutive 1-hrly time steps. Formed tracks are filtered through criteria specifying e.g. the maximum intensity or duration of storm.

Three physical parameters defining the tracking criteria are: surface wind speed, sea level pressure and selected-scale sea level pressure. A meso-scale part of sea level pressure is extracted with a spatial digital band-pass filter ([Feser and von Storch, 2005]).

A TC was identified when its lifetime maximum wind speed exceeded 18 [m s^{-1}], minimum core pressure reached 995 [hPa], and when the filtered pressure anomaly dropped below -9 [hPa]. Additionally cyclonic disturbance had to last more than 48 hours.

These criteria were adjusted to extract TCs with a frequency that matches the observed climatological mean. For this purpose the period 1980-2007 was analysed, due to best quality of the reference data then. In that time the contribution of satellite observations improved significantly the homogeneity in observed TC records.

More strict criteria have to be satisfied to detect only the strongest TCs. For this purpose the tracking algorithm was calibrated to identify mainly TC tracks which resemble BTD tracks of category 2 to 5. An intense TC in CCLM was identified when the TC lifetime maximum wind speed exceeded 24 [m s^{-1}], minimum core pressure reached 995 [hPa], and the filtered pressure anomaly dropped below -18 [hPa]. Cyclonic disturbances had to last more than 48 hours. Applying too severe conditions would reduce the overall number and also the number of intense TCs. Therefore in practise, the most accurate selection aimed to:

- capture the TC frequency close to the number of TCs recorded in BTD as intense ones
- maximize the amount of TCs which resemble the intense ones in BTD in relation to the number of overall detected TCs

Chapter 3. Tropical cyclone trends derived from observations and their reliability

3.1 Introduction

TC activity trends derived from available BTD observations are limited by their short length and deficient homogeneity. The quality of BTD sets before the satellite era (up to the 1970s) is hardly acceptable for use in statistical analysis, due to insufficient and changing observational techniques. Therefore the analysis of TC variability in the last century is generally constrained to the last four decades. However, the detection of significant climatic trends distinct from short-term oscillations within a 40-year period is very difficult.

Recent studies ([Ren et al., 2011, Song et al., 2010, Wu et al., 2006, Yu et al., 2007]) revealed that results are dependent on data sets and the statistics applied, confirming BTD data inhomogeneity and quality deficiencies for the WNP region. [Webster et al., 2005, Emanuel, 2005] claimed there would be an increase in the occurrence of the most intense TCs in the WNP. However, according to [Wu et al., 2006] who used several BTDs provided by different institutes, neither the numbers of the most intense TCs nor the power dissipation index defined by [Emanuel, 2005] shows an increasing tendency. Comparing three BTDs, [Ren et al., 2011] confirmed increasing TC tendencies for the Joint Typhoon Warning Center (JTWC) BTD, but they found decreasing tendencies in the data of the Japan Meteorological Agency (JMA) and the China Meteorological Administration (CMA). [Kamahori et al., 2006] found increasing numbers of TC days for categories 2 to 3 of the Saffir–Simpson Hurricane Scale (SSHS; Simpson 1974) and decreasing numbers in higher categories for JMA, while opposite trends were detected for the JTWC dataset. All these studies indicate a great dependency of the detected TC trends on the chosen BTD, pointing to data inhomogeneity

and quality deficiencies in the WNP region. [Knaff and Sampson, 2006] considered any detected intensity trend questionable before reanalyses employing datasets of TC intensity estimated with alternative techniques are incorporated.

Others attempted to identify the reasons for the differences between BTD that affect TC activity trends ([Kamahori et al., 2006, Nakazawa and Hoshino, 2009, Song et al., 2010]). Many studies highlighted the different operational procedures used by the individual meteorological agencies to estimate TC intensity as a main cause for differing TC activity results. [Knapp and Kruk, 2010] attempted to minimize discrepancies among BTD by applying unified algorithms to operational data from all centers, resulting in more comparable BTDs.

This chapter presents trends of TC activity for the WNP, derived from available BTD sets. Additionally, the reliability of given observational data sets is assessed.

The following work is structured accordingly:

- "Data and Methods" describes statistical methods applied in the study, and the data.
- The first part of the section "Results and discussion" presents annual variability of TC activity for the last three decades (1977-2008). The next part shows the skill of current solutions for achieving homogeneity between climate statistics derived from individual data sets. In the latter part, the remaining discrepancies between BTD sets are analysed and evaluated using independent reference data sets.
- Section 3.4 summarizes and concludes all given results.

3.2 Data and methods

Four different BTD sets were analysed in this study. They were provided by the following independent agencies: the China Meteorological Administration (CMA, www.typhoon.gov.cn), the Regional Specialized Meteorological Center, Tokyo of the Japan Meteorological Agency (JMA, www.jma.go.jp/jma/jma-eng/jma-center/rsmc-hp-pub-

eg/besttrack.html) and the Joint Typhoon Warning Center (JTWC, www.usno.navy.mil/NOOC/nmfc-ph/RSS/jtwc/best_tracks/wpindex.html). In addition, the International Best Track Archive for Climate Stewardship, (IBTrACS, http://www.ncdc.noaa.gov/oa/ibtracs/index.php?name=ibtracs-data) was used. This product combines BTD from different operational centers to create a global best track dataset (Knapp et al., 2010). Although IBTrACS can not serve as independent data, it provides useful information as it gives a merged BTD solution for which a data quality control was applied. BTD sets for the WNP contain TC centre, maximum sustained wind and central pressure at 6-hour intervals. JTWC and CMA intensity values start with Tropical Depression strength, and JMA starts with Tropical Storm category.

From 1977 JMA began recording maximum sustained wind speeds using the Dvorak technique ([Dvorak, 1972, Dvorak, 1973, Dvorak, 1975]). Since 1987, when aircraft reconnaissance flights ended in the WNP, this method became the main tool for compiling BTD sets. The technique estimates TC position and intensity using visible and infrared imagery from geostationary and polar-orbiting weather satellites. Cloud patterns identified from satellite sources serve as a basis for operational estimates of the TC development phase, namely Dvorak parameters (T-number and Current Intensity number).

However, procedural rules to process satellite data differ among meteorological agencies. Dvorak parameters are related to TC intensity through conversions which were independently established for differing wind speed definitions in each operational center. While the JTWC uses 1-minute mean sustained 10 m wind speed, as designed originally by the Dvorak technique, other agencies use 10-min averaged values. JMA established a new conversion table in 1990 ([Koba et al., 1991]), which transfers operational parameters (Current Intensity) directly to TC intensity described as 10-min maximum sustained wind speed.

The CMA data set specifies intensity in terms of "2-min mean maximum sustained wind speed [m s^{-1}] near the storm centre". However, this procedure contradicts the description in [Yu et al., 2007] which states that the CMA agency uses an empirically established linear relationship between 1-min and 10-min averaged values and multiplies wind values by a factor of 0.871. The assumed application of a 10-min-average definition in the CMA data set is supported by findings of relatively small differences among JMA and CMA ([Knapp and Kruk, 2010]). IBTrACS data use 10-min sustained wind speed.

In order to evaluate the BTD additional observational data sets were tested for their ability to serve as a reference. Blended Sea Winds provided by the National Oceanic and Atmospheric Administration's National Climatic Data Center (http://www.ncdc.noaa.gov/oa/rsad/air-sea/seawinds.html , denoted as "NOAA") contain ocean surface wind speed on a global 0.25° grid in 6 hourly time steps ([Zhang et al., 2006a, Zhang et al., 2006b]). The data are created by blending observations from multiple satellites with a simple spatial-temporally weighted interpolation.

The quality of the blended product is related to the accuracy of the input data and sampling scheme of the observations. The number of long-term US satellites providing wind observations increased from one in 1987 to five in 2000. In this study years 2000 to 2008 were analysed as they constitute a rather homogeneous temporal and spatial coverage. For this period wind observations are retrieved from: Quik Scatterometer (QuikSCAT), SSM/I (DMSP Special Sensor Microwave/Imager), AMSR-E (Advanced Microwave Scanning Radiometer of NASA's Earth Observing System) and the Tropical Rainfall Measuring Mission (TRMM) Microwave Imager (TMI).

Scatterometers measure instantaneous ocean surface wind vectors at 10m height with a grid-typical resolution of 25 km and are widely used in operationally prepared analyses and forecasts ([Bourassa, 2010, Brennan et al., 2009, Hoffman and Leidner, 2005]). They are intended to provide accurate ocean surface winds in all weather conditions except for rain

conditions that occur often during high winds. QuikSCAT data, evaluated against buoys, is adhered to an 8-minute average. QuikSCAT winds were shown ([Brennan et al., 2009]) to have high skills in intensity estimation for tropical storms strength. However, enhanced backscattering by rain may introduce a positive bias during tropical depressions and rain attenuation causes large negative biases for very high winds. Microwave observations flagged as contaminated by precipitation were excluded from the analysis.

As reference data for the TCs of the strongest intensity, aircraft measurements were used. For the analysed period 2000-2008 the THORPEX Pacific Asian Regional Campaign (TPARC-2008) aircraft campaign took place in the WNP, which provided measurements of wind speed during TC events. Observations were obtained from Stepped-Frequency Microwave Radiometer (SFMR). Additionally we used the measurements from a field experiment in 2010: Impacts of Typhoons on the Ocean in the Pacific (ITOP-2010). The databases for both campaigns are available online: http://www.aoml.noaa.gov/hrd/data_sub/hurr.html.

3.2.1 Quantifying tropical cyclones trend differences derived from BTD sets

TC trends for the period 1977-2008 were derived from several BTD sets and compared in the form of annual number of TC-days categorized by the SSHS scale. The analysis is constrained to TC observations recorded concurrently in all independent BTD sets. This excludes contributions of differing TC frequency among BTD sets to trend discrepancies and enables the identification of the reasons for differences in estimated intensity.

Discrepancies among trends derived from 1-min (JTWC) and 10-min (JMA) sustained wind speed are discussed with regard to the impact of intensity definition on the derived climate statistics. The accuracy and effectiveness of two methods unifying wind definitions is assessed with respect to reduction of trend discrepancies.

The methods adjusting TC intensity definitions from 10-to-1 min averaging period were applied to JMA and CMA. The first method is based on the statistical, linear relationship between 10-min and 1-min averaged intensity ([Atkinson, 1974]). The data from JMA and CMA (for CMA a 10-min average is assumed as stated in the previous section) multiplied by a factor of 1.14 are hereafter referred to as JMA*1.14, and CMA*1.14.

[Knapp and Kruk, 2010, Kruk et al., 2011] proposed an alternative method unifying wind definitions. They and other authors ([Song et al., 2010, Wu et al., 2006]) highlighted the problem of different algorithms applied during compilation of BTD sets, that convert operational parameters (derived from satellite imagery) to wind speed. Therefore the method proposed here reverses intensity values back to operational parameters (Current Intensity parameter) and then applies a single conversion table to all data sets. Following these guidelines, the JMA data set was reverted to Current Intensity numbers, using the conversion tables described in [Koba et al., 1991]. In a second step, we derive wind speed from Current Intensity numbers by applying the original Dvorak conversion table [Dvorak, 1984] used in JTWC. It is possible that the Koba conversion table was applied only to intensity records starting in 1991 and previous years were not updated to the new procedures ([Nakazawa and Hoshino, 2009]). However, the remapping method using the Koba conversion table was applied for the complete analysis. Consequently, years before 1987 should be analysed with extreme caution and have only minor impact on the conclusions derived in this article.

The remaining reasons for BTD trend discrepancies are examined by comparing data sets with the same wind speed definition (JTWC and JMA/CMA adjusted to 1-min averaging period). The statistical analysis additionally includes yearly mean differences for TC center locations, annual distributions of differences between BTD sets for Current Intensity numbers, and TC center locations. The difference in TC location is estimated by a measure of distance (ΔP) between two geographical points (x_1, y_1) and (x_2, y_2) on the Earth's surface:

$$\Delta P = r_0 \cdot \cos^{-1}\{\sin(y_1)\cdot\sin(y_2)+\cos(y_1)\cdot\cos(y_2)\cdot\cos(x_1-x_2)\}, \qquad (1)$$

x and y are longitude and latitude, r_0 is the radius of the Earth.

3.2.2 BTD-reference data comparison methods

Independent reference data were employed to evaluate the remaining discrepancies between BTD sets. Due to a positive bias which occurs in QuikSCAT data for tropical depressions ([Hoffman and Leidner, 2005]) and frequently changing procedures in operational centers to identify this phase, the analysis focuses on concurrent records in BTD sets during tropical storm stage. As JTWC and JMA provide information about conversion tables in use, we use the JMA data set remapped to 1-min averaged wind speed using the Dvorak conversion table (as described in the previous section). Concurrent TC observations in BTD were compared with the NOAA wind data for the period 2000-2008, when QuikSCAT had a large impact. To derive maximum TC wind speeds from NOAA, the center positions given by JMA were used. TC circulation in developed systems vanishes at a finite horizontal radius with an upper boundary of approximately 1000 km ([Dean et al., 2009]). For small, developing or already dissipated cyclonic systems, it was assumed that the maximum wind speed is within a 500 km radius around a given location. Maximum intensities between the two data sets were compared for all concurrent TC cases.

As microwave signal is vulnerable to heavy rain conditions, the NOAA data exclude such values of reduced accuracy. Therefore time steps with a number of missing values around a TC centre potentially high enough to mask a region of maximum wind speeds were also excluded from the comparison.

For the comparison of the highest intensity typhoons the SFMR observations were used. Observations were obtained during several flights targeting TC centers of typhoons Sinlaku (2008), Jangmi (2008) and Megi (2010). SFMR measures wind speed values in 1 s intervals. To use these wind speeds compatible with BTD, the values were used in two forms:

averaged over a 10 second and 1 minute interval. Similar to the previous method, the value of the maximum wind speed was derived by choosing the highest value within a certain radius from the TC center given by JMA.

3.3 Results and discussion

3.3.1 Trends of tropical cyclones activity in WNP for 1977-2008 given by observations

The following section compares TC activity over the WNP, inferred from different BTD sets. As intense and long-lasting TCs are most significant for socio-economic consideration, the analysis takes into account not only TC frequency, but also intensity and duration. BTD sets are examined in terms of the annually integrated TC lifetime, and analysed separately for intense (category 2-3, 4-5) and weaker TCs. The analysis takes into account only the observations recorded in all BTD concurrently, thus total TC records are the same for every data set. However, the number of records falling into individual intensity categories differs among data sets.

Figure 3.1 presents annually accumulated TC-day records during the time period 1977-2008 for categories 2-5, 4-5 and 2-3. Original data sets are IBTrACS, JMA and JTWC (reporting 1-min sustained wind speed). Data sets adjusted to a 1-min averaging period are JMA*1.14 and CMA*1.14 (which result from applying a multiplication factor to JMA and CMA) and JMADT (where a remapping method – using the original ([Dvorak, 1984]) conversion table - was applied to JMA Current Intensity numbers).

JMA, IBTrACS and CMA show very similar TC-day numbers within categories 2-5 (Figure 3.1 a,b,c). Records for JTWC are very close to the other BTD sets only for categories 2-3 (Figure 3.1c). For the highest categories (4-5), and consequently – in the category range 2-5, JTWC numbers are substantially larger. Previous studies ([Knapp and Kruk, 2010, Song et al., 2010, Ren et al., 2011]) confirmed that fact by showing very strong discrepancies between JTWC and JMA wind speed values.

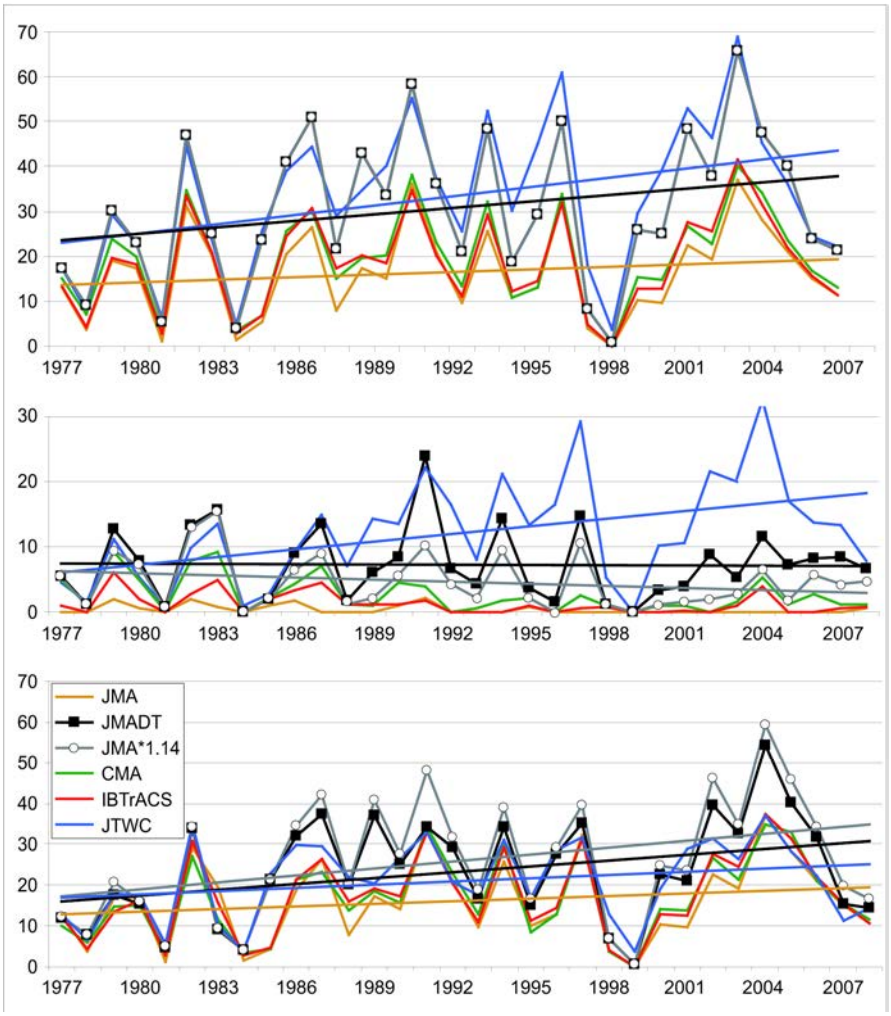

Figure 3.1 Annual TC-day numbers for SSHS intensity categories: top) 2-5, middle) 4-5, bottom) 2-3 for original BTD sets: JMA, CMA, JTWC, IBTrACS and modified BTD sets: JMA*1.14 (JMA multiplied by a factor), JMADT (JMA using the Dvorak conversion table). The x-axis shows years from the period 1977-2008.

Trends in all independent data sets (JMA, CMA, JTWC) and IBTrACs show an increase for the intense TCs (category range of 2-5). However, TC activity in JMA, CMA and IBTrACS shows relatively small change (factor of 0.18) compared to the steady, strong upward trend in JTWC (factor of 0.65). This fact is related to the large trend discrepancies between JTWC and other BTD sets in the highest categories (4-5). In this intensity range JTWC shows a strong upward trend (0.27), while JMA, CMA and IBTrACs show oppositely- a downward or no trend.

Some studies analysed the reasons for apparent discrepancies. [Song et al., 2010, Kruk et al., 2011] suggested, that differences in records falling into individual categories are related to the intensity estimation methods, applied in operational centers producing BTD sets. [Song et al., 2010] pointed specifically to differing algorithms, used to convert operational parameters to TC intensity.

[Knapp and Kruk, 2010] demonstrated that such discrepancies can be partly reduced by application of the same conversion algorithms to all BTD sets. Following this idea the conversion methods were unified and applied to JMA (CMA) in order to minimize trend discrepancies. 10-min intensity in JMA intensity was recalculated with application of the original Dvorak conversion table, applied in JTWC to estimate 1-min intensity (hereafter referred to JMADT). Alternatively, wind speed values in JMA (CMA) were adjusted to 1-min intensity by multiplying it with a factor of *1.14 (hereafter referred to JMA*1.14, CMA*1.14) suggested by [Atkinson, 1974].

Results of applied methods are shown in Figure 3.1a and confirm that the differences between BTD sets for categories 2-5 are significantly reduced. The average of annual relative differences between JMA (CMA) and JTWC decreased from 0.77 (0.57) to 0.19 (0.22) for JMA*1.14 (CMA*1.14). Trends of JMA increased from 0.18 to 0.45 (JMADT) and became more close to JTWC (0.65). Reduction of uncertainty range for derived trends confirms the increase of the intense TCs activity (category 2-5) observed in period 1977-2008.

The impact of unification the conversion methods is less significant when adjusted data sets are analysed separately for categories 2-3 and 4-5 (Figure 3.1b,c). For categories 2-3 BTD trends are similar, with upward trend of 0.22 for JMA and 0.27 for JTWC. Adjusting the estimation methods of JMA to those applied in JTWC, increased the ratio of changes up to: 0.38 in JMADT and 0.56 in JMA*1.14. As the result, the uncertainty range for BTD trends increased towards higher values.

For the highest intensity categories (4-5) unification of conversion procedures reduced the differences between BTD, but not sufficiently to unify the trends among them.

Figure 3.1c shows that trends in modified data sets (JMA*1.14, CMA*1.14, JMADT) still retain the decreasing character of 10-min wind speed BTD (JMA, CMA, IBTrACS). In contrast, 1-min wind speed BTD (JTWC) shows upward trends (0.39). The results for CMA*1.14 are almost identical to JMA*1.14 which suggests that 10-min-averaged wind speed values were used in CMA (see section 1.2).

Figure 3.2 presents annually accumulated TC-day records for BTD sets for the Tropical Storm category. The picture shows, similarly to Figure 3.1, the original data sets (JMA, JTWC, IBTrACS) and the modified ones (JMA*1.14, CMA*1.14, JMADT), adjusted to wind speed definition with 1-min averaging period. The results show that both adjusting methods lead to smaller TC-day numbers for the tropical storm category. JMADT has systematically lower numbers because application of the Dvorak conversion degraded over 30% of all records from the tropical storm to the tropical depression category. In contrast, application of the multiplication factor upgraded values to higher categories. Nevertheless the TC activity tendencies of the analysed records are in good agreement showing a slight increase until the mid-1990s and a decrease for the last decade.

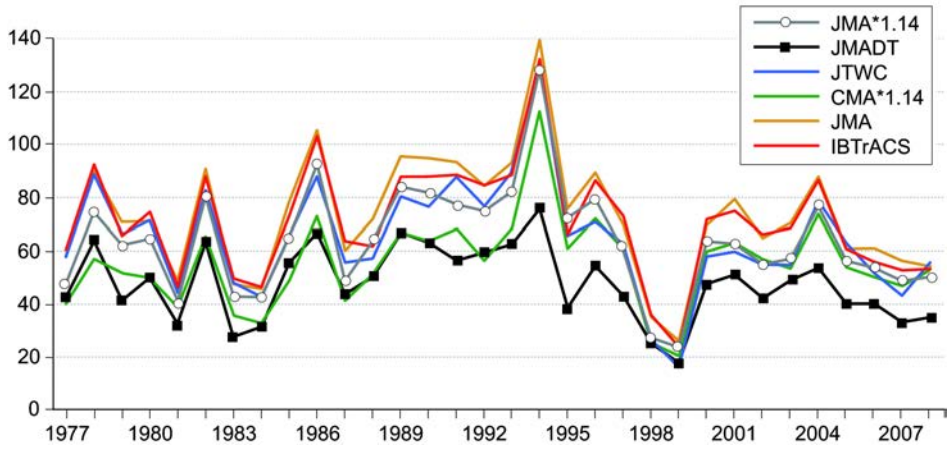

Figure 3.2 Annual TC-day numbers in the tropical storm intensity category, for original BTD sets: JMA, JTWC, IBTrACS and modified BTD sets: JMA*1.14, CMA*1.14 (JMA and CMA multiplied by a factor), JMADT (JMA using the Dvorak conversion table). The x-axis shows years from the period 1977-2008.

3.3.2 Impact of unification of conversion tables in BTD on climate statistics – discussion

Results of trends, presented in the previous section, only show agreement among all independent BTD data sets when TC days of category 2 -5 (intense TCs) are considered together. JMA, CMA and JTWC all indicate an increase in TC activity for the last three decades. However, for the highest intensity categories (4-5) these BTD sets show different tendencies. Such differences are caused by intensity- estimation methods, which vary between agencies producing BTD sets.

It has been shown that unification of intensity- estimation methods can partially reduce existing discrepancies. Consequently, the uncertainty range in derived trends became smaller, confirming upward tendencies of TC activity for category range: 2-5. The impact of different conversion tables and theirs unification (with remapping and rescaling methods) on TC intensity estimation is visualized in Figure 3.3. It presents the functions, converting Current Intensity parameters to TC intensity, which are used in operational centers in the WNP region. For wind speed of category 1 and higher, both conversions – the Dvorak table used in JTWC and the linear factor (JMA*1.14) - provide higher wind speed values for the same Current Intensity parameter than the Koba conversion. Therefore application of such methods to JMA increases wind values, shifts TC records toward higher (2-5) categories, and consequently reduces differences between JMA (CMA) and JTWC.

For categories 2-3, and 4-5 (Figure 3.1b,c) the unification of conversion methods did not relieve the uncertainty range among derived trends. A rescaling method applied to JMA*1.14 even increased the differences, compared to the JTWC in category 2-3. This is due to the fact that the multiplication factor is sufficiently high to increase and upgrade intensity records into categories 2-3, but not to the higher categories. Consequently TC records in JMA*1.14 are accumulated in the lower range (2-3), and show a much higher trend than JTWC in category 2-3. For the category 4-5 the trend remains negative, oppositely to JTWC.

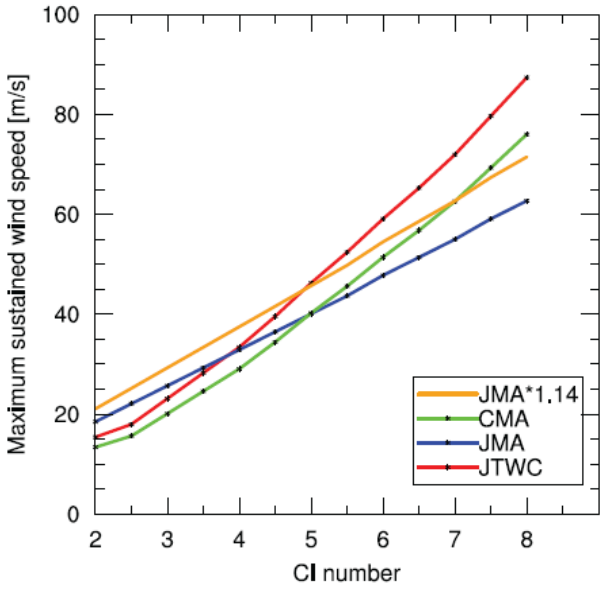

Figure 3.3 Relationship of Current Intensity parameter to maximum sustained 10 m wind speed [m s^{-1}] using conversion tables used in JTWC (Dvorak), JMA (Koba), JMA*1.14 (Koba multiplied by a factor of 1.14), CMA (Dvorak multiplied by a factor of 0.87). The x-axis shows the Current Intensity numbers, while the y-axis shows wind speed [m s^{-1}].

Such results indicate that conversion from 10-to-1 min averaged intensity with a rescaling method is not suitable for extreme winds. The multiplication factor enhances wind speed values linearly, for the whole data set distribution (Figure 3.3). However, the nonlinear sensitivity of high wind speed to the averaging period, which makes Atkinson's (1974) linear relation less accurate, creaks the risk of overestimating values in the lower intensity categories (2-3), while underestimating the highest ones.

[Kamahori et al., 2006] confirmed such findings, showing high discrepancies in trend tendencies between JTWC and linearly modified JMA, but this comparison included all identified TCs in both data sets and not only the concurrent ones. They also found a strong increase in JMA TC-days for categories 2-3, and a decrease for categories 4-5, while JTWC showed opposite tendencies.

Application of the original Dvorak conversion method is more suitable for the extreme winds, because it takes into account the non-linear effects of the averaging time interval. Consequently, for the categories 2-3 and 4-5 the trend discrepancies between JMA and JTWC

were reduced more efficiently, than with the linear method (Figure 3.1b,c). Especially for the extreme winds Dvorak conversion method shows higher skill, because it upgrades more records to categories 4-5. However, it is still not sufficient to reduce the trend differences completely. JMADT shows rather no trend, while JTWC demonstrates strong increase.

Assuming the different conversion algorithms as the main reason of trend discrepancies, application of the same algorithms to BTD sets should reduce the difference in wind speed to zero. Although the remapping method leads to enhanced agreement in TC-days statistics for the highest wind speeds, the relatively high differences are still present. This indicates that there are additional contributing factors, which, in the earlier TC intensity estimation stage, cause discrepancies in operational parameters (T number, Current Intensity).

The differences among BTD sets have shown also temporal variation. High agreement in TC-day records is visible in the first years of the analysis (1977-1987). As a possible explanation, [Knapp and Kruk, 2010] suggested that the same Dvorak procedures (e.g. the same conversion algorithm) were applied for this period. In the second period (1988-1997) numbers and trends among original BTD sets differ to a great degree. However, unifying wind speed definitions (application of the Dvorak table to BTD) did not efficiently resolve differences in the highest categories. Discrepancies among BTD sets in this period are increased, very similar to the strong increase of TC-day records in JTWC. To conclude, the unifying of conversion algorithms, and thus wind speed definitions, is necessary for an accurate assessment of BTD sets. However, the trend statistics derived from the given datasets remain inconsistent. This requires an explanation of the remaining differences, as presented in the following.

3.3.3 Can the reasons for discrepancies between BTD and the discrepancies themselves be evaluated? Reliability of climate statistics derived from BTD sets

This part of the analysis focuses on additional reasons for discrepancies among trends derived from BTD, remaining after unification of wind speed definitions. The resulting discrepancies between JTWC and JMADT point to the differences among Current Intensity numbers provided by the BTD agencies. To visualize the problem, which cannot be resolved by applying the same Dvorak conversion algorithm, two intense typhoons, Isa (1997) and Dianmu (2004), are presented in Figure 3.4a,b.

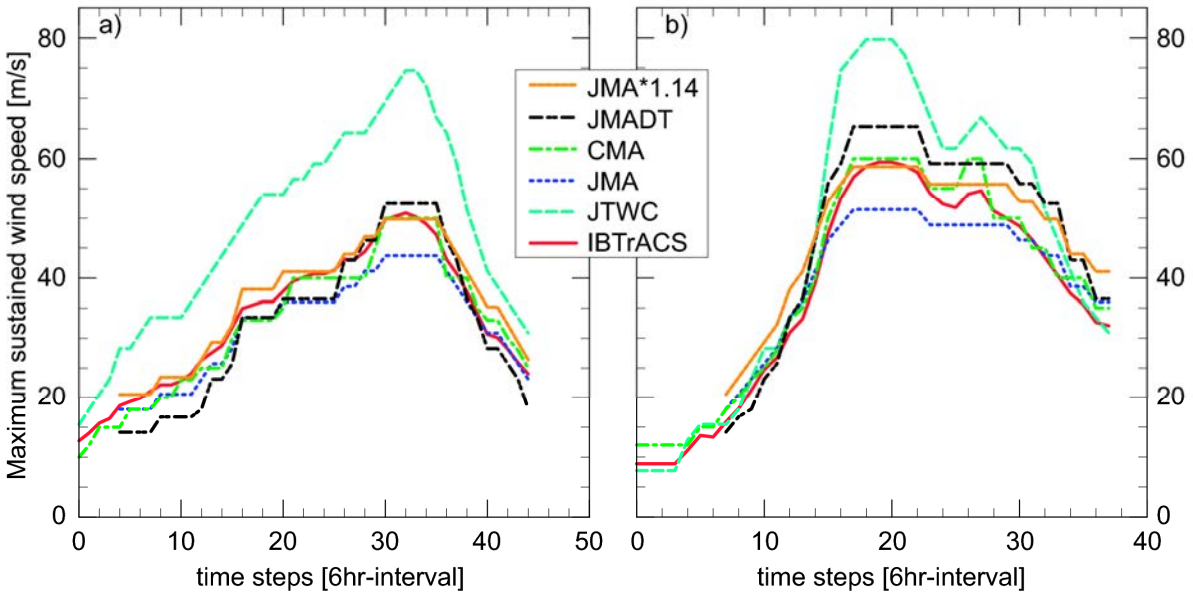

Figure 3.4 Wind speed time series for two TC events: a) Isa (1997), b) Dianmu (2004) for original BTD sets: JMA, CMA, JTWC, IBTrACS and modified BTD sets: JMA*1.14, (JMA multiplied by a factor), JMADT (JMA using the Dvorak conversion table). The x-axis shows time steps along the typhoon track, for which intensity in BTD sets was provided.

The picture shows a time series of maximum wind speed given by different BTD. Differences between original 10-min JMA data and 1-min JTWC reach 30 [m s^{-1}] during peak winds. Adjusting JMA to 1-min wind speed using a multiplication factor reduces the differences up to 25 [m s^{-1}] for Isa and 20 [m s^{-1}] for Dianmu. After applying the same Dvorak conversion table, differences with magnitude of 20 and 15 [m s^{-1}] still remain, which correspond to a difference in Current Intensity parameters of 1.75 and 1 (Figure 3.3). For TC Isa, a high discrepancy is noticeable during the whole TC lifetime. For Dianmu, the main differences occur during the highest-intensity phase, when the TC in JMADT reaches the

fourth category. It is also worthy to note how the multiplication factor shapes the values during the TC lifetime. JMA*1.14 shows higher intensity than JMA/JMADT intensities in the categories tropical depression, tropical storm and 1, but lower intensity than JMADT in the peak categories. [Kruk et al., 2011] stated that for most TCs Current Intensity parameters estimated by the BTD agencies in the WNP are almost identical. However, it is worth pointing out that, for the highest-intensity categories, noticeable differences appear, as shown by the examples of TC Isa and TC Dianmu.

Figure 3.5 presents these differences in a more systematic way. The picture shows the yearly distributions of differences between Current Intensity parameters in JTWC and JMADT, for years 1977- 2008. The x-axis shows years, while the y-axis shows Current Intensity difference. Size of the circles for a given Current Intensity difference indicates the percentage of a yearly sample (yearly number of joint for JTWC and JMADT TC occurrences). Given Current Intensity differences are presented for intensities separated into three categories: tropical depression-1, 2–3, and 4–5. Current Intensity parameters were derived from the wind speed, after the unification of intensity definition among BTDs (1-minute averaged wind speed). Therefore presented differences correspond to the intensity differences, which are independent of intensity definition.

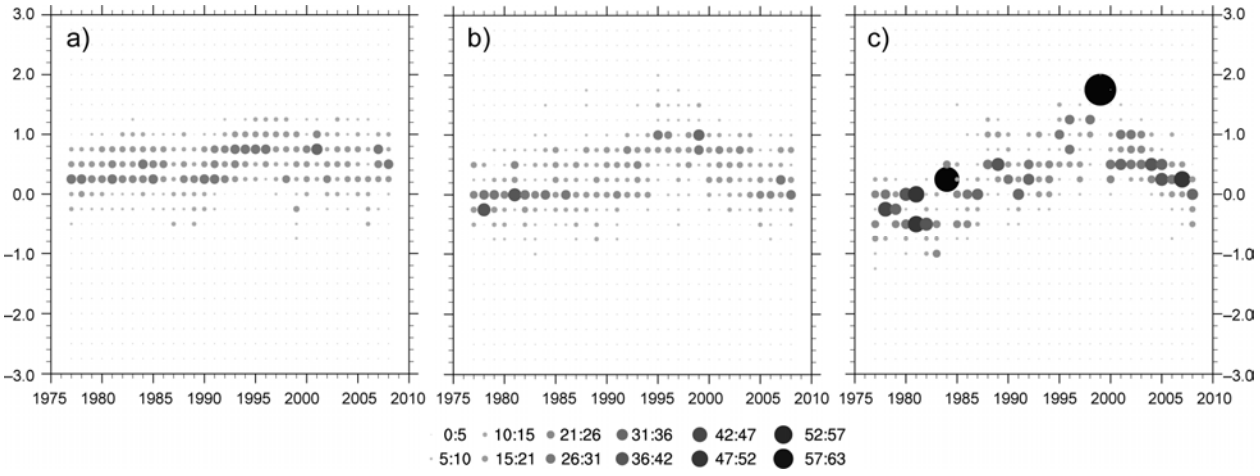

Figure 3.5 Yearly distributions of Current Intensity number differences for JTWC- JMADT assigned to intensity categories: a) tropical depression, tropical storm, 1, b) 2-3, c) 4-5. The x-axis shows years, while the y-axis shows Current Intensity difference. The size of the circles indicates the percentage of the occurrence number, counted for each year separately.

The distribution of differences in Current Intensity parameters reflects the discrepancies in the numbers of TC days falling into certain intensity categories (Figure 3.1b,c). The most pronounced differences in Current Intensity parameters are visible for the period 1988–97, especially for the highest intensity categories (Figure 3.5c). In this period, the Current Intensity differences were increasing in time and in 1997 reached the magnitude of 2. For TCs of lower categories (Figure 3.5a,b), the Current Intensity differences are smaller. In the early 2000s Current Intensity discrepancies are still higher, especially for categories 4–5. Two periods of the strongest Current Intensity discrepancies were also identified by [Nakazawa and Hoshino, 2009], who analyzed operational parameters from 1987–2006. They found a significantly higher numbers in JTWC for 1992–97 and 2000–05 in comparison to JMA.

The reasons for enhanced Current Intensity discrepancies in 1990s and the early 2000s can be related to separately evolving practices and usage of different information sources by operational centers. JMA reports geostationary satellites to be the principal source of TC localization and intensity estimation. In contrast, JTWC emphasizes supplementing these data with other: remotely sensed and in situ observations that are useful for TC-center identification, defining TC structure, and providing more direct intensity estimation. To analyse the possible impact of different satellite-based sources on intensiaty estimation, the differences in TC position between BTDs were presented on Figure 3.6

Figure 3.6a shows yearly distributions of differences between TC-center location in JTWC and JMA/JMADT, for years 1977- 2008. The x-axis shows years, while the y-axis shows distance between TC-center locations. Size of the circles for a given TC position difference indicates the percentage of a yearly sample (yearly number of joint for JTWC and JMADT TC occurrences).

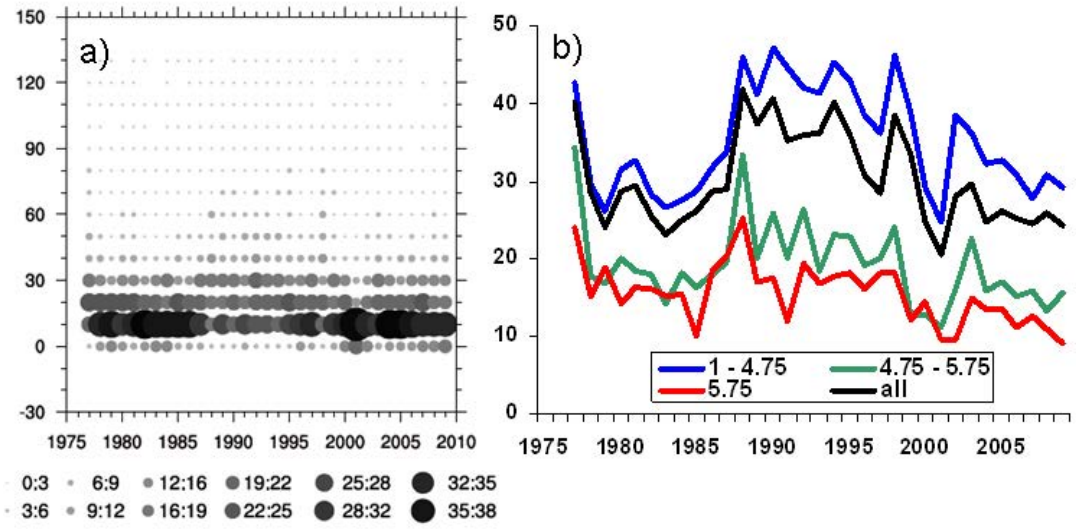

Figure 3.6 a) Yearly distributions of TC position differences [unit: km] between JTWC and JMA. The x-axis shows years, while the y-axis shows TC-position difference. The size of the circles indicates the percentage of the occurrence number, counted for each year separately. b) Annual mean differences in TC position between JTWC and JMA. Differences including all intensities are shown in black. Differences separated by categories given by Current Intensity number: 1-4.75, 4.75-5.75, higher than 5.75 are shown in blue, green and red, respectively.

Figure 3.6b shows annual means of TC center differences provided by JTWC and JMA. The mean annual differences in TC center position decrease with increasing intensity. The highest discrepancies occur for weak TCs (Current Intensity parameter range of 1–4.75), where often intensity and centers are difficult to estimate by low-resolved observations. In contrast, there is better agreement in locating the strongest TC centers. The most striking values are visible for the period 1988–98, when the aircraft reconnaissance era in the WNP was replaced by intensively developing satellite measurements. In that time widely distributed differences in TC locations were up to 150 [km] with mean annual differences varying between 30 – 50 [km]. After 1998 these differences are significantly smaller and do not exceed 30 [km]. The relationships between BTD trends in these distinct three periods correspond well with those of annual Current Intensity differences and TC-days trends (Figure 3.5 and Figure 3.1, respectively). The larger TC location differences for the midperiod correlates well with strong discrepancies in estimated Current Intensity parameters and in the numbers of TC-days falling into certain intensity categories. In the last decade the differences

in both: TC location and Current Intensity parameters show downward tendencies. The TC activity trends in that time are similar for JTWC and JMADT, even for the strongest categories.

3.3.4 Additional contributors for BTD inconsistencies

The analysis shows that differences in Current Intensity numbers and TC locations share a strong relationship. They are most distinguishable in the years 1987-1998, when the aircraft reconnaissance terminated and development of the intense satellite measurements began. Such coincidence suggests the usage of different information sources by JTWC and JMA may be a reason for the given TC trend differences. JMA reports usage of geostationary imageries only as a source for intensity estimation. In contrast, JTWC's operational center uses all available satellite data to ascertain the location and underlying storm structure and therefore improves the information used for imagery processing with the Dvorak technique. Such practises in JTWC might increase intensity values and contribute strongly to increasing tendencies of intense TC-days.

Increasing coverage of microwave observations (SSMI) from 1987 onwards which reached the maximum in 1997, together with high-resolution scatterometer (ERS2) measuring in 1995-1997, helped in TC center positioning and analysis of the lower intensity systems. Enhanced radar usability and additional information of higher-resolution TRMM in 1997 improved the accuracy of Dvorak-based estimations in JTWC. Introducing more and better spatially-resolved data certainly could affect the data set homogeneity and statistical information concerning derived trends. Extensive and irregular use of additional supplementary sources by one operational center and not the other, might lead to large Current Intensity discrepancies and opposite trends of intense TCs activity in comparison to other BTD. The strong, increasing tendency in intense TC-days found in JTWC, especially

for the period 1987-1999, might be severely biased by inhomogeneities introduced by changing procedures and different information sources applied in the operational centers.

It is suggested that apart from differing methods for converting Current Intensity numbers to intensities, Current Intensity discrepancies are the main contributor to differences between TC activity trends. The analysis indicates that discrepancies among operational parameters occur due to different data used as input for the Dvorak method applied in JTWC. However, to check the credibility of these parameters, they need to be compared with reference data.

3.3.5 Can the Current Intensity discrepancies between BTD sets be evaluated? A NOAA-BTD, aircraft-BTD comparison

To evaluate Current Intensity discrepancies, records for the years 2000-2008 in NOAA, JTWC and JMADT were analysed for the tropical storm category. The main input of NOAA, QuikSCAT is stated as having highly reliable values for moderate and high tropical storm values, while slightly overestimating wind of tropical depression strength. However, it provides data adhered to 8-min average. For this reason, NOAA can underestimate values up to 2 [m s^{-1}] when comparing with 1-min wind speed values within tropical storm category.

Figure 3.7 presents the yearly distributions of differences between TC intensity in concurrent records of JTWC and JMADT. The x-axis shows years, while the y-axis shows intensity difference for the period 2000-2008. Size of the circles for a given intensity difference indicates the percentage of a yearly sample (yearly number of joint for JTWC and JMADT TC occurrences). In this comparison JTWC reveals systematically higher values compared to JMADT.

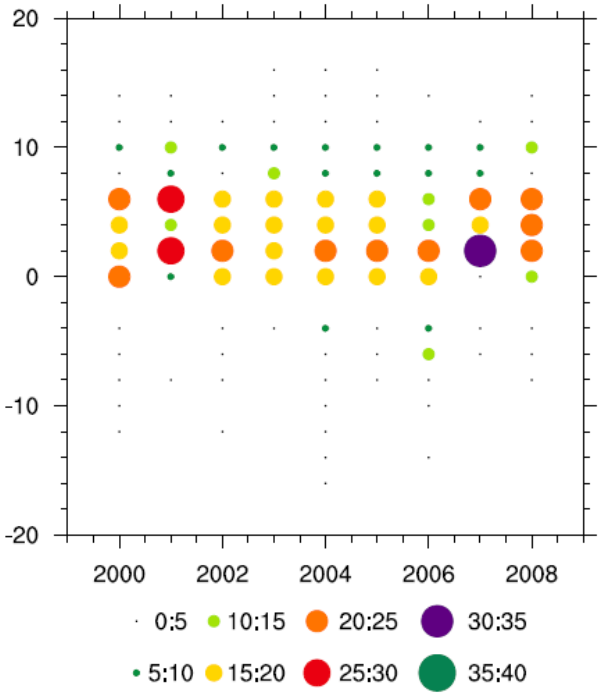

Figure 3.7 Yearly distributions of TC intensity differences [unit: m s^{-1}] for JTWC-JMADT, when intensity given by JTWC is in tropical storm category. The x-axis shows years, while the y-axis shows TC intensity difference. The circles indicate the percentage of the occurrence number, counted for each year separately.

For less than 15 % of all cases the absolute difference is smaller than 2 [m s^{-1}] which, according to [Kruk et al., 2011], is within the range of the remapping method's accuracy. However, for the majority of cases (60 %) JTWC is higher than JMADT by 2-8 [m s^{-1}]. For our comparison the data was divided into two groups according to these relationships. For the first one, representing almost 60 % of cases, JMADT remains like JTWC within the tropical storm category. For the second group, representing over 40 % of the cases, JMADT is low enough to fall into the tropical depression category. To assess which agency gives more reliable parameters, these two groups are compared with NOAA. They are analysed separately, with a greater focus on the first one (tropical storm) due to high reference data reliability.

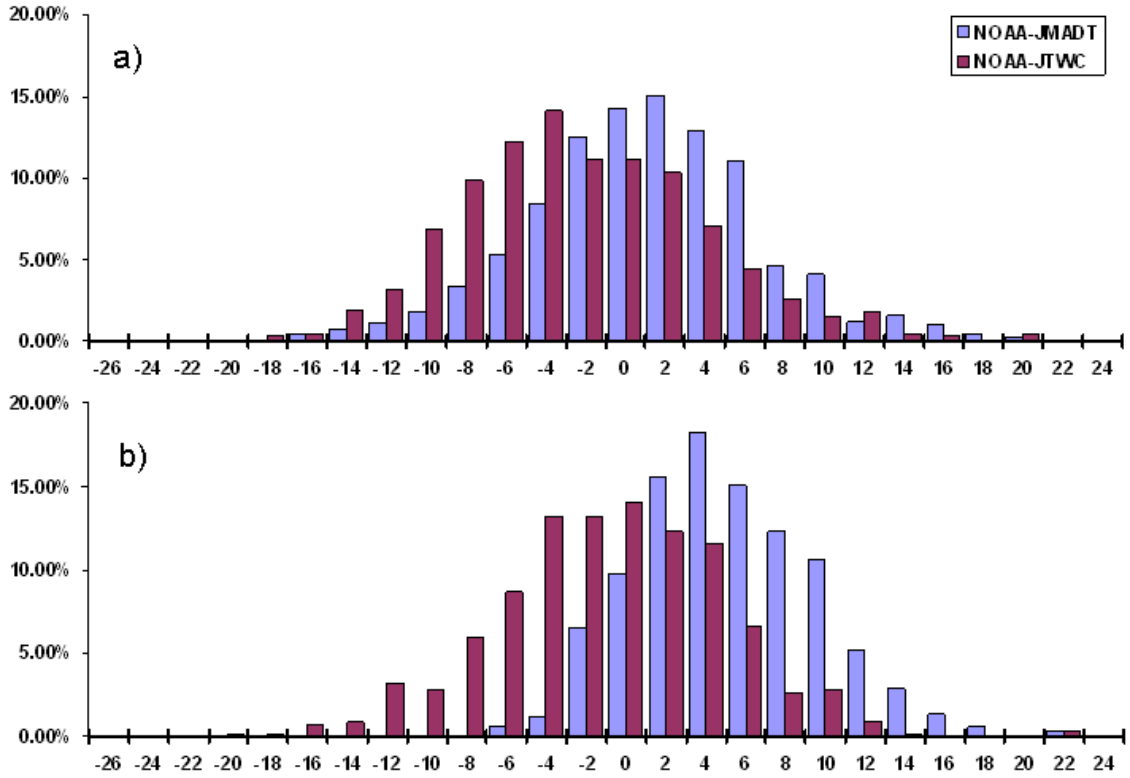

Figure 3.8 Distribution of TC intensity differences [unit: m s^{-1}] for NOAA – JMADT (blue) and NOAA – JTWC (purple), for 2000-2008 period. In a) TC intensity in JTWC and JMADT is in the tropical storm category, b) intensity in JTWC is in the tropical storm category and JMADT degraded to the tropical depression. The x-axis shows TC intensity difference, while the y-axis shows percentage of analysed sample (number of joint for JTWC, JMADT and NOAA TC occurrences).

Figure 3.8a,b presents differences for NOAA minus JMADT and for NOAA minus JTWC, computed for the 2000-2008 period, for both groups. For the group that contains data of both analysed BTD within the tropical storm category, NOAA remains closer to JMADT with 26% of the records remaining within absolute difference of 2 [m s^{-1}] and 50 % within 4 [m s^{-1}]. However, NOAA presents slightly higher values than JMADT with a median for the differences in the range <0;2> [m s^{-1}]. In comparison with JTWC, NOAA has lower values for more than 60% of the records, with the median within the range of <-4;-2> [m s^{-1}].

For the second group, where JMADT indicates the tropical depression phase, only 15 % of the NOAA values remain within an absolute difference of 2 [m s^{-1}] of JMADT. Here NOAA presents stronger tendencies towards higher values with a median of the difference in the

range of <4;6> [m s^{-1}]. However, this might be caused by a positive bias introduced by scatterometer data during rainy conditions for tropical depressions. Despite this fact, JTWC still remains higher than NOAA in almost 50 % of the cases. Figure 3.9a is a good example, showing the correspondence between intensity estimated by JTWC, JMADT and NOAA. The picture presents intensity time series for a TC Dolphin in 2008 provided by BTDs and NOAA. JTWC intensity show the highest values during the whole event, except for the tropical depression and early tropical storm phase when NOAA showed the highest values. For this TC the NOAA values remained noticeably closer to JMADT.

The analysis in the previous sections has shown, that the highest intensity discrepancies still remain in the highest categories. Thus to evaluate TC intensity discrepancies in the highest categories, records for BTDs and aircraft measurements were compared. However after the termination of an aircraft reconnaissance over WNP in 1987, there were only two aircraft measurement campaigns focusing on the TCs intensity. Measurements during the maximum of TC lifetime intensity are available only for two intense TCs: Jangmi in 2008 (not shown) and Megi in 2010 (Figure 3.9c). For the TC Jangmi maximum wind speed estimates of JTWC (72 [m s^{-1}]) match the observed ones better than JMADT. For this case JMADT presents the highest values (79 [m s^{-1}]), while SMFR 60-sec observations show 68 [m s^{-1}]. Figure 3.9c shows the intensity time series for supertyphoon Megi in 2010. For this event, SFMR measurements, even after averaging by 60 s interval, show the highest values (90 [m s^{-1}]), while BTD estimations are 87 [m s^{-1}] for JMADT and 82 [m s^{-1}] for JTWC.

3.3.6 Accuracy of intensity estimations given by BTD sets - discussion

To evaluate Current Intensity number discrepancies, BTD records were compared with satellite-based NOAA data and aircraft observations. NOAA serves as reference data for the

lower intensity categories, while aircraft observations are used for the highest wind speed evaluation.

Wind values derived from NOAA that provides data with reliable accuracy for the tropical storm phase, remain closer to JMADT than JTWC. Nevertheless, still a wide spread of differences exists among the data. JTWC shows much higher values than NOAA and JMADT, even in the group where JMADT falls into the tropical depression category and if a possible positive bias in NOAA has been taken into account. This indicates possible intensity overestimations in JTWC due to an erroneous contribution of Current Intensity parameters. Such overestimations may also be caused by supplementary data usage of JTWC, e.g. QuikSCAT, which gives values averaged over a 25 km area and an 8-minute interval. These values would be treated as the minimum threshold for maximum wind speed estimated by a forecaster. In the result, JTWC may increase the final wind estimates to compensate for possible underestimations due to wind retrieval limitations. Figure 3.9a shows time series of TC intensity for typhoon Dolphin in 2008 and serves as an example for pronouncedly higher wind speed values of JTWC in comparison to reference data (NOAA) and alternative BTD. However, the indirect way of choosing the maximum wind speed for NOAA winds (which provide reliable information only for lower TC intensity categories), as well as the limited accuracy of the remapping method still contribute to the uncertainty in the estimation of BTD reliability.

The strongest discrepancies still remain in the higher part of the SSHS intensity scale. Therefore an evaluation of BTD categories 4-5 is crucial for determining trends in TC activity. As aircraft sensors are unable to provide direct measurements of 10 m 1min sustained wind speed, they only serve as input to prepare surface wind analyses. Here the initialization conditions and assimilation techniques are crucial to construct reliable analyses.

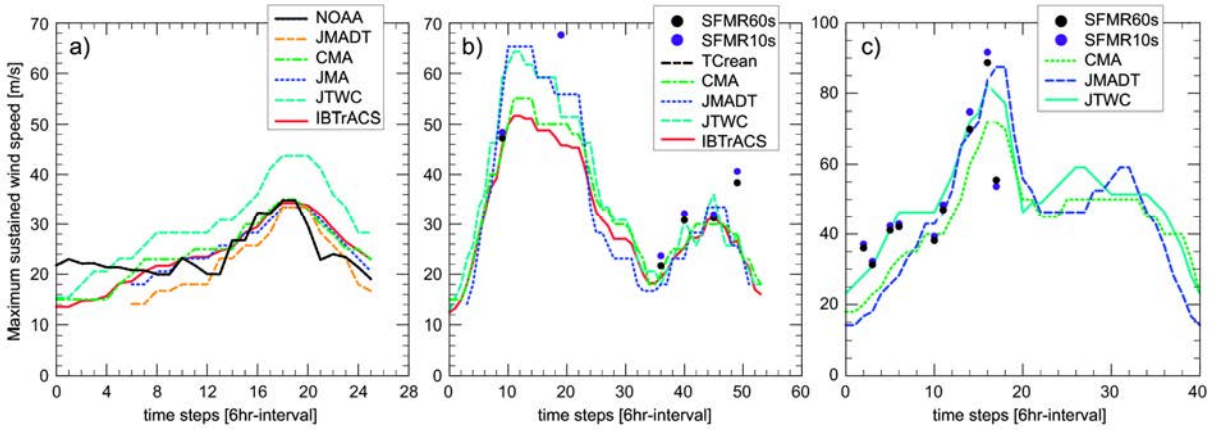

Figure 3.9 TC intensity time series [unit: m s^{-1}] for the: a) TC Dolphin (2008) for different best track data sets and NOAA, b) TC Sinlaku (2008), for BTD sets, TC reanalysis including aircraft reconnaissance (TCrean), and aircraft observations, c) TC Megi (2010) for BTD sets and aircraft observations (SFMR10s, SFMR60s). SFMR10s and SFMR60s are intensities averaged over 10 sec and 60 sec - time interval. The x-axis shows time steps within TC lifetime range, for which intensity was provided.

Figure 3.9b presents BTD, aircraft observations provided by SFMR taken during the TCS-08 2008 campaign, and an analysis reconstructed with those observations ([Zhang et al., 2007]) for typhoon Sinlaku in 2008. The initialization scheme assimilates TC central minimum pressure given by JTWC, but the maximum wind speed for higher categories does not reach JTWC values. As the provided TC reconstruction may be also biased due to the 10 km horizontal resolution, this can complicate the evaluation of BTD. On the other hand, the JTWC report [JTWC, 2009] states, that the aircraft measurements themselves for this TC had decisive impact on intensity estimation. Aircraft reconnaissance in this case helped to identify the second intensification phase. While for the first intensification phase the Dvorak technique estimated intensity with good accuracy, it underestimated the TC intensity during the second phase. The reconstructed reanalysis for the second period matches the observed values.

The maximum TC lifetime intensity, measured during aircraft campaigns differs remarkably from intensity provided by BTDs. For typhoon Jangmi aircraft from TPARC campaign measured mean 60-sec value of 68 [m s^{-1}] while JMADT estimated the highest values (79 [m s^{-1}]). For TC Megi, SFMR 60-sec measurements show the highest values (90

[m s^{-1}]) of maximum wind speed. Additionally, the SFMR recorded the weakening of TC Megi faster than estimated by the Dvorak method. Landfalling TC situations, for which the reliability of Dvorak relationships is limited, require in-situ observations. [Nakazawa and Hoshino, 2009] also noticed differences in operational (Current Intensity- and T-) numbers among various BTD, both for intensification and weakening phases. Differing weakening ratios, after reaching TC maximum intensity in BTD sets, indicate that there may be differences between definitions for allowable intensity change (in the form of Current Intensity and T parameters). Such constraints ([Dvorak, 1984]) were gradually relaxed by JTWC during the 1990s ([Velden et al., 2006]), allowing for a faster weakening of intense TCs. These procedural changes possibly contributed to the existing discrepancies among BTD.

Additionally, it is noticeable that in the developing stage of a typhoon, BTD in JTWC is strongly influenced by aircraft measurements (Figure 3.9c). These were possibly used to supplementary identify the early intensification phase.

3.4 Trends of tropical cyclones activity for the period 1978-2008 and the reliability of statistics derived from observations - summary

The analysis in this chapter presents variability of TC activity observed over the WNP for the period 1977-2008. Climate statistics, derived on basis of independently compiled data sets (BTD), indicate an increasing activity of intense TCs (category 2-5). The contribution to this trend by records of category 2-3 and 4-5 is ambiguous, therefore additionally the reliability of given BTD sets was investigated.

It was confirmed that different methodologies, deriving TC intensities used by the meteorological agencies to produce BTD, influence TC activity trends. In order to minimize discrepancies existing between the individual data sets, two methods were applied.

Both methods: the commonly used rescaling with a linear factor (used to homogenize BTD with different wind speed definition) as well as the remapping method proposed by [Knapp and Kruk, 2010] show high skill to reduce trend discrepancies, but only when categories 2-5 are considered together. Then all BTD sets show increasing numbers of annually accumulated TC-days for the period 1977-2008.

However, when analysing categories 2-3 and 4-5 separately, the methods' skill differ. Rescaling with a multiplication factor leads to overestimated trends of TC-days for lower categories (2-3) while still underestimating the highest ones (4-5). An alternative method, which reconstructs TC intensity by remapping Current Intensity parameters with a Dvorak technique conversion ([Knapp and Kruk, 2010]) reduces most discrepancies for categories 2-3. For the highest categories, the technique minimizes discrepancies only partly, TC activity trends in JMADT show no trend while strongly increasing trends are visible for JTWC.

An application of the same converting procedures to retrieve TC intensities should theoretically reduce the difference between the individual BTD to zero. However, remaining differences indicate that there are additional contributing factors leading to discrepancies in operational Current Intensity numbers.

The distribution of the Current Intensity discrepancies in time corresponds to the differences in TC center positions. The largest discrepancies occur in the 1990s when higher-resolution satellite observations were developing. The reduction and phasing out of aircraft data sources in the late 1980s may also have had an influence.

This indicates that extensive and irregular use of additional supplementary sources by JTWC might cause huge Current Intensity discrepancies and opposite trends of intense TCs activity with other BTD. The strong increasing tendency in intense TC-days found in JTWC, especially for the period 1987-1999, may be severely biased by inhomogeneities introduced by changing procedures and information sources. On the other hand JMA use mainly the geostationary satellite imagery for the intensity estimations. This might limit accuracy of the

estimations, however it maintains homogeneity within the data set and makes this source more reliable for deriving climate statistics.

For direct evaluation of accuracy in intensity estimated by BTD sets, JTWC and JMADT were compared to NOAA sea surface wind speeds and aircraft measurements. JTWC shows a systematic overestimation of both NOAA and JMADT for the tropical storm category, where NOAA data is considered to be very accurate. For the tropical storm category JMADT wind speed values remain closer to NOAA, although visible differences still exist. Higher Current Intensity parameter estimates as well as subjective interpretation of additional sources in JTWC (e.g. microwave wind retrievals) likely contribute to such results. It is concluded that JMA provides more reliable Current Intensity parameters than JTWC for the tropical storm wind speed range.

Sparse in-situ data limit the evaluation effort of BTD accuracy for the highest wind regimes. Aircraft campaign measurements in 2008 and 2010 show some agreement with maximum intensity estimations in BTD. For a more complete evaluation, aircraft data for the earlier period would be needed, when the accuracy uncertainties were the highest.

Additionally, the analysis of some strong TC events like Sinlaku (2008) and Megi (2010) suggests that there are some deficiencies within the Dvorak technique procedures. Slow weakening ratios for BTD in comparison to in-situ observations indicate that not only the homogeneity has to be assured, but also that temporal non-changing methods to estimate TC intensities should be applied in all operational centers.

Ultimately, the analysis presented demonstrates the importance to document those operational procedures that are applied for the Dvorak technique by the meteorological agencies; otherwise the interpretation of the results can lead to misleading conclusions. This may happen when considering ambiguously specified wind speed definitions in CMA or intensity in JMA before applying the [Koba et al., 1991] conversion table. It is suggested to pay special attention with regard to the highest wind regimes as the largest differences

between BTD sets were found here. The differences in TC activity trends may require academic agreement on a set of procedures and a reanalysis of existing storm data.

Chapter 4. Capability of CCLM to dynamically downscale tropical cyclones

4.1 State of regional climate model's abilities to simulate tropical cyclones and related uncertainties

RCMs become a powerful tool in reproducing the climate variability on different time scales as well as extreme climate events, when driven by good quality reanalysis ([Wang et al., 2004]). Since the first successful applications of RCMs by [Dickenson et al., 1989] and [Giorgi and Bates, 1989], much effort was focused on RCMs development and evaluation. Uncertainties in RCMs, as well as in GCMs come from many sources like: physical parameterizations, initial conditions, numerical algorithms, surface forcing, etc. Therefore for simulations of realistic TC features, the convective parameterization and horizontal resolution ([Walsh, 2004, Walsh et al., 2004, Bender et al., 2010, Knutson et al., 2007, Grossmann and Morgan, 2011]) are of high importance. RCMs have also another, important source of error. It is related to the lateral boundary conditions, through which the large-scale atmospheric fields are prescribed ([Warner et al.1997]). Small RCM domains may constrain the solution to follow the conditions imposed from the forcing fields and inhibit development of the small-scale features. Oppositely, for RCMs with large domains the 'internal variability' induced by initial conditions may deteriorate the large-scale fields. It happens especially when the forcing fields are provided only by lateral boundaries ([von Storch et al., 2000, Miguez-Macho et al., 2004, Waldron and Horel, 1996]). Many studies ([Seth and Giorgi, 1998, Nutter et al., 2004, Wu et al., 2005, Nicolis, 2007, Vanvyve et al., 2008, Landman et al., 2005]) have shown that lateral boundary conditions are essential for successful long-term regional climate simulations. [Landman et al., 2005, Wu et al., 2012] found that the RCM domain choice and lateral boundary conditions location have a large impact on interannual variability of TC

activity. [Kanamitsu et al., 2010] stated that ill-posed lateral boundary conditions cause a large error in the low-frequency (climate time scale) atmospheric variability of downscaled fields. This significantly contaminates the interannual variability of the synoptic- and planetary-scale fields and consequently affects its long-term linear trend.

To prevent the RCM solution from redundant deviating from the large-scale forcing fields, RCM simulations often use a spectral nudging technique ([SNT, [Kanamitsu et al., 2010, Knutson et al., 2007, Castro et al., 2005]). SNT is based on the view ([von Storch, 1999]), that small-scale features result from the interactions between large-scale atmospheric flow and smaller-scale geographic features (e.g. topography, land-sea interaction). Therefore, in contrast to the standard approach, SNT forces large-scale fields not only through the lateral boundaries, but also through the model interior. SNT forcing adds the nudging terms only to the large-scale solution and in the higher latitudes. This allows the smaller-scale processes, influenced by surface geographic features, to develop. Some studies applied this technique successfully also for the SE Asia domain ([Cha et al., 2011, Song et al., 2011, Yhang and Hong, 2011, Tang et al., 2010, Cha and Lee, 2009, Feser and von Storch, 2008a, Feser and von Storch, 2008b]). SNT effectively improves simulated mean climate in the WNP, namely: monsoon circulation, precipitation patterns, subtropical circulation ([Cha et al., 2008, Cha and Lee, 2009, Miguez-Macho et al., 2004, Wu et al., 2012]). The impact of spectral nudging on TC formation, development and associated large-scale circulation patterns has not yet been thoroughly explored. Some sensitivity experiments for a single typhoon case were shown in [Feser and von Storch, 2008b], but this case study cannot give answers for longer time periods. This work aims to answer the remaining questions related to the SNT impact on simulated TC climatology. Finally, it will assess the general capability of RCM (in this study - CCLM, Cosmo-Climate Lokal Model) with SNT applied to downscale TC intensity.

The following part shows an analysis of the typhoon season 2004 simulated by CCLM, with- and without application of the SNT. Results are then compared with observational data sets (satellite data and reanalyses).

4.2 Experimental design, analysis methods, observational data

Ten ensemble simulations with CCLM were computed, five - with application of SNT (SN), and five - without the SNT (NN). Simulations differ only by starting dates, which were set to consecutive days between 01- 05.03.2004, for both ensemble members. The CCLM is configured according to the model description and settings provided in Chapter 2. The model domain, presented in Figure 2.1, includes the main TC genesis regions in the WNP. Therefore TCs are mainly generated within the model domain and not prescribed by lateral boundary conditions. Due to the large domain, the internal model variability should be large as well ([Alexandru et al., 2007]). It describes the model's ability to generate several possible atmospheric states for the same lateral boundary conditions. Spectral nudging reduces this internal model variability ([Weisse and Feser, 2003]) and thus leads to fewer differences between individual ensemble members and a smaller ensemble spread.

The first simulated month wasn't analysed to avoid possible spin-up effects on the computed climatology. Therefore ensemble simulations were analysed for the period April-December 2004 during which 29 TCs were recorded by BTD over the WNP.

To extract TCs from modelled data, a simple Lagrangian tracking algorithm ([Feser and von Storch, 2008a]) was applied. The description and settings of the algorithm are provided in Chapter 2.

Simulated CCLM TC were defined as 'overlapping' the observed one (given by BTD), when the distance between both tracks was shorter than 500 [km] in at least 10 % of the longer track's length. If several CCLM tracks corresponded to the same BTD track, then the

one with the higher percentage of matching track's length was chosen. The distances between simulated RCM and BTD tracks were computed with the great circle distance formula.

As a reference for simulated TCs, BTD records provided by JMA were used. For evaluation purposes observations and reanalysis data were used: TRMM satellite precipitation data (horizontal resolution 0.25° (~ 28 km)); ERA-Interim ([Dee, 2011], horizontal resolution T255 (~ 80 km)) and NCEP CFSR reanalysis data ([Saha, 2010], horizontal resolution 0.5° (~ 55 km)).

4.3. Representation of tropical cyclones features simulated with CCLM

4.3.1. Impact of spectral nudging on tropical cyclones frequency, track patterns and spatial density

The numbers and patterns of TC tracks simulated by CCLM are analysed and compared with the observed ones during the typhoon season 2004. Table 1 shows the total TC frequency and the number of TCs matching the observed ones for all simulations in both ensembles. The frequency of TCs identified in CCLM depends on the subjectively established tracking algorithm settings, therefore the relation between TC numbers in SN and NN is brought into focus. Results show that TC frequency is two times lower when the SNT is applied. However, the number of tracks matching the observed ones is two times higher. In CCLM-SN about 50 % of all TCs overlapped the observed ones, while in CCLM-NN - less than 20 %. This relation consequently influences the spatial patterns of TC track density, presented in Figure 4.1.

Figure 4.1 shows the fields of TC density normalized by its spatial mean, for observed TCs (Figure 4.1a) and the simulated ones (CCLM-NN and CCLM-SN, Figure 4.1b and 4.1c, respectively). Both CCLM ensembles show realistic features of spatial density, with the highest TC density in the western part of the WNP (120°-150° E), where tracks often advance towards the SE Asian coast. The NN ensemble mean shows a more outspread pattern than the

BTD, which is mainly due to enhanced TC activity along the SE Asian coast and in the eastern part of the WNP. The pattern of the SN ensemble mean resembles the features of the observed one much more. Consequently the pattern correlations between spatial track densities (Table 4.1) are higher for SN members than for NN, with values varying from 0.61-0.67 and 0.50-0.61 respectively.

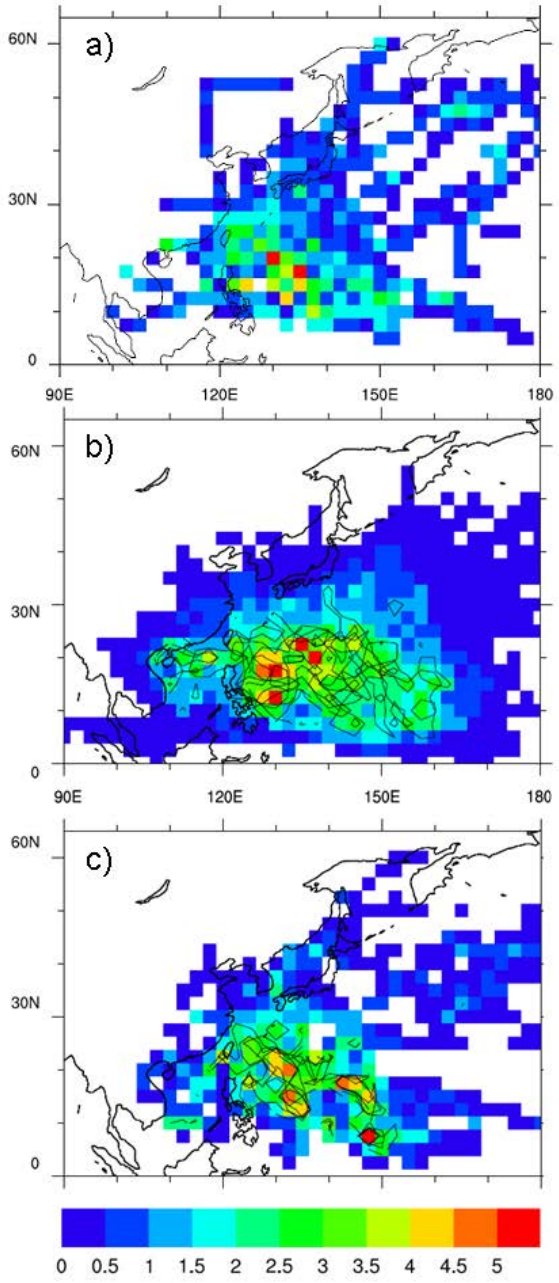

Figure 4.1 TC spatial densities (TC occurrence within 2.5° latitude x 2.5 longitude grid boxes; normalized by the mean spatial density) for a) BTD; b) CCLM-NN; c) CCLM-SN. TC densities in BTD and CCLM ensemble mean are shaded. TC densities in the individual simulations of CCLM are shown as black contour lines and stand for the value 3. White color denotes the regions, where TC didn't occur.

Table 4.1 The table shows the regional climate simulation ID, if spectral nudging was used, the simulation start date, the total track number and the number of tracks which overlap JMA best tracks. The last column shows the spatial pattern correlation (PC SPD) between spatial track densities of the individual CCLM simulations and the BTD. The simulations were all started at 12:00 am, the only difference between simulations 10-14 (without spectral nudging) and between runs 20 and 24 (with spectral nudging) is the starting date.

Simulation ID	**Spectral nudging**	**Start date**	**Total track number**	**Overlapping tracks number**	**PC SPD**
10	No	03/01/2004	66	12	0.50
11	No	03/02/2004	65	10	0.59
12	No	03/03/2004	65	9	0.61
13	No	03/04/2004	64	7	0.55
14	No	03/05/2004	62	10	0.57
20	Yes	03/01/2004	40	21	0.67
21	Yes	03/02/2004	31	20	0.61
22	Yes	03/03/2004	31	22	0.64
23	Yes	03/04/2004	29	19	0.66
24	Yes	03/05/2004	28	20	0.64

Figure 4.2 shows simulated TCs matching the TCs recorded in BTD in a systematic way. The picture presents a distribution of deviations [km] between simulated TC tracks and the observed ones for CCLM-NN (left) and CCLM-SN (right) ensemble members. Every TC observed in the typhoon season 2004 is shown separately. The size of the circles relates to the number of track points falling into the given distance interval. The color of the circles assigns individual ensemble member. The picture confirms that CCLM-SN simulates more TCs matching the observed ones, than CCLM-NN. Five TCs recorded in BTD were simulated only when the SNT was applied (CCLM-SN). Two other TCs were found only in CCLM-NN simulations. Three TCs from the season 2004 weren't identified in any of the CCLM simulations. The distribution of distances between modeled and observed TCs has different features for NN and SN simulations. Deviations between tracks in CCLM-NN and BTD are

large (up to 800 [km]) and differ significantly among ensemble members. In contrast, simulated TC tracks within the SN ensemble converge towards smaller distance intervals (100 ~ 200 [km]) and become less frequent towards larger distance intervals.

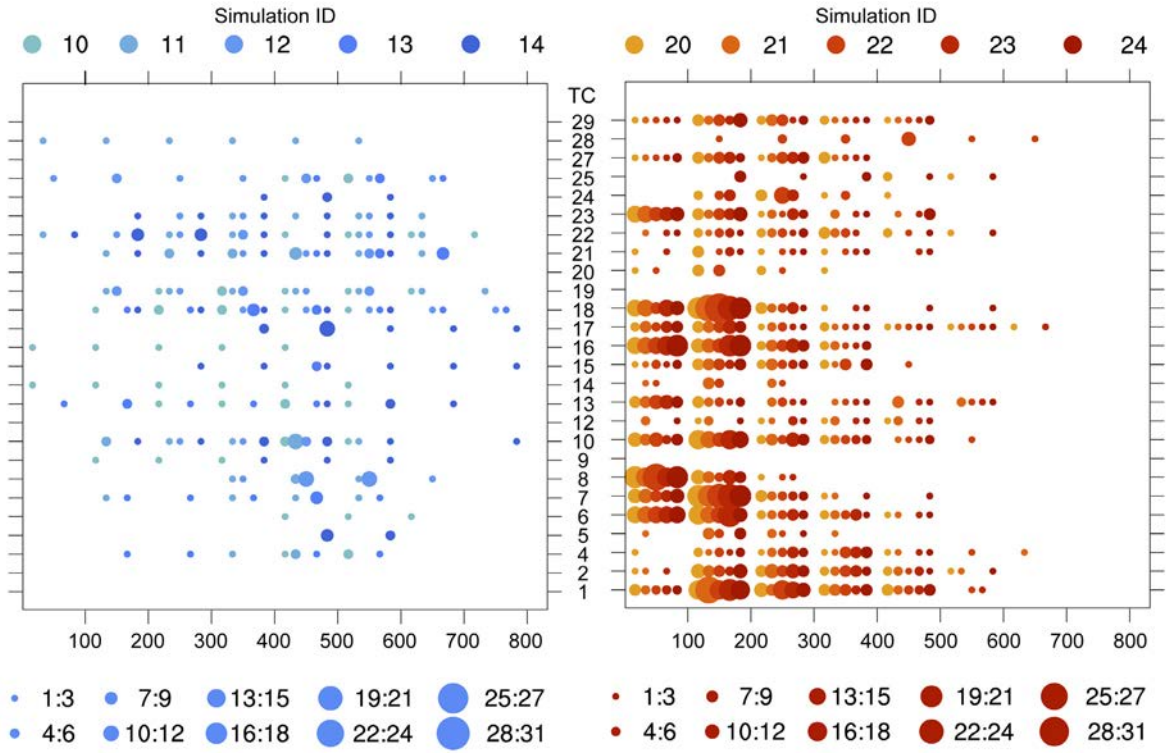

Figure 4.2 Differences of simulated TCs compared to BTD for the year 2004 for CCLM-NN (left) and CCLM-SN (right). The y-axis shows the individual TC IDs, those TCs which were not tracked in either NN or SN simulations were omitted (3, 11, 26). The x-axis shows distance intervals of 100 km. The size of the circles gives the number of track points classified into given distance intervals. The different colours depict the individual CCLM ensemble members.

Such features of TCs simulated in SN and NN ensembles are well represented by Typhoon Songda, found in at least four members of each ensemble. Figure 4.3 shows the track of TC Songda, given by BTD observations and CCLM simulations. Observations recorded TC Songda's formation in the eastern part of the WNP. The TC moved towards the SE Asian coast and recurved in the vicinity of Taiwan towards the North-East. NN tracks do not converge and spread into diverse directions, far from the observed TC. Two of the tracks didn't recurve and hit the SE Asian coast, another two moved towards the North. In contrary,

the SN tracks merged after a short while and then followed the TC track in BTD. Such features indicate that initial conditions have negligible impact on TCs simulated in CCLM-SN. In other words, the SNT reduces the internal variability of simulated TC tracks which greatly improves its track patterns and spatial density.

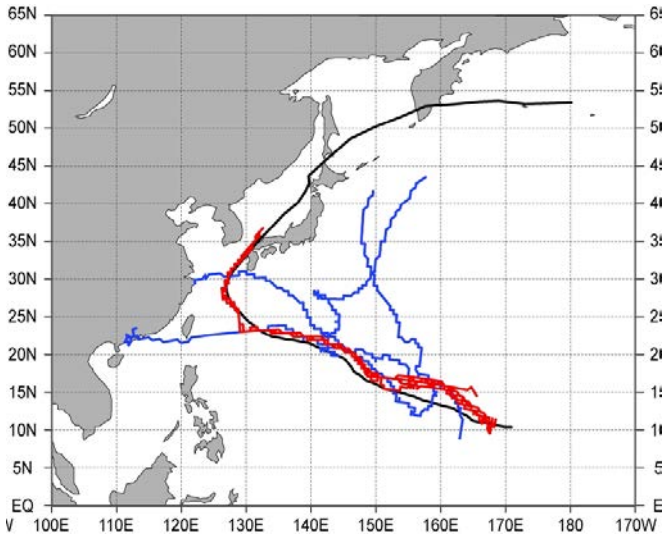

Figure 4.3 Tracks of Typhoon Songda, given by best track data of BTD (black), CCLM–SN (red) and CCLM-NN (blue).

4.3.2. Impact of spectral nudging on tropical cyclones intensity

This section demonstrates the effect of spectral nudging on simulated TC intensity. The analysis focuses on maximum wind speed, vertical profiles of TC temperature anomalies and wind speed - pressure relationship. As TC Songda is representative for TC features in SN and NN simulations it will be referred to throughout the chapter.

Figure 4.4 shows the surface horizontal wind fields of TC Songda for CFSR reanalysis (left), CLM-NN (middle), CLM-SN (right), at the time when observed and simulated TCs were relatively close to each other (Figure 4.3, 01.09.2004). The shaded pattern in CCLM-NN and CCLM-SN describes the first ensemble member. The contour lines are assigned to the remaining ensemble members.

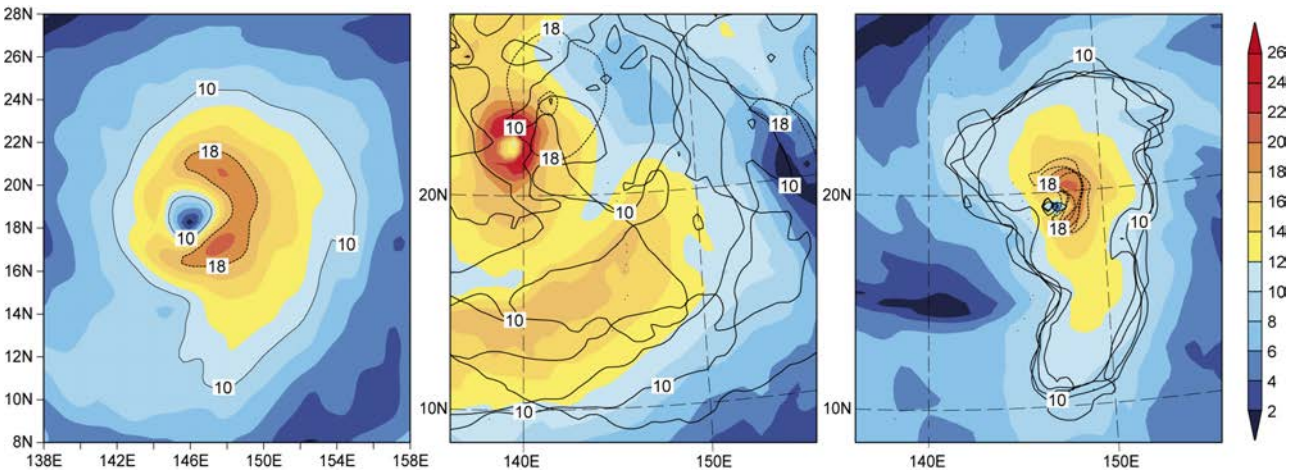

Figure 4.4 Horizontal surface wind speed fields [m s^{-1}] for TC Songda, on 1st September 2004, 00:00. From left: CFSR reanalysis, CCLM-NN, CCLM-SN. For CCLM the first simulation (simulation no 10 and 20) of each ensemble is shaded, the other simulation are shown as contour lines: 10 [m s^{-1}] as solid lines, 18 [m s^{-1}] as dotted lines.

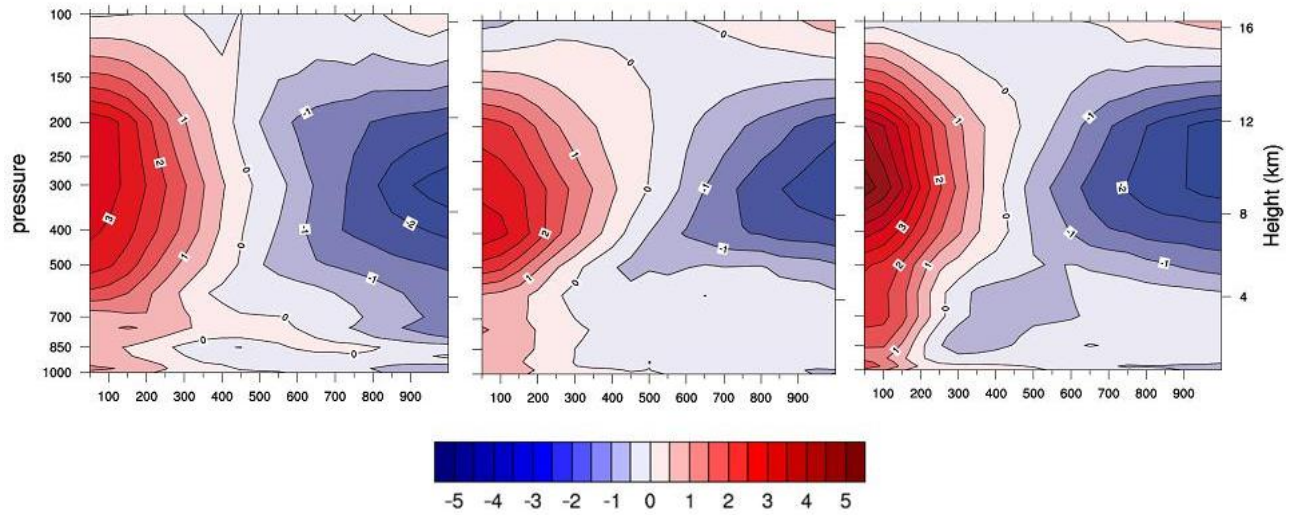

Figure 4.5 Vertical temperature anomalies [unit: K degrees] averaged over the radial distance from the TC centre for typhoon Songda at its stage with maximum near-surface wind speed for NCEP CFSR (left), and CCLM-NN (middle) and CCLM-SN (right) ensemble means. The x-axis shows the radial distance [unit: km]. The left y-axis shows pressure levels [unit: hPa], the right y-axis shows height [unit: km].

The cyclone in CFSR has a mature structure with a well-developed eye. TCs in all CCLM-SN members are located close to the observed one, but their evolving rainbands, small eye and eyewall indicate an early intensification phase. In contrast, to CCLM-SN, wind patterns and associated TC intensity in CCLM-NN vary among each member and deviate extensively from observations. For example, the first NN ensemble member (Figure 4.4, shaded with color) shows a well developed structure and wind speed higher than in SN and

CFSR. In the latter time steps, differences in the TC development phase between CCLM-NN and CCLM-SN become more distinct. While in SN simulations TC Songda constantly follows the track observed in CFSR, in CCLM-NN TCs deviate into diverse directions and reach different intensities.

To understand the effect of the SNT on surface and higher atmospheric layers, vertical profiles of temperature anomalies for TC Songda are analysed. Figure 4.5 shows these profiles averaged over the radial distance from the TC center, for the CFSR reanalysis (left), CCLM-NN ensemble mean (middle) and CCLM-SN ensemble mean (right) at the time of maximum intensity recorded by BTD observations (04.09.2004-05.09.2004). Only two TCs from the CCLM-NN ensemble survived till the given time step and reached their highest intensity at the same day or six days later (04.09.2004;10.09.2004). Four TCs from the SN ensemble followed the observed track and reached their highest intensity at the same day or one day later (05.09.2004; 06.09.2004). Simulated and observed TCs show well-developed, anomalously warm cores and cold areas in surrounding areas. CFSR and both ensembles extend their anomalies down to the sea surface. However, anomalies in the NN ensemble mean are slightly weaker than CFSR, while anomalies in SN are much stronger. Large deviations among CCLM-NN members, induced by internal variability of the model, have shown a counterbalancing effect on their mean TC intensity development. Oppositely, reduced internal variability in SN simulations has a positive impact on TC vertical development in the ensemble mean.

Cha et al. (2011) recently suggested that nudging the large-scale solution to the higher model levels inhibits the TC intensification process. To verify that, the wind-pressure relationships in CCLM-NN and CCLM–SN TCs were compared. Figure 4.6 presents simulated intensities of all 6-hrly track points in the CCLM-NN and CCLM-SN simulations, in terms of wind speed and pressure. Blue lines show wind speed-pressure relationship, derived by a cubic spline fit for intensities given in CCLM and the black lines for BTD.

The relationship is in both cases quite similar, but values in NN show a wider spread around the fitted curve. For both ensembles, wind speeds shows underestimation, compared to BTD. Such underestimation occurs mainly when pressure drops below ~ 980 [hPa]. This implies that the resolution in CCLM is not sufficient to resolve the strong pressure gradients featuring intense TCs. The values in CCLM-NN reach lower minimum pressure, up to ~ 920 [hPa], than CCLM-SN (~ 940 [hPa]). However, coinciding wind speed values in CCLM-NN don't show significantly higher values. For both ensembles TC wind speed can not exceed the value of 40 [m s^{-1}]. This result indicates an inhibiting impact of the SNT on low pressure core development. However, impact of the SNT on TC wind speed is negligible, due to other limiting factors related to model dynamical characteristics (e.g. resolution, convection scheme).

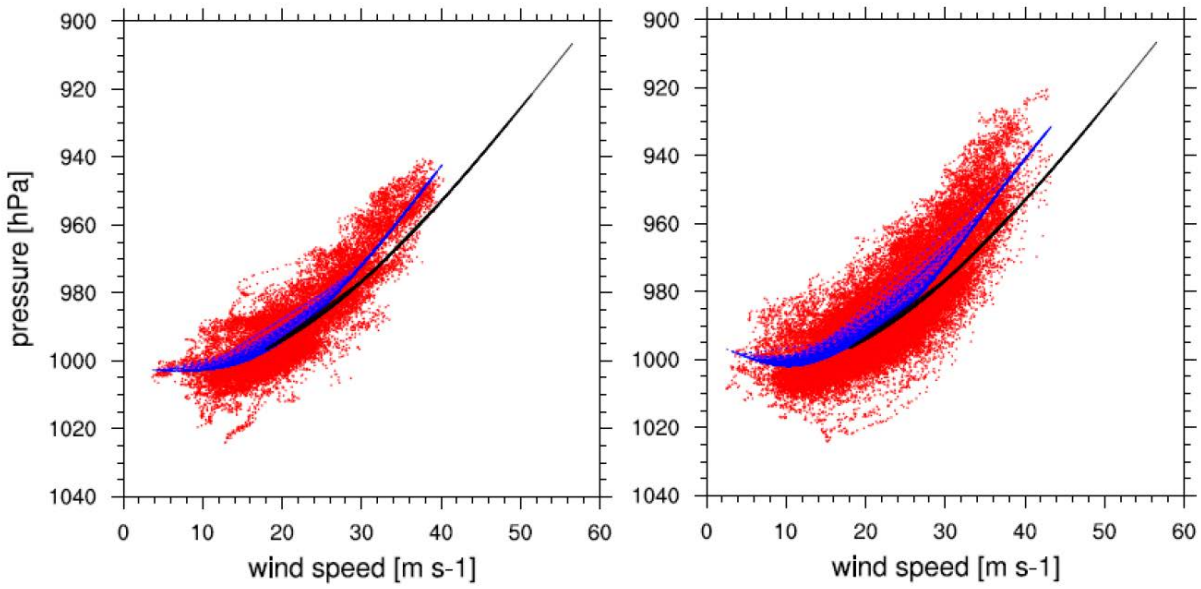

Figure 4.6 Scatterplot of maximum surface wind speed [unit: m s^{-1}] versus minimum pressure [unit: hPa] for all TCs during their lifetime for CCLM –SN (left) and CCLM –NN (right). Blue and black lines are cubic spline fits for CCLM and BTD observations, respectively.

An inhibiting effect of the SNT may explain the slow intensification of TC Songda in CCLM-SN, compared to CCLM-NN and CFSR (Figure 4.4c, CCLM-SN). However, the intensity of this TC, at the maximum stage recorded by BTD, was lower in the CCLM-NN ensemble mean (Figure 4.5b, CCLM-NN). This indicates that the large internal variability,

when no SNT is applied, may have even stronger, negative impact on simulated TC intensity. For TC Songda a positive effect of the SNT, related to the reduction of internal variability, possibly compensates an inhibiting effect of the SNT (Figure 4.5c, CCLM-SN).

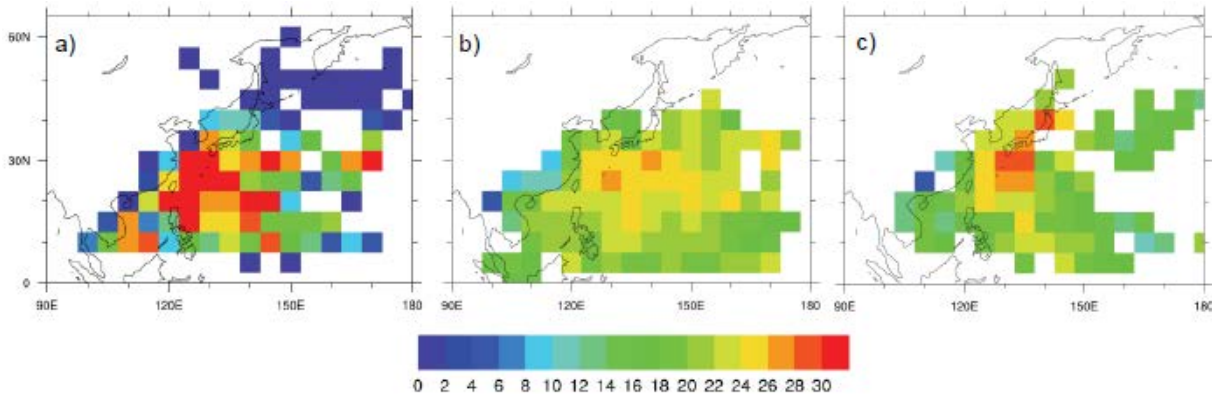

Figure 4.7 TC mean wind speed spatial distribution (TC wind speed cumulated within 5° latitude x 5° longitude grid boxes; normalized by the mean TC spatial density) for a) BTD; b) CCLM-NN; c) CCLM-SN. Gridboxes where TC occurred less than 3 times are not shaded.

A comparison of spatial distribution of mean TC intensity in simulations and BTD, shown in Figure 4.7, supports the previous findings. The picture presents the fields of accumulated TC maximum wind speed normalized by the number of TC occurrences falling into each grid box, for BTD (a), CCLM-NN ensemble mean (b) and CCLM-SN ensemble mean (c).

BTD reaches the highest values, often exceeding 30 [m s^{-1}], distributed mainly in the vicinity of the SE Asian coast. Mean TC intensity fields in CCLM-NN follow an outspread pattern of spatial TC density (Figure 4.1b). This implies that for the eastern part of the WNP, the NN ensemble shows higher values than BTD. In SN such a deviation is reduced, as an aftermath of the improved TC track patterns (Figure 4.1c). For the regions in the vicinity of Taiwan, where TCs reach the highest intensities, SN shows values higher than NN. Mean TC intensity in that regions exceeds 28 [m s^{-1}] for CCLM-SN but does not exceed 26 [m s^{-1}] in CCLM-NN. The results indicate that the SNT improves fields of spatial mean TC intensity.

Overall, the influence of the SNT on TC intensity results from two counteracting effects. The reduction of the model's internal variability shows a positive effect on the spatial distribution of TC tracks and intensity, which outweighs the inhibiting impact on TC vertical development processes.

4.3.3 Impact of spectral nudging on tropical cyclones climatology

The formation and development of tropical cyclones are strongly associated with environmental conditions. Sufficient ocean thermal energy, enhanced mid-troposphere relative humidity, and conditional instability support deep convection. Enhanced lower troposphere relative vorticity, weak vertical shear of horizontal winds and minimum distance by at least 5° in latitude from the equator are dynamical parameters which are necessary for tropical cyclogenesis. This section analyses the impact of the SNT on the large-scale atmospheric circulation shaping the TC activity climate. To understand this, the simulated TC climatology (for SN and NN) is compared with the observed one.

Figure 4.8 presents atmospheric fields for June, July and August 2004 for CFSR (left column), CCLM-NN ensemble mean (middle column) and CCLM-SN ensemble mean (right column). Fields assessing the dynamic conditions for tropical cyclogenesis are: a) geopotential height, b) zonal wind and c) relative vorticity, all on the pressure level of 850 hPa. Fields related to the thermodynamic conditions are: d) relative humidity on the pressure level of 600 hPa, e) convective available potential energy, f) hourly precipitation. Fields of 850 hPa geopotential height and 850 hPa zonal wind (Figure 4.8a,b) show that CCLM simulates realistic features of low-level circulation, similar to observed ones. However, CCLM-NN reveals much stronger than CFSR cyclonic anomaly in the subtropical WNP, which is associated with the Asian monsoon circulation. Anticyclonic circulation, forming as a subtropical high eastward from Japan, is weaker. In contrast, CCLM-SN captures the pattern and magnitude of monsoon circulation correctly. This has a positive impact on the simulated

subtropical high circulation. The strength and location of the subtropical high in CCLM-SN is close to the observed one (CFSR).

The monsoon trough provides favourable conditions for TC genesis in the WNP. Therefore the skill of the model to reproduce monsoon environment determines the simulated TC activity. Westerly winds, relative vorticity and precipitation characterizing monsoon phenomena are in CCLM-NN largely overestimated (Figure 4.8b,c,f). The SNT substantially reduces such deviation, which consequently impacts TC activity in CCLM-SN. A reduced error of overestimated cyclonic circulation and an underestimated subtropical high in CCLM-SN decreases TC activity and improves spatial track patterns (e.g reduces the TC outspread towards the eastern part of the WNP).

Some downscaling studies ([Wu et al., 2012, Cha and Lee, 2009, Miguez-Macho et al., 2004]) confirmed the positive impact of the SNT on monsoon circulations and related spatial precipitation patterns. [Cha et al., 2008] additionally explained the mechanism causing enhanced precipitation when no SNT is applied. They have shown that strong zonal flow increases the planetary boundary layer mechanical mixing and consequently enhances latent surface heat fluxes. This in turn increases convective available potential energy, stimulates convective processes and may lead to intensified precipitation when no SNT is applied.

Figures 4.8b,d,e,f confirm such findings. The strong westerly flow in the monsoon region, reproduced by CCLM-NN, coincides with an intensified and eastwardly extended convective available potential energy, relative humidity and precipitation patterns. In CCLM-SN such deviation is reduced. This also explains the improvement of TC track and intensity patterns (Figure 4.1 and 4.7), e.g. reduction of TC activity in the eastern WNP.

To conclude, the SNT shows a positive impact on both: dynamic and thermodynamic conditions, which significantly control TC activity. Large-scale circulation patterns associated with monsoon circulation and the subtropical high are improved. Consequently, the strong positive feedback between surface low-level winds, convective available potential energy and

precipitation is reduced. Results provided in this chapter indicate that TC climatology shows more realistic features when the SNT is applied.

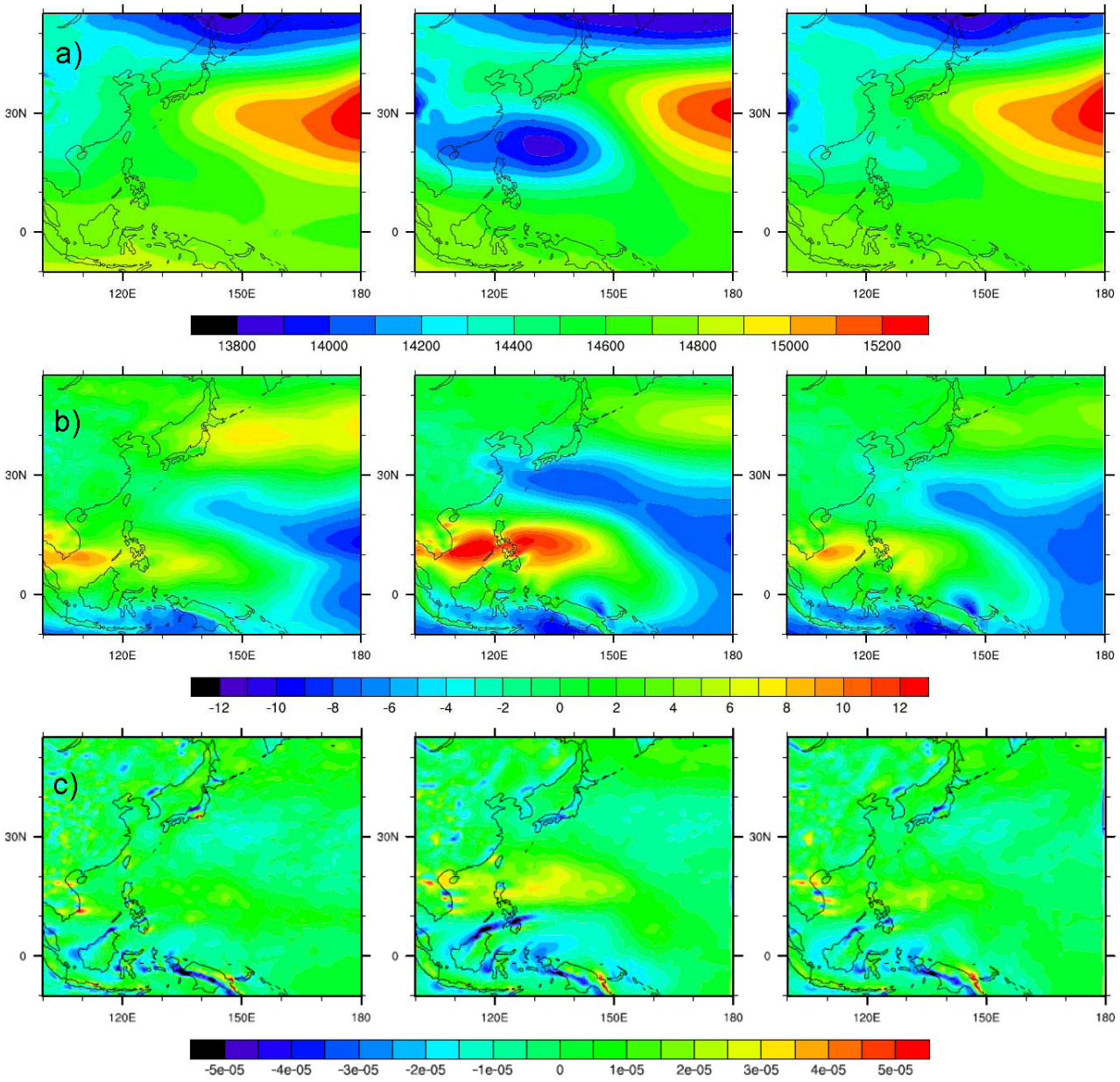

Figure 4.8 Time mean for June, July August season 2004 for: a) geopotential height on 850 hPa [unit: m s^{-2}], b) zonal wind on 850 hPa [unit: m s^{-1}], c) relative vorticity on 850 hPa [unit: s^{-1}], in CFSR (left column), CCLM-NN ensemble mean (middle column) and CCLM-SN ensemble mean (right column),

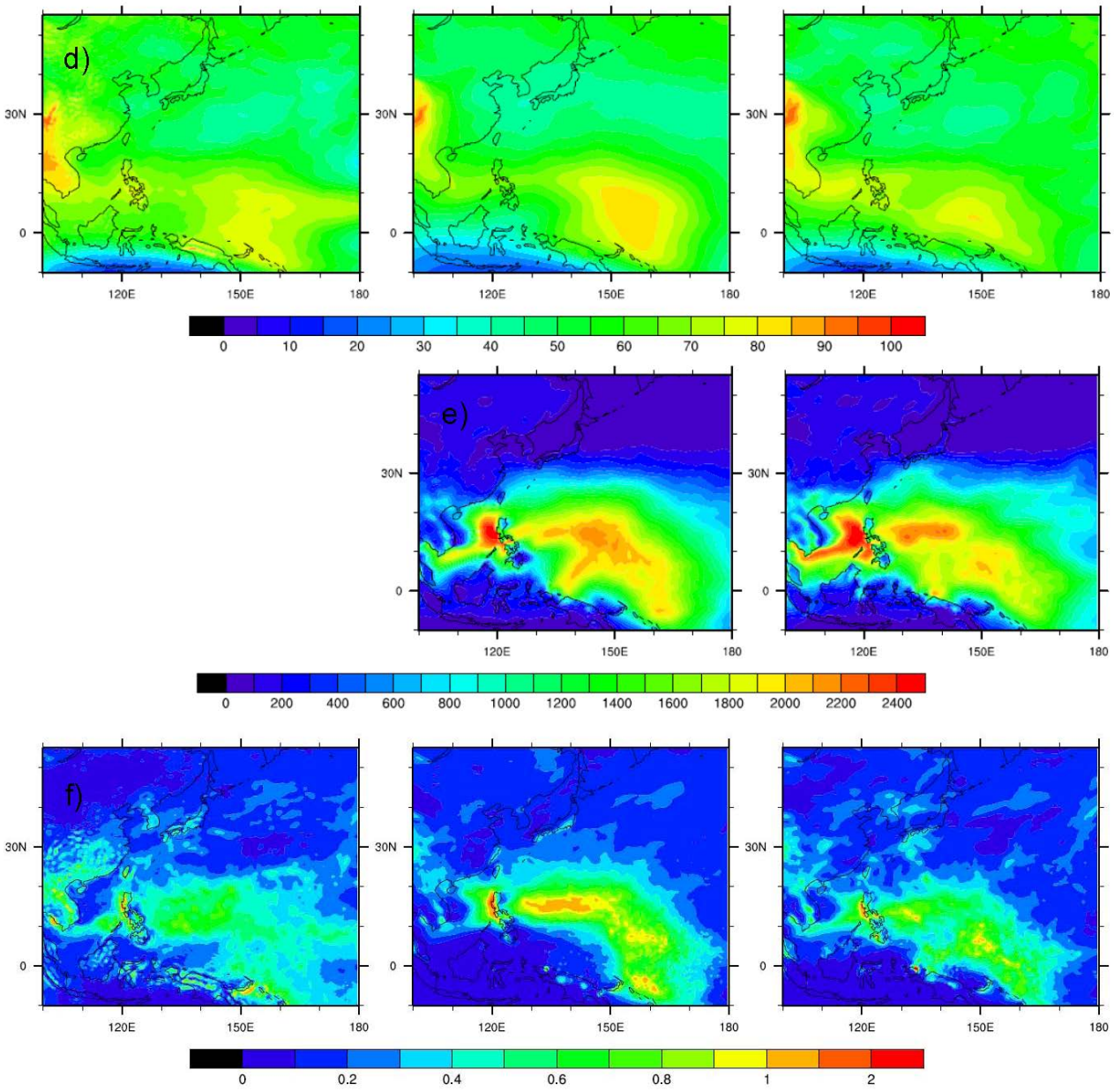

Figure 4.8 cd..: d) relative humidity on 600 hPa [unit: mm], e) convective available potential energy [unit: J kg^{-1}], f) hourly precipitation [unit: mm] in CFSR (left column) CCLM-NN ensemble mean (middle column) and CCLM-SN ensemble mean (right column). Convective available potential energy is not provided by CFSR, therefore it is shown only for CCLM-NN and CCLM-SN.

4.3.4. Representation of the meso-scale features in TCs simulated by CCLM

Following the results from the previous section, this part assesses the skill of the CCLM with the SNT applied (CCLM-SN) to add meso-scale value to the large-scale atmospheric information provided by the driving data. The performance of the CCLM is analysed with a focus on TCs wind speed and sea level pressure using Brier Skill Score (BSS) statistics. The BSS is estimated accordingly:

$$BSS=1- (RMSE(Ycclm,Yref)/RMSE(Yncep,Yref)), \quad (2)$$

where: Ycclm and Yncep are the variables for CCLM and NCEP reanalysis respectively, Yref is the reference variable given by JMA, at a given time step. The BSS varies from 1, when CCLM perfectly fits the reference data, and tends to "– infinity" when CCLM deviates from the reference stronger than NCEP does. BSS equal zero would mean that CCLM is of equal skill as NCEP.

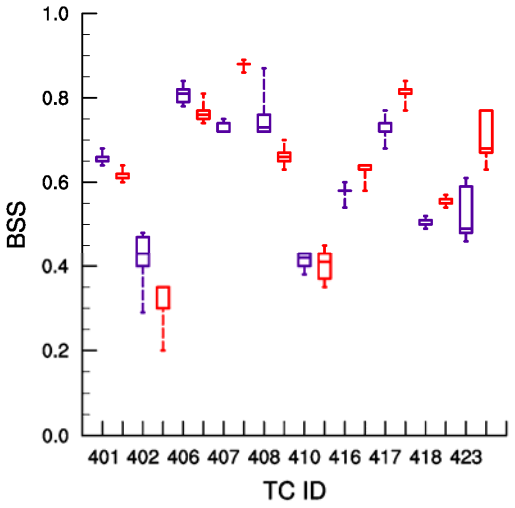

Figure 4.9 Brier Skill Score (BSS) for CCLM wind speed (blue) and sea level pressure (red) between BTD and NCEP for ten chosen TCs. The x-axis shows ID number for each TC. The y-axis shows the BSS for each member of the five CCLM-SN ensemble simulations.

Figure 4.9 presents BSS estimated for maximum sustained wind speed and minimum sea level pressure for ten TCs, which were found in all SN simulations and which matched the TCs observed in BTD. The BSS shows positive skill in all simulated TCs. For wind speed, BSS varies from 0.49 (for the 0.25th percentile) to 0.73 (for the 0.75th percentile), while for

pressure the scores are slightly higher and vary from 0.55 to 0.77. The scores among the SN simulations vary in a small extent. In seven cases, the spread is smaller than 10 % of an average TC score. TC 402 showed the largest spread (up to 30 % from the average score), with BSS values varying from 0.3 to 0.5 in wind speed. The results indicate that CCLM improves the representation of TC features by adding meso-scale information to coarsely resolved reanalysis. The skill is higher for sea level pressure. However, simulated TCs are still much weaker than observed.

Figure 4.10 shows maximum lifetime TC intensity for the same ten TCs, shown in Figure 4.9. The picture shows wind speed underestimation of at least 10 [m s^{-1}] and sea level pressure overestimation of at least 10 [hPa]. None of the simulated TCs exceeds the intensity of 40 [m s^{-1}]. Consequently, TC lifetime maximum intensity is limited to the first SSHS intensity category in terms of maximum surface wind speed (< 43 [m s^{-1}]), and the third category in terms of core pressure (> 945 [hPa]).

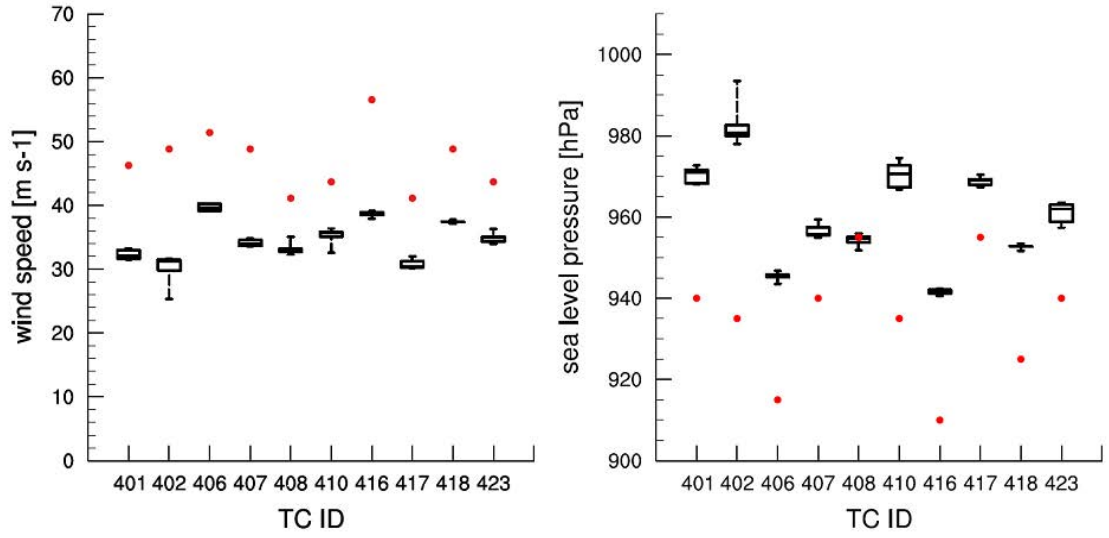

Figure 4.10 Maximum lifetime TC intensity for all CCLM-SN simulations (black) and BTD observations (red dots), in terms of: wind speed [unit: m s^{-1}] (left) and sea level pressure [unit: hPa](right). The x-axis shows ID number for each chosen TC.

Figure 4.11 shows the distribution of TC intensity given by maximum lifetime sustained wind speed of all TCs in the CCLM-SN ensemble mean and for BTD for the

typhoon season 2004. The result suggests that CCLM simulates TCs which are two categories lower than observed ones, in terms of maximum wind speed.

[Feser and von Storch, 2008a] confirmed that downscaling NCEP reanalysis to 55 km resolution with the RCM CCLM improves the representation of TC features. But many other studies ([Stowasser et al., 2006, Camargo et al., 2007, Knutson et al., 2007, Knutson et al., 2008]) stated that 50 km resolution is too coarse for models to simulate realistic TC intensity. Some research ([Feser and von Storch, 2008a, Knutson et al., 2007]) also indicated that downscaling to finer resolutions may not have necessarily an additional impact on simulated TC intensity. [Knutson et al., 2007] showed that downscaling to 18 km results in hurricanes of 3rd SSHS category in terms of pressure and 2nd category in terms of wind speed.

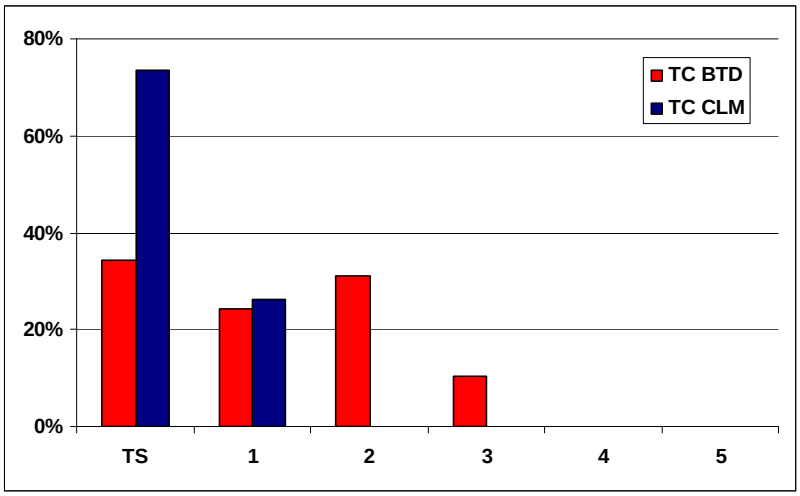

Figure 4.11 Distribution of TCs in the CCLM-SN ensemble mean (blue) and in BTD observations (red) sorted by SSHS intensity categories, based on TC lifetime maximum wind speed. The x-axis shows SSHS categories extended by tropical storm category.

Results of [Knutsona and Tuleya, 2004] suggested that without a convective parameterization scheme which appropriately resolves small-scale processes, increasing horizontal resolution will have negligible impact on the structure and intensity improvements. [Moon et al., 2007] gave another explanation for deficiently simulated winds. They relate these to reduced surface drag in high wind conditions resulting from surface flux parameterizations. To conclude, CCLM shows positive, but limited skill to simulate realistic

TC intensity. This has to be taken into account while analysing TC climatologies, TC variability and trends in the following section.

4.4 Capability and limitations of CCLM to simulate tropical cyclones climatology using spectral nudging

In the first part of this chapter, the impact of the SNT on simulated TC activity was investigated. For this purpose TC frequency, spatial track patterns, TC intensity and related large-scale atmospheric fields simulated by CCLM with- and without SNT were compared with observations. Analysis has shown advantages and disadvantages of the SNT application.

The SNT has shown a notable impact on TC intensity development. The maximum TC intensity is higher when no SNT is applied. The core pressure of the most intense TCs are up to ~ 20 [hPa] deeper in CCLM-NN. Differences in maximum TC wind speed are less distinct. Values in both analysed ensembles have shown an upper threshold of 40 [m s^{-1}], which may result from additional, limiting factors e.g. resolution. Therefore these differences can be even higher for simulations of finer horizontal resolution.

Given results may not necessarily indicate the negative, inhibiting impact of SNT on TC intensity. In contrary, absence of SNT may lead to enhanced TC intensity values. As shown in the previous sections, higher TC activity (intensity and frequency) in CCLM –NN results from the biased representation of mean TC climate.

CCLM without spectral nudging showed large variability in simulated track patterns and associated TC intensity. Fields of TC track density showed systematic errors, which are associated with the simulated mean climate over SE Asia and WNP. In the CCLM – NN ensemble the mean monsoon circulation was amplified and the circulation in the subtropical high was weakened, compared to CFSR. This changed spatial track pattern and increased TC formation in the eastern part of the WNP. An ensemble simulation using five members turned

out to be not sufficient to capture the whole spectrum of internal model variability and to represent the TC climatology correctly.

The SNT has shown a positive impact on the simulated TC climate and consequently spatial distribution of TCs and their intensity. Application of the SNT greatly reduced variability in TC track patterns, improved the skill of CCLM to reproduce TC activity and related large-scale atmospheric circulation. Simulated TC frequency decreased by a factor of 2. But the number of TCs, matching the observations, increased by a factor of 2. Spatial fields of TC tracks and mean TC intensity were more accurate compared to observations. Exaggerated TC activity in CCLM-NN over the eastern part of the WNP was, after application of the SNT, significantly reduced. Moreover, for the regions with the highest observed intensities (in the vicinity of the SE Asian coast and Japan) the mean TC intensity increased, thus showing values more similar to the observed ones. This improvement results from the higher CCLM skill to reproduce large-scale patterns of dynamic and thermodynamic conditions when using spectral nudging.

The second part of this chapter analyses the skill of CCLM-SN to downscale meso-scale features of TCs of the typhoon season 2004. The results showed that CCLM has skill in adding meso-scale information to the large-scale reanalysis and this skill is higher for sea level pressure than for wind speed. However, CCLM is not capable to simulate TC intensities higher than the 2nd category. Consequently, the most intense TCs are weaker and the mean TC intensity distribution in CCLM is lower than observed. Therefore, in order to identify only the intense TCs, the intensity criteria defining TC events in the tracking algorithm had to be adjusted toward lower values.

Overall, the SNT has demonstrated to be an efficient tool to control the internal model variability and consequently - to produce reliable TC climatologies. Therefore the SNT will be applied in a long-term simulation of past TC climate, which will be presented in the

following part. However, the limitations of the regional model to simulate realistic intensity features must be taken into account while interpreting the RCM simulation.

Chapter 5. A long-term tropical cyclones climatology over the period 1948-2011

5. 1 Introduction

This work presents TC climatology for the last six decades (1948-2011) over the WNP and SE Asia using a dynamical downscaling approach with the regional climate model CCLM. While many downscaling studies focused on a shorter time scale, this is the first such long-term regional hindcast simulation of TC variability in the given region.

In the previous chapter it was shown that CCLM using the spectral nudging technique (SNT) has high capability to reproduce TC climate. However, a numerical simulation running on a 50 km horizontal resolution leads to underestimation of TC intensity.

[Knutson et al., 2007] stated that for successful downscaling, models also have to be able to reproduce the relationship between TC activity and environmental factors controlling them. As shown in Chapter 3, feasibility of establishing such a relationship is limited, given the relatively short and inhomogeneous TC observations. While for the North Atlantic region TC activity was mostly associated with average sea surface temperature (SST) variations ([Webster et al., 2005, Emanuel, 2005, Holland and Webster, 2007]) for the WNP region many studies failed to confirm such a relationship. [Wang and Chan, 2002] stated that SST anomalies do not determine the TC genesis location. [Chan and Liu, 2004] showed a negative correlation between TC number and SST in the WNP. [Chan, 2007, Chan, 2009] suggested that interannual variations of the intense TC numbers may be affected by both thermodynamical and dynamical environmental factors. Dynamical simulations give an alternative possibility to analyse the link between TC activity and environmental factors. Thus

the following work will present also the relation between TC activity and thermodynamic factors (Maximum Potential Intensity (MPI) and SST) on interannual- and decadal time scale.

The following work is structured accordingly:

- "Data and Methodology" describes statistical methods applied in the study, and the data.
- In the first part of the section "Results" spatial and temporal TC variability simulated by CCLM is compared with the observed one (BTD), for the period 1978-2011. The second part shows a comparison of the simulated and observed relationship between TC activity and environmental factors. The association with the environmental large-scale patterns is quantified by means of Canonical Correlation Analysis. Finally, the TC activity changes for the whole period 1948-2011 are presented.
- The "Summary and Conclusions" part provides an interpretation for the given results and summarises the main findings.

5.2 Data and Methodology

For comparison purposes we use BTD provided by the Japanese Meteorological Agency (JMA, www.jma.go.jp/jma/jma-eng/jma-center/rsmc-hp-pub-eg/besttrack.html). These were found to be the most reliable BTD in terms of TC trends [Barcikowska et al., 2012]. The records from 1978, when the satellite observations allowed for better spatial homogeneity of TC observations, were chosen.

Statistics derived from the CCLM and observations are annually accumulated numbers of TC days and spatial density of TC occurrences. TC day numbers for all identified storms are provided for the years 1948-2011 in CCLM and 1951-2011 in BTD, in the summer season (July-October, hereafter JASO months). However, since TC intensity was recorded by BTD only since 1978, observed TC days of intense storms can be calculated only for the years

1978-2011. For computing the spatial density of TC occurrences each 6-hourly TC position within a 5° latitude x 5° longitude grid box was counted. To define the dominant modes of TC variability an empirical orthogonal function (EOF) analysis was applied for yearly spatial density fields for 1978-2011. The EOF ([North et al., 1982]) analysis defines the 'key' patterns featuring the variability of the input data. The importance of the patterns is given by the percentage of the variance they explain in the input data.

The long-term trend in CCLM (1948-2011) was derived from spatial density fields counting 1-hourly TC positions within 2° x 2° grid boxes. Spatial density fields were calculated for all identified storms and also just for the intense ones. Trends were computed with a linear regression approach using the least squares fit. Additionally, for five regions, where the most distinct long-term changes were found, a piecewise linear trend model was derived. The model was fitted to the data using a least squares method and it was assumed that there was at most one slope change.

The influence of large-scale circulation patterns on hindcasted TC variability was quantified with a Canonical Correlation Analysis (e.g.[von Storch and Zwiers, 1999]). The method estimates the maximum correlation between two multidimensional data sets. Here we analysed the association of TC spatial density with Maximum Potential Intensity (MPI) patterns and SST. For this purpose the first five EOFs were computed using yearly anomalies of atmospheric variables calculated during JASO (July-October, hereafter JASO months) months. It is assumed that the first five EOFs represent the main patterns of variability and those were used for further analysis ([Leoncini et al., 2008, von Storch and Zwiers, 1999]).

Spatial density fields are discontinuous fields with high spatial variability. Therefore they were divided into subregions with distinct features of TC frequency (Figure 5.4). Table 5.1 represents the statistics for the selected regions: average TC number (avg), average TC number for 2° latitude x 2° longitude grid boxes (avg norm), standard deviation (std dev), and least squares slope (lsq) of 6-hourly TC occurrences in 1978-2011. The MPI [Emanuel, 1988]

is computed with a program provided by K. Emanuel on the website ftp://texmex.mit.edu/pub/emanuel/TCMAX/.

The yearly values of MPI and SST for the WNP region were calculated with the sea surface temperature (SST) fields that were used to drive the regional model as well as RCM temperatures and specific humidity content.

Table 5.1 The statistics of TC occurrences in the regions selected for Canonical Correlation Analysis for 1978-2011: average number (avg), average number for 2° latitude x 2° longitude grid boxes (avg norm), standard deviation (std dev), and least squares slopes (lsq).

	Region	avg	avg norm	std dev	lsq
1	105-122°E, 10-20°N	12.2	2.6	12.2	0.28
2	122-138°E, 10-20°N	27.9	7.0	20.1	-0.03
3	138-150°E, 10-20°N	15.5	5.2	16.5	-0.16
4	150-160°E, 10-20°N	6	2.4	9.4	0.16
5	105-115°E, 20-30°N	4.4	1.8	4.5	0.04
6	115-130°E, 20-30°N	29.3	7.8	17.7	0.57
7	130-145°E, 20-30°N	29.7	7.9	22.8	0.59
8	145-160°E, 20-30°N	9.5	2.5	11.3	0.14
9	120-130°E, 30-40°N	6.3	3.1	7.5	0.16
10	130-145°E, 30-40°N	10.8	2.9	8.8	0.23
11	145-160°E, 30-40°N	5.4	1.5	7.9	0.14

5.3 Results

5.3.1 Tropical cyclones spatial and temporal variability for the western North Pacific in modelled and observational data

The spatial and temporal variability of hindcasted regional model TC activity is compared to an observational data set (BTD). The analysis focuses mainly on the last three decades (1978-2011) when satellites were used for constructing the best track data sets. However, due to the lack of in-situ measurements suitable for validation of BTD and inhomogeneities introduced by operational methods which changed over time during

compilation of the data sets ([Barcikowska et al., 2012, Landsea et al., 2006]) BTD does not serve as a reference.

As shown in Chapter 1 statistics of TC frequency variability recorded by BTD give the most robust results for the intense TC's (categories 2-5), showing agreement among all independent BTD sets. Thus temporal variability analysis is focused particularly on the intense TCs. The tracking settings were chosen so that the yearly mean number of simulated TCs is the same as observed, 25 TCs. However, for the main typhoon season (JASO) CCLM underestimates the mean TC number, showing on average 14.3 TCs while BTD gives 17.8 TCs. The standard deviation remains the same (3.8) for both data sets. The RCM data set representing the most intense TCs shows mean frequency numbers twice as high (5.2 TCs, 48 TC days) as the observed ones (2.4 TCs and 28 TC days). This is the effect of the tracking algorithm settings chosen which allow partly for a weaker TCs detection. The standard deviation for both data sets remains relatively high and similar: 2.1 TCs; 22.1 TC days for CCLM and 1.9; 24.4 for BTD respectively. The total variance of intense TC frequency numbers in CCLM may have been artificially influenced by weaker TCs falling into the distribution.

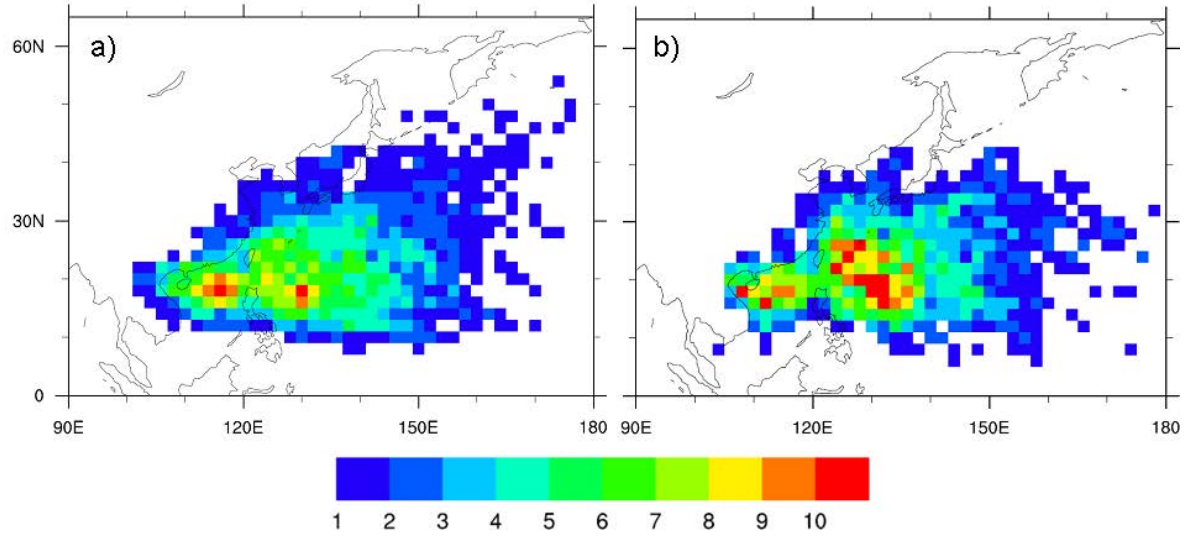

Figure 5.1 TC spatial densities (accumulated TC occurrence per every 2° latitude x 2° longitude grid box; normalized by the mean spatial density fields) for a) BTD, b) CCLM in the period 1978-2011.

Figure 5.1 shows maps of TC occurrences during the 30-year simulation period, in BTD observations and CCLM simulation. Simulated TC occurrences show fairly realistic features, although the numbers in the main development region (10°-30° N, 120°-150° E) are too high in comparison to BTD. Simulated TC tracks are less extensive in north-eastward direction and rarely exceed subtropical latitudes. The numbers over the South-East China Sea region is comparable for simulated and observed fields. However, in CCLM higher values slightly spread toward the coastal region.

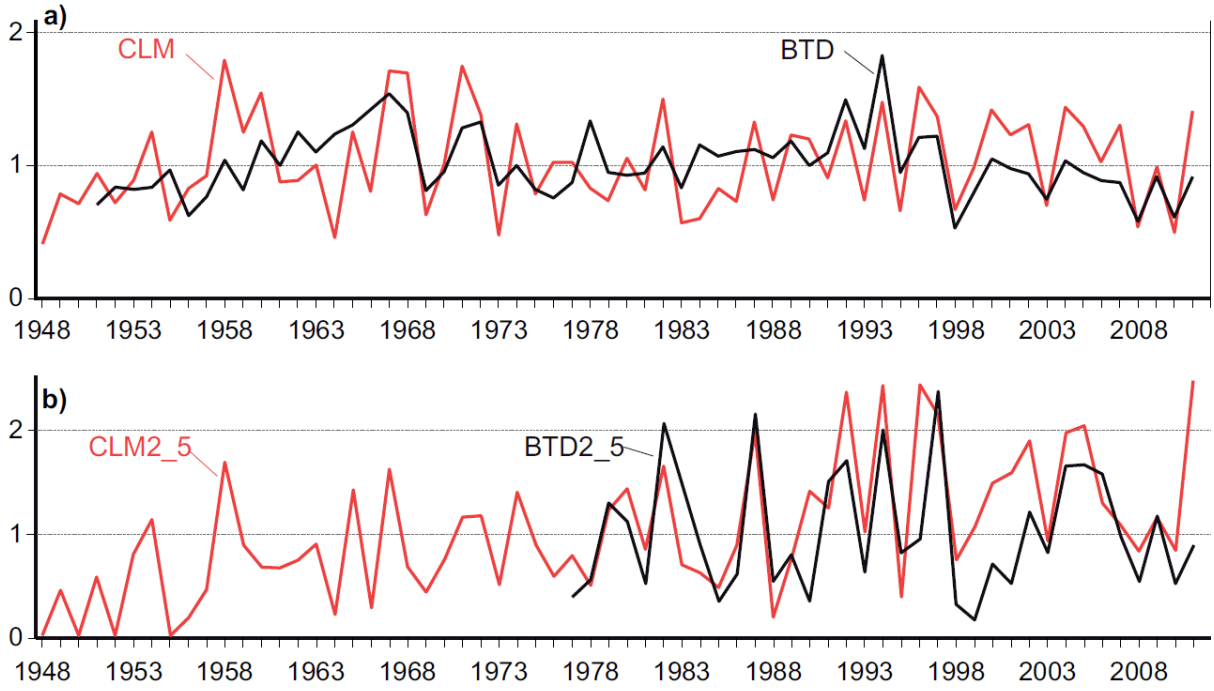

Figure 5.2 Annual TC days counted for July-October seasons, normalized by the climatological mean value for CCLM (red) and BTD (black). TC days are counted for a) all TCs (denoted as CLM and BTD) and b) for the intense TCs (denoted as CLM2_5 and BTD2_5). Climatological means are derived separately for the pre-satellite period: 1948-2077 and 1978-2011. BTD provides TC intensity estimations in the latter period, which limits its time series for the intense TCs to that period.

Figure 5.2a presents time series of annually accumulated TC days, given by the CCLM and the BTD observations in JASO months. The time series for the observed intense TCs (Figure 5.2b) are shown from 1978, when the BTD begun TC intensity recordings. Therefore, to achieve an objective comparison we present normalized numbers whereby the

mean was computed separately for the two periods: 1948-1977 and 1978-2011. For the first period, before the satellites era began (1950, 1960s, early 1970s), BTD (similar to CCLM) show a strong increase and an abrupt drop of TC days in the early 1970s. From the 1980s both data sets show an increasing phase up to the early 1990s and smaller numbers of TC days in the last decade. However, CCLM shows a rather gradual decrease while BTD drops off abruptly. These differences are partly reduced when only intense TCs (Figure 5.2b) are analysed: for the period 1978-1998 both data sets show increasing tendencies and again a shift to smaller numbers afterwards.

In order to analyse the spatial TC variability an EOF analysis is applied to the yearly occurrences of intense TCs in CCLM and BTD, for the period 1978-2011. Figure 5.3a and 5.3c shows the first EOFs (EOF-1), which represent the main modes of inter-annual variability for TCs in CCLM and BTD, respectively. PC-1 in CCLM indeed follows the time series of yearly TC days with a correlation of 0.87. However, its EOF explains less (19%) of the total variance than EOF-1 in BTD (26%). Additionally it is assumed that the first EOF represents the main TC track patterns. The comparison indicates similar features in modelled and observed data sets. Positive loadings spread from the south-eastern part of the WNP and extend toward the SE Asia coast or recurve towards Japan. Negative loadings occur in the northern part of the Philippine Sea and the South China Sea for CCLM, and in the southern parts for BTD. There is also a visible shift in the CCLM pattern towards the North. The time series of the analysed EOF modes (PC-1) in CCLM and BTD share a correlation of 0.63. The PC-1s show most similarities in the first decade, but less similarity in the later period (1998-2011).

To analyse the decadal TC variability an EOF analysis is applied to yearly TC occurrences filtered with a 10-years Gaussian filter. Figure 5.3b and 5.3d shows the first EOFs (EOF-1), which represent the main modes of decadal variability for TCs in CCLM and BTD, respectively. The EOFs of both data sets explain 43% (CCLM) and 49% (BTD) of the

total variance. The patterns show similar features and their PC-1s show a very strong correlation (0.92). Both cases indicate decreasing TC activity below 20° latitude of the WNP for the last three decades. In addition CCLM indicates an increase of TC activity in the higher latitudes, with a maximum in the region located southward from Japan. EOF-2 (not shown) explains 25% of the total variance in CCLM and 19 % in BTD. It shows similar patterns with positive loadings for the north-western part of the WNP and negative ones for the south–eastern part. Their PC-2s show a correlation of 0.66 and decreasing, negative values till the mid-1990s and an increase in the last decade. The EOF analysis suggests increasing TC activity in the subtropical latitudes related to a north-westward shift of TC tracks.

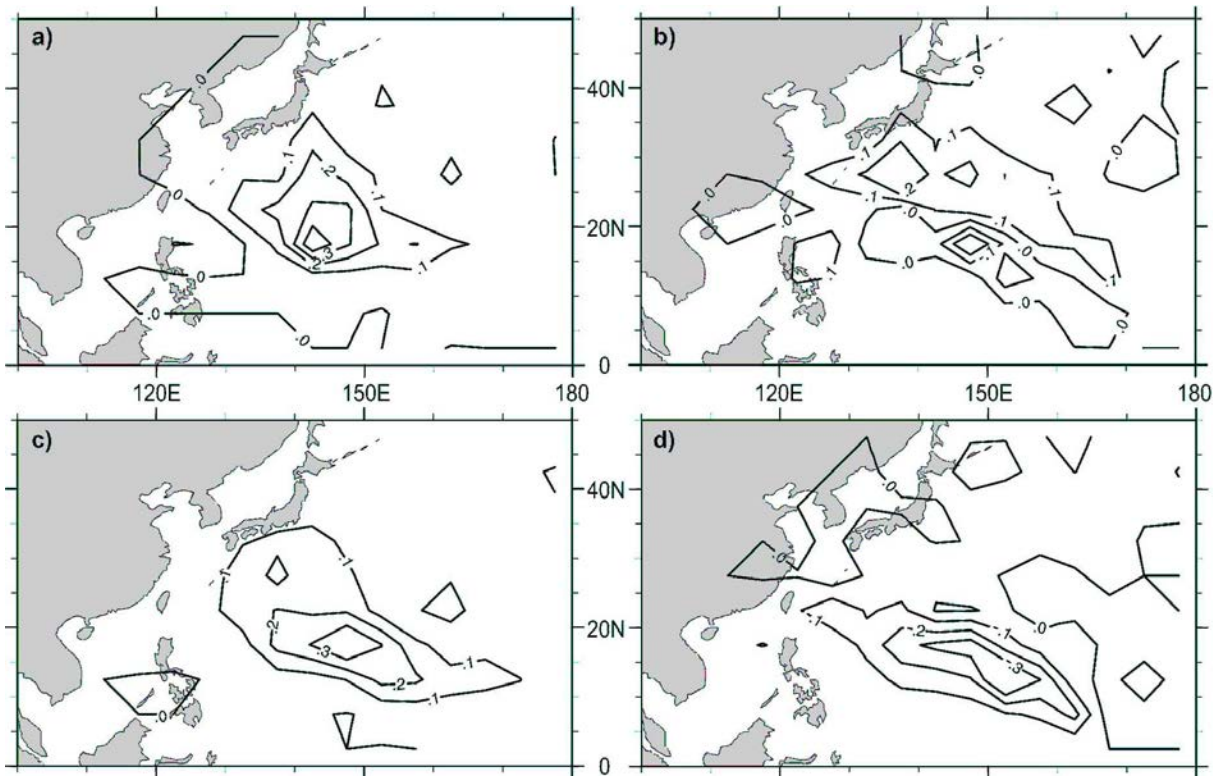

Figure 5.3 First EOFs for CCLM's a) inter-annual and b) decadal variability, for the intense TCs (category 2-5), explaining 19 % and 43 % of the total variance, respectively. First EOFs for BTD's c) inter-annual and d) decadal variability, for intense TCs (category 2-5), explaining 26 % and 49 % of the total variance, respectively.

5.3.2 Tropical cyclones variability and associated environmental factors

In the following we analyse the relation of intense TC variability to large-scale environmental patterns. We use MPI defined by [Emanuel, 1988] as the thermodynamic factor representing favourable conditions for TC genesis and intensification. Three factors shape the MPI value: sea surface temperature (SST), the outflow temperature, and convective available potential energy. A high MPI value indicates that a thermodynamic energy state exists prone for TCs to reach higher intensities.

The association of yearly, intense TC activity with MPI is quantified with the Canonical Correlation Analysis (CCA; e.g. [von Storch and Zwiers, 1999]). This method derives the maximum correlation between EOFs representing the main MPI variability patterns and anomalies of TC occurrences. The first 5 EOFs explain 71% of the total variance for MPI and 84% for TC occurrences. The first five modes can be considered as a large fraction of TC activity which shows diverse spatial variability.

Figure 5.4a shows the first pair of CCA patterns derived for fields of MPI anomalies (CCA MPI) and regionalized TC occurrences anomalies (CCA TC). CCA MPI pattern is shaded. Regions of CCA TC are marked with black lines, with region number (given in bracket) and corresponding correlation coefficients. CCA pair shares a correlation of 71%. MPI positive loadings are spread along the SE Asia coast towards the North-East. The associated pattern of CCA TC presents anomalously high values in the same regions with the maximum located in the subtropical latitudes (Figure 5.4, region numbers: 1,6,7). The time series of this pattern correlates well (0.88) with PC-1 which represents annual time series of the dominant EOF mode (EOF-1). Such a relation is reasonable since mainly those intense TCs which follow the track patterns of EOF-1 (Figure 5.4a) can cause anomalously high TC activity like in CCA TC (Figure 5.4, region numbers: 1, 6, 7). In other words only recurving TCs and those moving towards the North-East may influence TC activity in the mid-latitudes.

Figure 5.4b shows the time series of CCA MPI pattern (red) and yearly sea surface temperature anomalies (blue). The picture indicates that the yearly variability of CCA MPI pattern relates strongly to the mean SST anomalies in the WNP basin and follows its time series with a correlation of 0.85. This shows that SST determines MPI anomalies and influences the main mode of inter-annual variability of the intense TCs in the WNP.

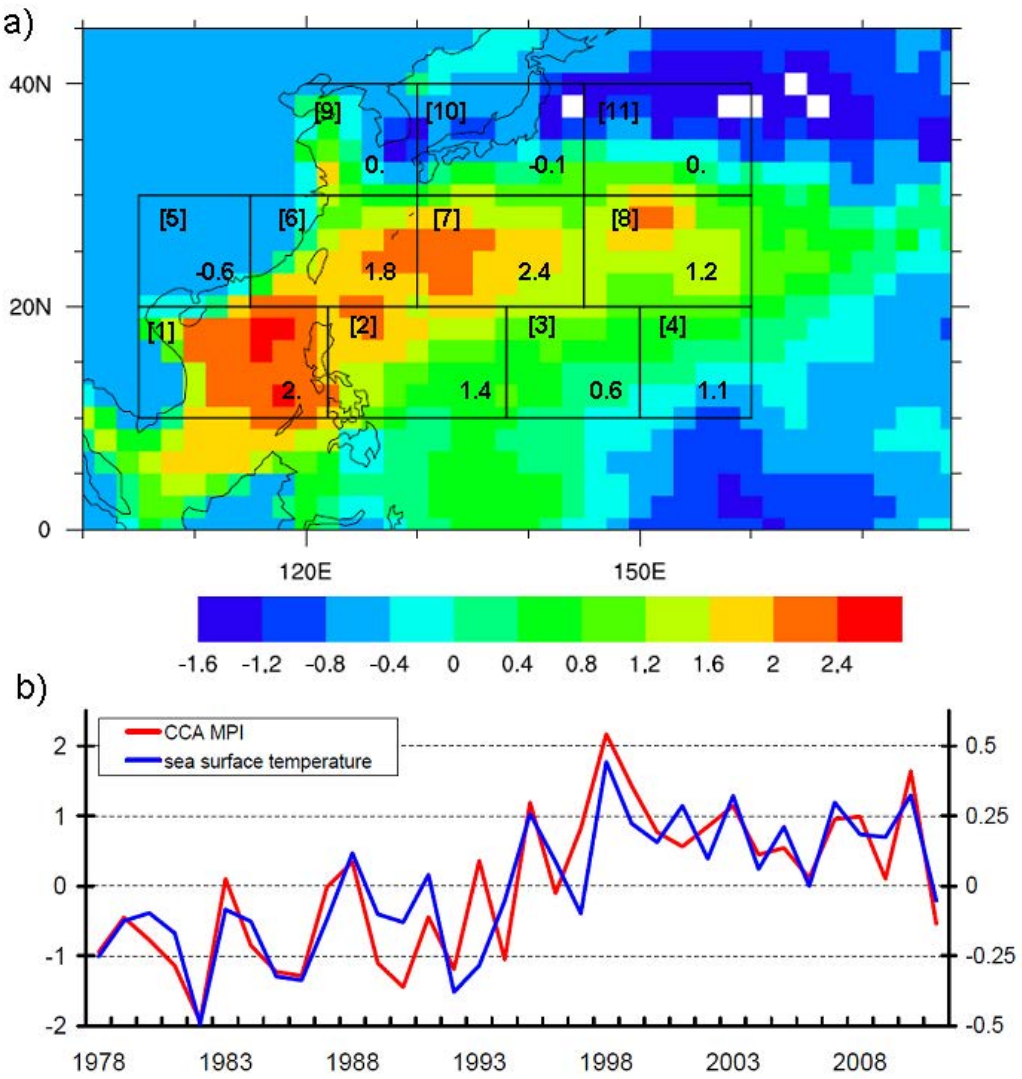

Figure 5.4 a) The first pair of canonical correlation patterns – derived between regional time series of TC occurrences anomalies (CCA TC) and fields of maximum potential intensity anomalies (CCA MPI). CCA pair shares a correlation of 71 % for the period 1978-2011. CCA MPI is color - shaded, CCA TC coefficients are given as numbers in each corresponding subregion. The number of the region is given in brackets. b) Time series of canonical coefficients of maximum potential intensity anomalies (CCA MPI, red) sharing a correlation of 85 % with mean sea surface temperature anomalies (blue) over the main TC genesis area in the WNP (100°E - 180°E, 5-30°N). The left y-axis shows canonical coefficients, the right y-axis corresponds to the sea surface temperature anomalies. The x-axis shows years from the period 1978-2011.

To verify whether such a relationship exist for the observed TC activity, CCA analysis is performed between observed SST and TC activity, given by BTD observations and CCLM simulations. Figure 5.5 shows that the first patterns of SST (CCA SST) correlating with TC anomalies (CCA TC) in CCLM are very similar to the ones derived for BTD. The canonical correlation shared by CCA pairs is 58 % for CCLM and 59 % for BTD. The time series of the first CCA TC explains most of the variance of the yearly intense TC occurrences, but notably more for CCLM (89 %) than BTD (69 %). This confirms that SST anomalies along the SE Asian coast and subtropics strongly influence the intense TCs activity in the WNP, but other factors affect observed TC activity more than the simulated one.

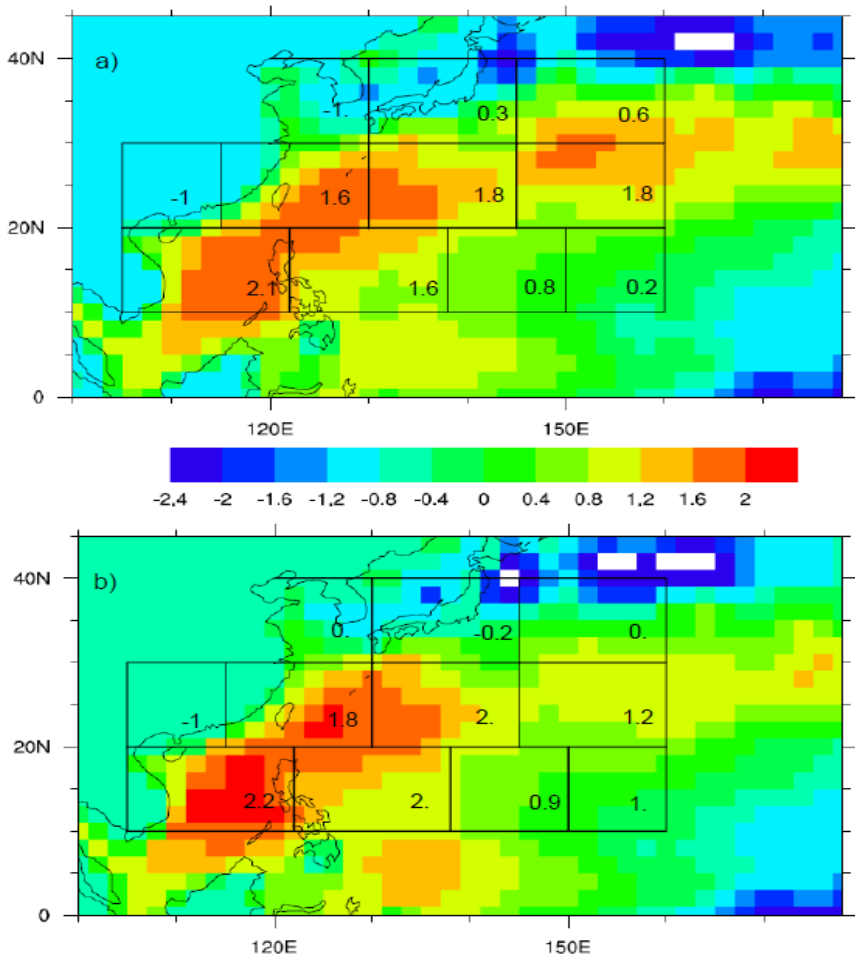

Figure 5.5 First pair of canonical correlation patterns derived between regional time series of TC occurrences anomalies (CCA TC) and fields of sea surface temperature anomalies (CCA SST). Sea surface temperature fields are provided by NCEP reanalysis. TC fields are derived from a) BTD observations, sharing a CCA correlation of 59 % b) CCLM, sharing a CCA correlation of 58 %. CCA SST is shaded, CCA TC coefficients are given as numbers in each corresponding subregion.

In order to relate the decadal variability of intense TCs to environmental factors a Gaussian filter with the window size of 10 was applied to the anomaly fields of TC occurrences and MPI. In the next step the first EOF of the filtered fields were compared. Figure 5.6 shows (a) the first EOF representing decadal variability of MPI, and (b) its time series (MPI PC-1) together with the PC-1 of decadal TC variability. The MPI pattern explains 33% of its total variance and the pattern of TC occurrences 43%. The first MPI EOF shows positive anomalies increasing towards coastal SE Asia areas and towards the mid-latitudes. The time series of MPI PC-1 (Figure 5.6b) indicates that these anomalies occur mainly during the last decade, again following the increase of mean SST in the WNP. For the same time period positive values of TC PC-1 indicate anomalously high TC activity in the subtropical part of the WNP. The time series MPI PC-1 and TC PC-1 share a high correlation (0.91) pointing to a large influence of environmental factors on decadal changes in TC variability.

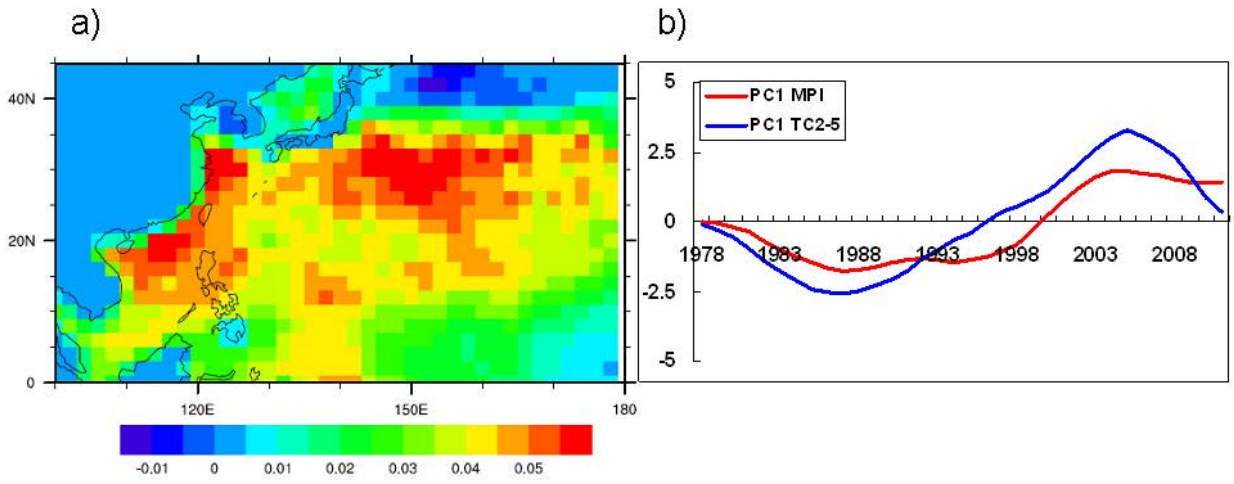

Figure 5.6 a) First EOF representing decadal variability of the Maximum Potential Intensity in CCLM. b) EOF time series for: Maximum Potential Intensity (PC1 MPI, red) and TC-days number for the intense TCs (PC1 TC2-5, blue). Time series share a correlation of 91 %. The x-axis shows years from the period 1978-2011.

5.3 Discussion of tropical cyclones variability and associated environmental factors

The time series of the annual occurrences of the intense TCs as well as the time series representing its dominant mode (PC-1) show reasonable agreement (r=0.63 for PC-1s) between CCLM and BTD. The spatial patterns of EOF-1 are also similar. CCLM explains less

(19%) of the total variance than the BTD (26%), which may result from different methodologies used for TC identification and tracking. Especially weaker TCs which fall into the analysed distribution of intense TCs in CCLM may increase spatial variability in the data set. The spatial nature of the weak TCs differs from that of the intense TCs. Therefore if the spatial TC variance in CCLM is biased due to weak TCs the main variability mode (EOF-1) explains less of the total variance.

A canonical correlation analysis demonstrated that simulated and observed TC activity is strongly related to thermodynamic factors. Anomalously high TC activity in the vicinity of the SE Asian coast and in the subtropics is massively influenced by MPI factors, showing high anomalies. The canonical correlation coefficient of 58 % for SST and 71 % for MPI anomalies in CCLM indicates that also other than thermodynamic factors contribute to TC variability. The time series of TC anomalies, represented by the first CCA TC pattern, determines almost 90% of simulated inter-annual TC variability. For the TC activity observed in BTD (JMA), canonical correlation patterns for CCA SST and CCA TC share a correlation of 59 %. However, CCA TC explains less variance (70 %) of observed inter-annual TC variability, which might be an effect of other climatic factors impacting TC activity or simply the inhomogeneities included in the BTD sets. [Chan, 2007, Chan, 2009] confirmed that inter-annual variability of the intense TCs provided by BTD (JTWC) can not be entirely explained by SST or MPI averaged over the WNP basin. Instead, he suggested, that dynamic conditions (e.g. relative vorticity or vertical wind shear) may determine the inter-annual variability of the intense TCs in WNP.

The dominant modes of interdecadal variability explain a high portion of the total variance in CCLM and BTD (43 % and 49 %, respectively) and share a high correlation. Both data sets show weakening TC activity for the tropical latitudes in the period 1978-2011. Such a decrease was shown also by [Liu and Chan, 2008] who examined EOFs of interdecadal TC variability given by different data sets (JTWC). Time series of the dominant EOF mode [Liu

and Chan, 2008] showed high TC activity over the tropical WNP in the 1980s and very low activity for the next decade. However, the EOF mode was derived for a longer period (1960-2005) and includes also weak TCs. Consequently its pattern is more complex and explains less of the total variance.

While CCLM shows weakening TC activity in the tropics, an increase can be seen for the subtropics. Such an increase occurs at the same time with an increasing MPI for the corresponding regions. The northward shift of TC tracks was analysed by [Tu et al., 2009], who associated it with warm SST anomalies over the equatorial and central WNP in the last four decades. The authors showed within a model experiment that warm SST anomalies over the equator and the mid-latitudes induce low-level cyclonic winds in these regions. However, for the mid-latitudes the author could not confirm such a relation with observations. For the short period of observed warm SST anomalies in the WNP (2000-2006), observation data did not show anomalous trends of TC activity. On the other hand, the authors point to uncertainties of these results due to a small sample size and possible different results for an extended analysis for ongoing years. The results presented here imply that CCLM simulates TC activity realistically on inter-annual and decadal time scales. Its variability strongly relates to the changes in large-scale environmental patterns.

5.4 Trend analysis 1948-2011

In the following the hindcasted trends for TC activity are analysed for the period 1948-2011. Thus all material presented in this subsection is simulated by CCLM data. Figure 5.7 presents trends for annually accumulated TC days for all storms and just for the intense ones, normalized by the according mean of the whole period. Both time series show an increasing trend, with a slope coefficient of 0.02 for the intense TCs and 0.009 for all storms. Additionally, there is also a shift towards less numbers visible, especially for the intense TCs in the last decade.

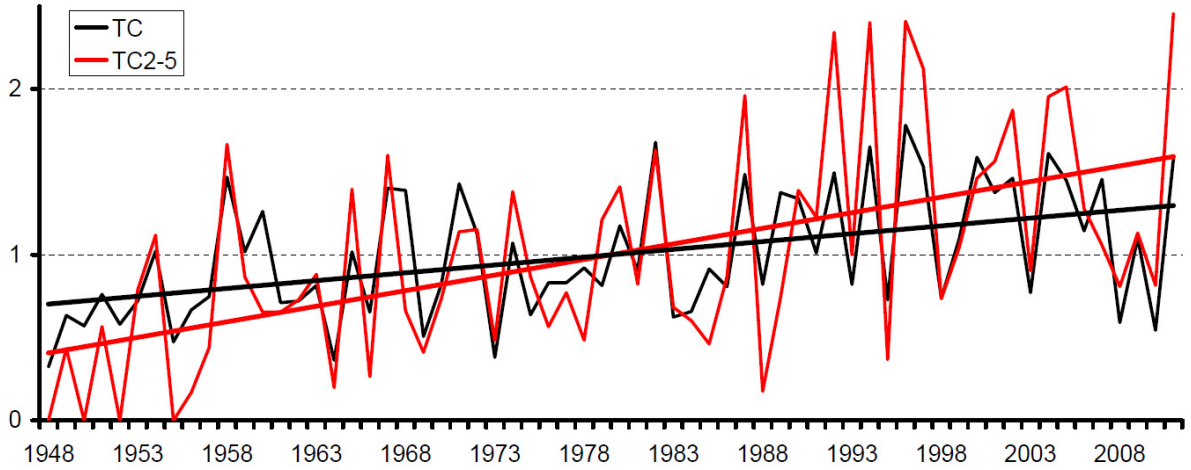

Figure 5.7 Annual TC days normalized by their mean values for the period 1948-2011, counted for JASO months in CCLM, and linear trends. The red curve represents all TCs and the blue curve represents only intense TCs (TC2-5). The x-axis shows years from the period 1948-2011.

TC variability is mainly associated with MPI anomalies. Figure 5.8a presents the first CCA pattern derived for MPI (CCA MPI) sharing a correlation of 72 % with the pattern of intense TC occurrences (CCA TC) in the period 1948-2011. CCA MPI shows positive anomalies spread along the SE Asian coast and subtropics with the maximum located in the vicinity of Taiwan. The associated CCA TC pattern presents anomalously high TC activity in the corresponding regions (Figure 5.8a, region numbers: 1, 6, 7). Time series of CCA TC describe (Figure 5.8b) about 90 % of the year-to-year variance of simulated intense TC days in the period 1948-2011.

The spatial features of TC activity long-term trends are different for the intense TCs and the weaker ones. Figure 5.9 presents the fields for the long-term trends derived for the occurrences of all TCs (a) and only for the intense TCs (b). For all TCs the maximum is located in the South China Sea region, while for the intense ones it is in the subtropical latitudes, in the vicinity of Taiwan. Downward tendencies of TC activity are focused mainly in the south-eastern part (130-150°E, 10-20°N) of the WNP.

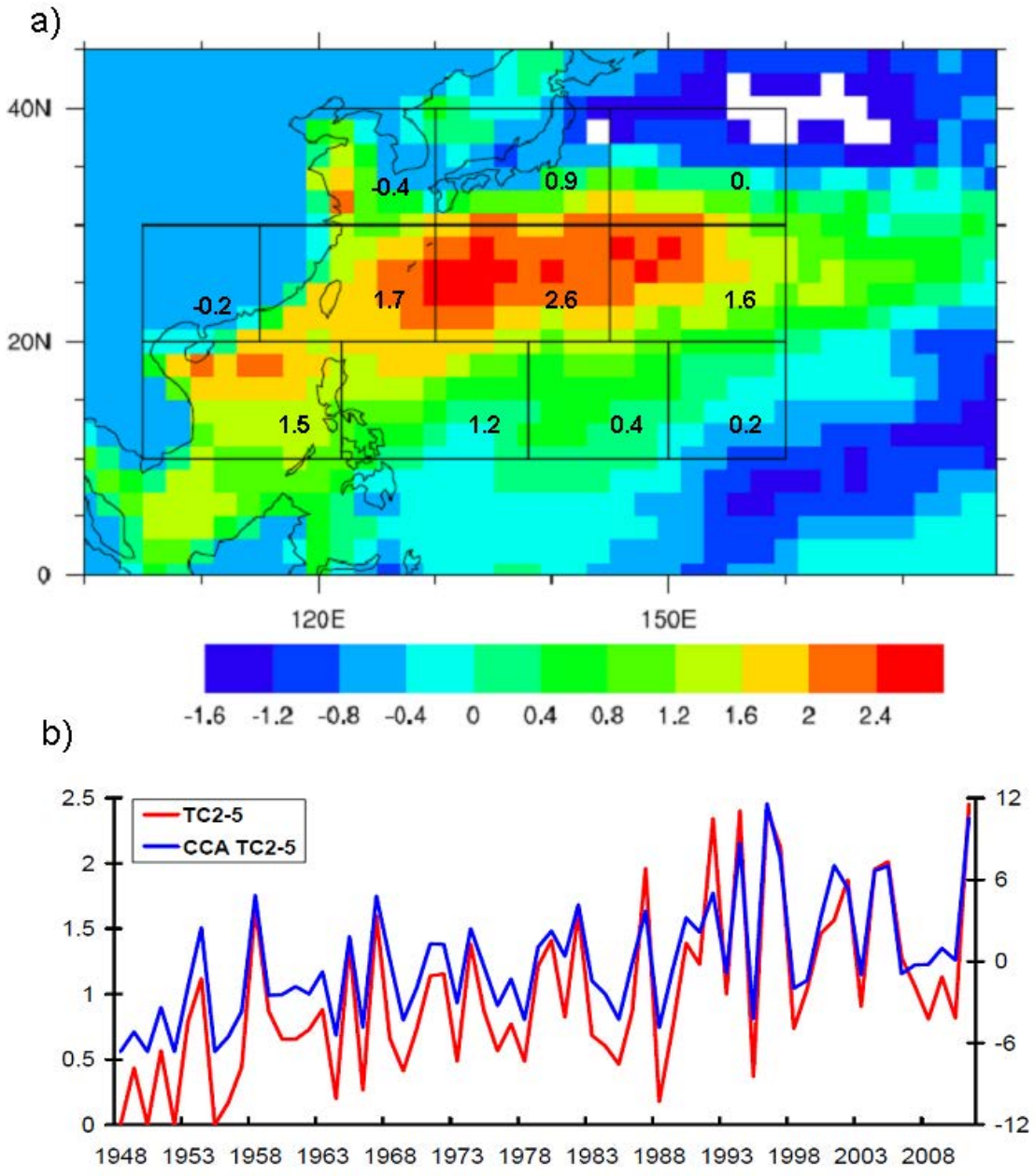

Figure 5.8 a) The first pair of canonical correlation patterns - derived between regional time series of TC occurrences anomalies (CCA TC) and fields of maximum potential intensity anomalies (CCA MPI). CCA pair shares a correlation of 72 % for the period 1948-2011. CCA MPI is shaded, CCA TC coefficients are given in each corresponding subregion. b) Annual TC days normalized by their mean values for the period 1948-2011, counted for JASO months in CCLM (red). Canonical coefficient time series of the TC occurrences anomalies (CCA TC) are shown in blue. The left y-axis shows the TC occurrences anomalies, the right y-axis shows canonical coefficients. The x-axis shows years from the period 1948-2011.

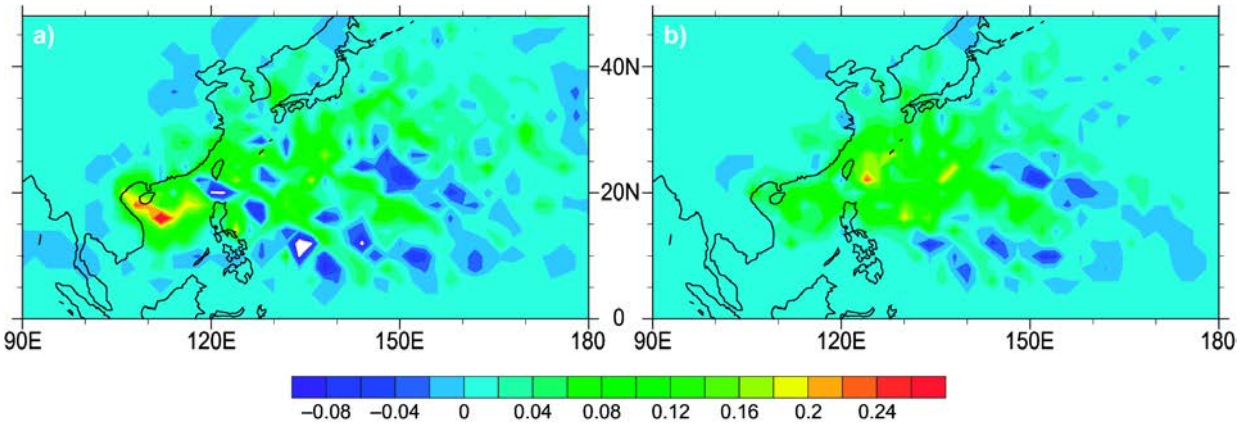

Figure 5.9 Trends for yearly TC occurrences, estimated with a linear regression using a least squares fit derived for every 2° latitude x 2° longitude grid box for a) all TCs and b) intense TCs; for the period 1948-2011.

Additionally, TC variability was analysed in the regions of: the South China Sea, vicinity of Taiwan, Philippine Sea, the north-eastern part of the WNP (145-160°E, 20-27°N), and the south-eastern part of the WNP (130-155°E, 5-15°N) in more detail. Figure 5.10 shows the annual variability and derived piecewise linear trends for all and only for intense storms in the given areas. The TC activity of all storms in the South China Sea (Figure 5.10a,b) shows a strong increase until the 2000s and a decrease in the last decade. It is also worthy to notice that the intense TCs did not enter this area at all in the first decade of the simulated period. The region in the vicinity of Taiwan (Figure 5.10c) is affected by increasing activity for all and for the intense storms starting in the 1980s. The trend for all storms in the Philippine Sea (Figure 5.10e) is less clear, but the intense storms show an increasing tendency. In the eastern parts of the WNP (Figure 5.10g,h) TCs occur sparsely, therefore counts of all storms were analysed in these areas. Here mainly a decrease for all storms in the analysed period can be seen. Additionally in the south-eastern part of the WNP (Figure 5.10h) numbers are increasing during the last decade.

Several observational studies that analysed the impact of typhoons in the WNP for shorter time periods [Ho et al., 2004, Wu et al., 2005] confirm partly our findings. [Ho et al., 2004] found that in the period 1951-2001 the TC passage frequency over the South China Sea

slightly increased, but it decreased for the Philippine Sea and for the East China Sea. [Tu et al., 2009] found strong TC variability after 1982 and an abrupt shift of TC activity in the vicinity of Taiwan in the 2000s. The authors concluded that there is a northward shift of typhoon tracks. [Wu et al., 2005] identified a westward shift of TC track patterns in the WNP for the last decades and stated that there is a rising influence of TCs on subtropical East Asia.

5.4 Tropical cyclones variability and changes during the last decades – analysis and comparisons with observations

Long-term hindcasts of TC variability for the western North Pacific and South East Asia, computed with the atmospheric regional model CCLM, are analysed in this study. First, the inter-annual and decadal variability of hindcasted TC activity are compared to observations (BTD). An analysis of intense TCs in the period of 1978-2011 shows remarkable agreement. Second, the linkage of inter-annual TC variability with a large-scale environmental pattern was quantified with a canonical correlation analysis. The results show that TC variability is strongly related to the changes of thermodynamic factors controlling TC genesis and development. It is stated that CCLM can successfully hindcast TC variability which allows to derive and to assess long-term changes in storminess in the WNP.

The last part of this analysis presents hindcasted TC activity trends for the period 1948-2011. The analysis takes into account all TCs and only the intense ones, identified in observations as category 2-5. For both analysed TC distributions, CCLM shows an upward trend. It is determined mostly by thermodynamic conditions, which in the vicinity of the SE Asian coast and subtropics are becoming more favourable for TC genesis and development.
The regional hindcast shows that TC activity in the South China Sea region increased mainly due to weaker storms, while intense TCs increasingly affect the subtropical latitudes in the WNP. A downward TC activity trend is found in the south-eastern part of the WNP. Hindcasted TC activity in the WNP indicates an increase and north-westward tendencies of

track patterns for the period 1948-2011. This is consistent with more recent and shorter-period observations.

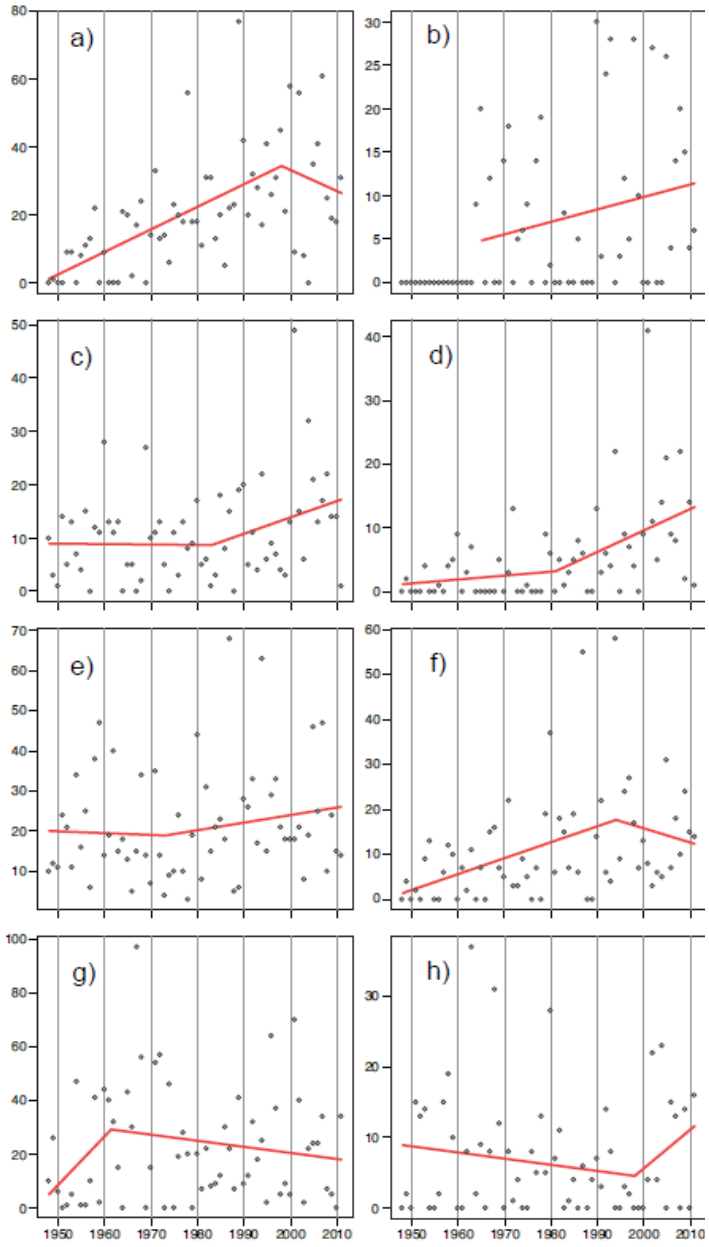

Figure 5.10 Annual variability and piecewise linear trends for TC days for (a) the South China Sea, (c) vicinity of Taiwan and (e) the Philippine Sea. b, d, and f show the according trends for the intense TCs. g) shows annual variability and piecewise linear trends for TC days for the region 145°-160°E, 20-27° N and h) the same for the region 130°-155°E, 5-15°N. The x-axis shows years from the period 1948-2011.

Chapter 6. Summary and Conclusions

The enhanced global TC activity in the last years stimulated the research community to validate TC climatologies and to analyse changes in TC statistics over the last decades. Analysing different observational data sets, TC activity over the western North Pacific leads to ambiguous trend results ([Kamahori et al., 2006, Ren et al., 2011, Wu et al., 2006]). This demonstrates that a detection of changes in observed TC activity, as well as their attribution to environmental factors, is of limited feasibility. Thus, an alternative data set is needed, which should be sufficiently long and homogenous to derive TC climate statistics.

This may be provided by high-resolution regional model simulations. Many studies ([Feser and von Storch, 2008b, Knutson et al., 2007, Walsh, 2004]) successfully applied dynamical downscaling to simulate meso-scale features of TCs. [Knutson et al., 2007] reproduced the observed variability of TC activity during the last three decades over the North Atlantic. Therefore, atmospheric reanalysis data were downscaled with the spectral nudging technique. The main goal of this study was to construct and analyse a long-term TC climatology over the western North Pacific and South - East Asia, using a similar approach.

For this purpose, NCEP reanalysis were downscaled with a regional climate model (CCLM) for the period 1948-2011. Additionally, a spectral nudging technique was applied, to prevent the model's large-scale circulation fields from deviating too far from the global forcing fields.

However, first it was required to assess TC climate on basis of observations of the last decades. Therefore the first part comprises TC frequency trends, derived from different observational data sets and evaluates their reliability. The analysis of BTD sets demonstrated a strong dispersion in TC trends, varying between decreasing and increasing trends. These discrepancies were mainly attributed to different methods, which were used by meteorological agencies to estimate TC intensities. These methods also changed over time. A

successive unification of these methods partly reduced these discrepancies. As a result, TC activity for higher intensity categories (category 2-5 according to the SSHS) showed an upward trend in all analysed BTD sets. However, intensity differences for the highest intensity categories (category 4-5) still remain. They are caused by changed usage of observational sources by JTWC. Therefore the interpretation of TC statistics derived from this BTD set requires special caution. In contrast, JMA uses only one source of satellite imagery. This maintains homogeneity within the data set and makes this source the most reliable for deriving climate statistics. In the latter part of the work it is used as a reference data set.

The second part of the study investigates the potential to construct an alternative long-term TC climatology through application of an RCM (CCLM). It presents an assessment of model skill to simulate TC climatologies, with a focus on the influence of the spectral nudging technique (SNT). Brier Skill Score statistics demonstrated high skill of the RCM to downscale TC meso-scale features from the large-scale reanalysis. However, the simulated TC intensities are lower than the observed ones by up to two SSHS categories. A comparison of wind speed - pressure relationship between simulations and observations shows that CCLM underestimates wind speeds when the pressure reaches values lower than ~ 980 [hPa]. This also indicates that the skill of CCLM is higher for sea level pressure than for wind speed. This may be caused by the insufficient horizontal resolution of the model (~ 50 km), which can not resolve realistic pressure gradients in intense TCs. Additionally, CCLM without the spectral nudging technique generates sometimes deeper TCs. CCLM – NN simulates core pressures up to ~ 20 [hPa] lower than CCLM - SN. Nevertheless, spectral nudging significantly improved the representation of the mean TC climate - and consequently - the spatial fields of TC occurrences and the mean TC intensity fields. These findings corroborate that the SNT has a positive impact on simulated TC climatologies, which justifies its application for regional long - term simulations of the past decades.

The last part of the study presents and analyses a long-term TC climatology, constructed for the western North Pacific for the period 1948-2011. A comparison with more recent observations (1978-2008) provided by JMA data set demonstrates that:

- the constructed data set represents realistic features of TC activity variability on inter-annual and inter-decadal time scales;
- the simulated TC climatology gives a realistic representation of the large-scale environmental fields, such as sea surface temperature and the Maximum Potential Intensity.

The long term TC climatology for the western North Pacific shows an increasing trend, with a short decrease in the last decade. Additionally the following features can be seen:

- an increasing activity of intense TCs is found in the subtropical latitudes,
- an increasing activity of weaker storms - over the South China Sea
- decreasing tendencies of TC activity in the south-eastern part of the western North Pacific

Overall, the constructed TC climatology shows an increase and a north-westward shift of intense TC tracks for the period 1948-2011. These TC activity features are related to the patterns of sea surface temperature and Maximum Potential Intensity. These fields also show a north-westward tendency (along the SE Asian coast and in the subtropical latitudes) towards favourable conditions for TC genesis.

This study demonstrated that the constructed data set can serve as an alternative for observations to assess TC activity changes during the last decades over the western North Pacific. However, due to specific characteristics of the CCLM model, the TC climatology has some deficiencies. The horizontal resolution, parameterization scheme or application of spectral nudging limits the capability of the model to simulate realistic TC intensities. Therefore the criteria of the tracking scheme were tuned accordingly to obtain the desired mean TC frequency. However, the TC data set may still be contaminated by other low-

pressure systems. Therefore, to reduce the uncertainty caused by the tracking methodology, the analysis of the TC data set was mainly focused on intense TCs. An analysis of weak TCs requires more objective tracking criteria. The application of a higher resolution, improvement of parameterization schemes, and a better representation of small-scales process might also improve the simulation. Alternatively, statistical methods to extrapolate the simulated TC intensity, e.g. Extreme Value Theory, could serve this purpose.

The impact of greenhouse gases on current and future TC activity is still an open question, puzzling both science and governments. This study showed that CCLM can be a useful tool, contributing to the answer for the pending question. The model gives a realistic relationship between TC activity and the thermodynamic conditions determining TC genesis and development. An agreement with observations was shown for intense TC variability at a decadal scale. It also had a high correlation with mean sea surface temperature anomalies over the western North Pacific. On the other hand, observational studies [Chan and Liu, 2004, Chan, 2007, Chan, 2009], as well as the CCLM simulation, indicate that there are other factors which shape TC activity, namely: vorticity, wind shear and relative humidity. The CCLM skill to reproduce the mean TC climate has been greatly improved by the SNT, thus a constructed long-term data set provides great potential for further diagnostic studies.

CCLM proves be a useful tool for future projections, while it reproduces realistic relationships, between TC activity and environmental patterns affecting TC genesis and development. However, spectral nudging applied in future projections is a controversial issue. The nudging techniques constrain the model solution to follow prescribed large-scale fields. Therefore it is of primary importance to obtain high – quality GCM projections, serving as driving fields, which will skilfully capture the large-scale circulation patterns.

REFERENCES:

[Alexandru *et al.*, 2007] A. Alexandru, R. de Elia, and R. Laprise. Internal variability in regional climate downscaling at the seasonal scale. *Mon. Weather. Rev.*, 135:3221–3238, 2007.

[Anderson-Berry and Weyman, 2008] L. J. Anderson-Berry and J. C. Weyman. Societal impacts of tropical cyclones. In *Fifth International Workshop on Tropycal Cyclones*. World Meteorological Organization. National Oceanic and Atmospheric Administration, 2008.

[Atkinson, 1974] G. D. Atkinson. Investigation of gust factors in tropical cyclones. *FLEWEACENTech. Note JTWC 74-1, Fleet Weather Center, Guam,*, page 9, 1974.

[Barcikowska *et al.*, 2012] M. Barcikowska, F. Feser, and H. von Storch. Usability of best track data in climate statistics in the western North Pacific. *Mon. Weather. Rev.*, 140:2818–2830, 2012.

[Bender *et al.*, 2010] M. A. Bender, T. R. Knutson, R. E. Tuleya, J. J. Sirutis, G. A. Vecchi, S. T. Garner, and I. M. Held. Modeled impact of anthropogenic warming on the frequency of intense Atlantic hurricanes. *Science*, 327(5964):454–458, 2010.

[Bengtsson *et al.*, 1982] L. Bengtsson, H. Böttger, and M. Kanamitsu. Simulation of hurricane-type vortices in a general circulation model. *Tellus B*, 34(5), 1982.

[Bengtsson *et al.*, 1995] L. Bengtsson, M. Botzet, and M. Esch. Hurricane-type vortices in a general circulation model. *Tellus A*, 47(2):175–196, 1995.

[Bister and Emanuel, 1998] M. Bister and Emanuel. Dissipative heating and hurricane intensity. *Meteorol. Atmos. Phys.*, 65:233–240, 1998.

[Bourassa, 2010] Bourassa et al., M. A. Remotely sensed windsand wind stresses for marine forecasting and ocean modeling. In *Proc. ‘‘OceanObs’09: Sustained Ocean Observations and Information for Society’’; Conf., Vol. 2, Venice, Italy, ESAPubl. WPP-306, doi:10.5270/OceanObs09.cwp.08. [Available online at http://www.oceanobs09.net/proceedings/cwp/cwp08/ index.php.]*, 2010.

[Brennan *et al.*, 2009] M. J. Brennan, C.C. Hennon, and R. D. Knabb. The operational use of QuikSCAT ocean surface vector winds at the National Hurricane Center. *Wea. Forecasting, 24*, 24:621–645, 2009.

[Broccoli and Manabe, 1990] A. J. Broccoli and S. Manabe. Can existing climate models be used to study anthropogenic changes in tropical cyclone climate? *Geophys. Res. Lett.*, 17(11):1917–1920, 1990.

[Camargo *et al.*, 2007] S. J. Camargo, H. Li, and L. Sun. Feasibility study for downscaling seasonal tropical cyclone activity using the NCEP regional spectral model. *International Journal of Climatology*, 27(3):311–325, 2007.

[Castro *et al.*, 2005] C.L. Castro, R. A. Sr. Pielke, and G. Leoncini. Dynamical downscaling: assessment of value retained and added using the regional atmospheric modeling system (RAMS). *J. Geophys. Res.*, 110:D05108, 2005.

[Cha and Lee, 2009] D.-H. Cha and D.-K. Lee. Reduction of systematic errors in regional climate simulations of the summer monsoon over East Asia and the western North Pacific by applying the spectral nudging technique. *J. Geohys. Res.*, 114, D14108, 2009.

[Cha *et al.*, 2008] D.-H. Cha, D.-K. Lee, and Hong S. Y. Impact of boundary layer processes on seasonal simulation of the East Asian summer monsoon using a regional climate model. *Meteor. Atmos. Phys.*, 100:53–72, 2008.

[Cha *et al.*, 2011] D.-H. Cha, C.-S. Jin, D.-K. Lee, and Kuo Y.-H. Impact of intermittent spectral nudging on regional climate simulation using Weather Research and Forecasting model. *J. Geohys. Res.*, 116, D10103, 2011.

[Chan and Liu, 2004] J.C.L Chan and K. S. Liu. Global warming and western north pacific typhoon activity from an observational perspective. *J. Climate*, 17:4590–4602, 2004.

[Chan, 2007] J.C.L Chan. Interannual variations of intense typhoon activity. *Tellus*, 59A:455–460, 2007.

[Chan, 2009] J.C. L. Chan. Thermodynamic control on the climate of intense tropical cyclones. *Proceedings of the Royal Society A*, 465:3011–3021, 2009.

[Dean *et al.*, 2009] L. Dean, K. A. Emanuel, and D. R. Chavas. On the size distribution of atlantic tropical cyclones. *Geophys. Res. Lett.*, 36:L14803, 2009.

[Dee, 2011] D. P. et al. Dee. The era-interim reanalysis: configuration and performance of the data assimilation system. *Q. J. R. Meteorol. Soc.*, 137:553–97, 2011.

[Dickenson *et al.*, 1989] R.E. Dickenson, R:M. Errico, F. Giorgi, and G.T. Bates. A regional climate model for western United States. *Clim. Change*, 15:383–422, 1989.

[Dvorak, 1972] V. F. Dvorak. A technique for the analysis and forecasting for tropical cyclone intensities from satellite pictures. *NOAA Tech. Memo. NESS 36, NOAA*, 36:15pp, 1972.

[Dvorak, 1973] V. F. Dvorak. A technique for the analysis and forecasting for tropical cyclone intensities from satellite pictures. *NOAA Tech. Memo. NESS 45, NOAA*, page 19, 1973.

[Dvorak, 1975] V. F. Dvorak. Tropical cyclone intensity analysis and forecasting from satellite imagery. *Mon. Weather. Rev.*, 103:420–430, 1975.

[Dvorak, 1984] V. F. Dvorak. Tropical cyclone intensity analysis using satellite data. *NOAA Tech. Rep. NESDIS 11, NOAA*, page 45, 1984.

[Emanuel, 1987] K. A. Emanuel. The dependence of hurricane intensity on climate. *Nature*, 326(6112):483–485, April 1987.

[Emanuel, 1988] K. Emanuel. The maximum intensity of hurricanes. *J. Atmos. Sci.*, 45(7):1143–1155, April 1988.

[Emanuel, 2001] K. Emanuel. Contribution of tropical cyclones to meridional heat transport by the oceans. *J. Geophys. Res.*, 106(D14):14771–14781, 2001.

[Emanuel, 2005] K. Emanuel. Increasing destructiveness of tropical cyclones over the past 30 years. *Nature*, 436(7051):686–688, August 2005.

[Emanuel, 2006] K. Emanuel. Environmental influences on tropical cyclone variability and trends. In *27th Conf. on Hurricanes and Tropical Meteorology, Monterey*, 2006.

[Feser and von Storch, 2005] F. Feser and H. von Storch. A spatial two-dimensional discrete filter for limited area model evaluation purposes. *Mon. Weather. Rev.*, 133(6):1774–1786, 2005.

[Feser and von Storch, 2008a] F. Feser and H. von Storch. Regional modelling of the western pacific typhoon season 2004. *Meteorolog. Z.*, 17 (4):519–528, 2008.

[Feser and von Storch, 2008b] F. Feser and H. von Storch. A dynamical downscaling case study for typhoons in Southeast Asia using a regional climate model. *Mon. Weather. Rev.*, 136(5):1806–1815, May 2008.

[Giorgi and Bates, 1989] F. Giorgi and G.T. Bates. The climatological skill of a regional model over complex terrain. *Mon. Weather. Rev.*, 17 17:2325–2347, 1989.

[Gray, 1968] W.M. Gray. A global view of the origin of tropical disturbances and storms. *Mon. Weather. Rev.*, 96:669–700, 1968.

[Grossmann and Morgan, 2011] I. Grossmann and M.G. Morgan. Tropical cyclones, climate change, and scientific uncertainty: what do we know, what does it mean, and what should be done? *Clim. Chang.*, 2011.

[Ho *et al.*, 2004] C.-H. Ho, J.-J. Baik, J.-H. Kim, and D.-Y. Gong. Interdecadal changes in summertime typhoon tracks. *J. Clim.*, 17,9:1767, 2004.

[Hoffman and Leidner, 2005] R. N. Hoffman and S. M. Leidner. An introduction to the near-real-time quikscat data. *Wea. Forecasting,*, 20:476–493., 2005.

[Holland and Webster, 2007] G. J Holland and P. J. Webster. Heightened tropical cyclone activity in the North Atlantic: natural variability or climate trend? *Philosophical Transactions of the Royal Society A: Mathematical, Physical and Engineering Sciences*, 365(1860):2695–2716, 2007.

[Holland, 1997] G. J. Holland. The maximum potential intensity of tropical cyclones. *J. Atmos. Sci.*, 54(21):2519–2541, November 1997.

[Hoyos *et al.*, 2006] C. D. Hoyos, P. A. Agudelo, P. J. Webster, and J. A. Curry. Deconvolution of the factors contributing to the increase in global hurricane intensity. *Science*, 312(5770):94–97, 2006.

[Hu and Meehl, 2009] A. Hu and G. A. Meehl. Effect of the atlantic hurricanes on the oceanic meridional overturning circulation and heat transport. *Geophys. Res. Lett.*, 36(3):L03702–, February 2009.

[JTWC, 2009] JTWC. 2008 annual tropical cyclone report. 116 pp. [available online at http://www.usno.navy.mil/nooc/ nmfc-ph/rss/jtwc/atcr/2008atcr.pdf.]. Technical report, Joint Typhoon Warning Center, Pearl Harbor, HI, 2009.

[Kain, 2004] J. S. Kain. The Kain-Fritsch convective parameterization: An update. *J. Appl. Meteor.*, 43(1):170–181, January 2004.

[Kalnay *et al.*, 1996] E. Kalnay, M. Kanamitsu, R. Kistler, W. Collins, D. Deaven, L. Gandin, M. Iredell, S. Saha, G. White, J. Woollen, Y. Zhu, A. Leetmaa, R. Reynolds, M. Chelliah, W Ebisuzaki, W. Higgins, J. Janowiak, K.C. Mo, C. Ropelewski, J. Wang, R. Jenne, and D. Joseph. The NCEP/NCAR 40-year Reanalysis Project. *Bull. Amer. Meteor. Soc.*, 77:437–470, 1996.

[Kamahori *et al.*, 2006] H. Kamahori, N. Yamazaki, N. Mannoji, and K. Takahashi. Variability in intense tropical cyclone days in the western North Pacific. *SOLA*, 2:104–107, 2006.

[Kanamitsu *et al.*, 2010] M. Kanamitsu, K. Yoshimura, Y.-B. Yhang, and S-Y. Hong. Errors of interannual variability and trend in dynamical downscaling of reanalysis. *J. Geohys. Res.*, 115:D17115, 2010.

[Kistler, 2001] R. et al. Kistler. The NCEP-NCAR 50-year reanalysis: Monthly means CD-ROM and documentation. *Bull. Amer. Meteor. Soc.*, 82:247–267, 2001.

[Knaff and Sampson, 2006] J.A. Knaff and C. Sampson. Reanalysis of West Pacific tropical cyclone intensity 1966-1987. In *27th Conference on Hurricanes and Tropical Meteorology, Monterey,* 2006.

[Knapp and Kruk, 2010] K. R. Knapp and M. C. Kruk. Quantifying interagency differences in tropical cyclone best-track wind speed estimates. *Mon. Weather. Rev.*, 138(4):1459–1473, November 2010.

[Knutson *et al.*, 1998] T. R. Knutson, R. E. Tuleya, and Y. Kurihara. Simulated increase of hurricane intensities in a CO2-warmed climate. *Science*, 279(5353):1018–1021, 1998.

[Knutson *et al.*, 2007] T. R. Knutson, J. J. Sirutis, S. T. Garner, I. M. Held, and R. E. Tuleya. Simulation of the recent multidecadal increase of Atlantic hurricane activity using an 18-km-grid regional model. *Bulletin of the American Meteorological Society*, 88, 10:1549–1565, 2007.

[Knutson *et al.*, 2008] T. R. Knutson, J. J. Sirutis, S. T. Garner, G. A. Vecchi, and I. M. Held. Simulated reduction in Atlantic hurricane frequency under twenty-first-century warming conditions. *Nature Geosci*, 1(6):359–364, June 2008.

[Knutsona and Tuleya, 2004] T. R. Knutsona and R. E. Tuleya. Impact of CO2-induced warming on simulated hurricane intensity and precipitation: sensitivity to the choice of climate model and convective parameterization. *J. Clim.*, 17(18):3477–3495, 2004.

[Koba *et al.*, 1991] H. Koba, T. Hagiwara, Osano, and S Akashi, S. Relationships between ci number andminimum sea level pressure/maximum wind speed of tropical cyclones. *Geophys. Mag.*, 44:15–25, 1991.

[Kossin and Velden, 2004] J. P. Kossin and C. S. Velden. A pronounced bias in tropical cyclone minimum sea level pressure estimation based on the Dvorak Technique. *Mon. Weather. Rev.*, 132, 1:165, 2004.

[Kruk *et al.*, 2011] M. C. Kruk, K. R. Knapp, and P. A. Hennon. On the use of Dvorak current intensity as a climate data record in the western North Pacific. In *91st American Meteorological Society Annual Meeting*, 2011.

[Lander, 2008] M. A. Lander. A comparison of typhoon best track data in the western North Pacific: irreconcilable differences. In *28th Conference on Hurricanes and Tropical Meteorology*, 2008.

[Landman *et al.*, 2005] W. A. Landman, A. Seth, and S. J. Camargo. The effect of regional climate model domain choice on the simulation of tropical cyclone-like vortices in the Southwestern Indian Ocean. *J. Climate*, 18(8):1263–1274, April 2005.

[Landsea *et al.*, 2004] C. W. Landsea, C. Anderson, N. Charles, G. Clark, J. Dunion, J. Fernandez-Partagas, P. Hungerford, C. Neumann, and M. Zimmer. The Atlantic hurricane database re-analysis project: Documentation for the 1851-1910 alterations and additions to the HURDAT database. Hurricanes and typhoons: Past, present and future. *Columbia University Press,R. J. Murname and K.-B. Liu, Eds.*, pages 177–211, 2004.

[Landsea *et al.*, 2006] C. W. Landsea, B. A. Harper, K. Hoarau, and J. A. Knaff. Can we detect trends in extreme tropical cyclones? *Science*, 313:452–454, 2006.

[Landsea, 2005] C. W. Landsea. Hurricanes and global warming. *Nature*, 438:E11–13, 2005.

[Leduc and Laprise, 2009] M. Leduc and R. Laprise. Regional climate model sensitivity to domain size. *Climate Dynamics*, 32:833–854, 2009.

[Leoncini *et al.*, 2008] G. Leoncini, R.A. Sr Pielke, and P. Gabriel. From model based parameterizations to lookup tables: An EOF approach. *Wea. Forecasting*, in press, 2008.

[Liu and Chan, 2008] K. S. Liu and J. C. L. Chan. Interdecadal variability of western North Pacific tropical cyclone tracks. *J. Clim.*, 21:4464–4476, 2008.

[Manabe *et al.*, 1970] S. Manabe, J. L. Holloway, and H. M. Stone. Tropical circulation in a time-integration of a global model of the atmosphere. *J. Atmos. Sci.*, 27(4):580–613, July 1970.

[Mann and Emanuel, 2006] M. E. Mann and K. A. Emanuel. Atlantic hurricane trends linked to climate change. *Eos Trans. AGU*, 87(24):–, 2006.

[Miguez-Macho *et al.*, 2004] G. Miguez-Macho, G.L. Stenchikov, and A. Robock. Spectral nudging to eliminate the effects of domain position and geometry in regional climate model simulations. *J. Geophys. Res.*,109:109 D13104, 2004.

[Moon *et al.*, 2007] I.-J. Moon, I. Ginis, T. Hara, and B. Thomas. A physics-based parametrization of air-sea momentum flux at high wind speeds and its impact on hurricane intensity predictions. *Mon. Weather. Rev.*, 135:2869– 2878, 2007.

[Murakami *et al.*, 2011a] H. Murakami, B. Wang, and A. Kitoh. Future change of western North Pacific typhoons: Projections by a 20-km-mesh global atmospheric model. *J. Climate*, 24(4):1154–1169, October 2011.

[Murakami *et al.*, 2011b] H. Murakami, Y. Wang, H. Yoshimura, R. Mizuta, M. Sugi, E. Shindo, Y. Adachi, S. Yukimoto, M. Hosaka, S. Kusunoki, T. Ose, and A. Kitoh. Future changes in tropical cyclone activity projected by the new high-resolution MRI-AGCM. *J. Clim.*, 25(9):3237–3260, November 2011.

[Nakazawa and Hoshino, 2009] T. Nakazawa and S. Hoshino. Intercomparison of dvorak parameters in the tropical cyclone datasets over the western North Pacific. *SOLA*, 5:33–36, 2009.

[Nicolis, 2007] C. Nicolis. Dynamics of model error: The role of the boundary conditions. *J. Atmos. Sci.*, 64:204–215, 2007.

[North *et al.*, 1982] G. R. North, F. J. Moeng, T. J. Bell, and R. F. Cahalan. Sampling errors in the estimation of empirical orthogonal functions. *Mon. Weather. Rev.*, 110(7):699–706, 1982.

[Nutter *et al.*, 2004] P. Nutter, D Stensrud, and M. Xue. Effects of coarsely resolved and temporally interpolated lateral boundary conditions on the dispersion of limited-area ensemble forecasts. *Mon. Weather. Rev.*, 32:2358–2377, 2004.

[Oouchi *et al.*, 2006] K. Oouchi, J. Yoshimura, H. Yoshimura, R. Mizuta, I, S. Kusunoki, and A. Noda. Tropical cyclone climatology in a global-warming climate as simulated in a 20 km-mesh global atmospheric model: Frequency and wind intensity analyses. *Journal of the Meteorological Society of Japan*, 84, No. 2:259–276, 2006.

[Pasquero and Emanuel, 2008] C. Pasquero and K. Emanuel. Tropical cyclones and transient upper-ocean warming. *J. Climate*, 21(1):149–162, January 2008.

[Pielke *et al.*, 2008] R. Pielke, J. Gratz, C. Landsea, D. Collins, M. Saunders, and R. Musulin. Normalized hurricane damage in the United States: 1900-2005. *Natural Hazards Review*, 9(1):29–42, 2008.

[Rapaic *et al.*, 2011] M. Rapaic, M Leduc, and Rene Laprise. Evaluation of the internal variability and estimation of the downscaling ability of the canadian regional climate model for different domain sizes over the North Atlantic region using the big-brother experimental approach. *Climate Dynamics*, 36:1979–2001, 2011.

[Ren *et al.*, 2011] F. Ren, J. Liang, G. Wu, W. Dong, and X. Yang. Reliability analysis of climate change of tropical cyclone activity over the western North Pacific. *J. Climate*, 24(22):5887–5898, June 2011.

[Saha, 2010] S. Saha et al.. The NCEP climate forecast system reanalysis. *Bul*, 91:1015–1057, 2010.

[Saunders and Lea, 2008] M. A. Saunders and A. S. Lea. Large contribution of sea surface warming to recent increase in Atlantic hurricane activity. *Nature*, 451(7178):557–560, January 2008.

[Seth and Giorgi, 1998] A. Seth and F. Giorgi. The effects of domain choice on summer precipitation simulation and sensitivity in a regional climate model. *J. Clim.*, 11:2698–2712, 1998.

[Song *et al.*, 2010] J.-J. Song, Y. Wang, and L. Wu. Trend discrepancies among three best track data sets of western North Pacific tropical cyclones. *J. Geophys. Res.*, 115(D12):D12128–, June 2010.

[Song *et al.*, 2011] S. Song, J. Tang, and X. Chen. Impacts of spectral nudging on the sensitivity of a regional climate model to convective parameterizations in East Asia. *Acta Meteorologica Sinica*, 25, 1:63–77, 2011.

[Southern, 1979] R. L. Southern. The global socio-economic impact of tropical cyclons. *Australian Meteorological Magazine, Bureau of Meteorology, Melbourne*, pp 175–195, 1979.

[Sriver and Huber, 2007] R. L. Sriver and M. Huber. Observational evidence for an ocean heat pump induced by tropical cyclones. *Nature*, 447(7144):577–580, May 2007.

[Steppeler *et al.*, 2003] J. Steppeler, G. Doms, U. Schättler, H.-W. Bitzer, A. Gassmann, and and Gregoric G. Damrath, U. Meso-gamma scale forecasts using the nonhydrostatic model lm. *Meteorol. Atmos. Phys.*, 82:75–96, 2003.

[Stowasser *et al.*, 2006] M. Stowasser, Y. Wang, and Hamilton K. Tropical cyclone changes in the western North Pacific in a global warming scenario. *J. Clim*, 20:2378–2396, 2006.

[Sugi *et al.*, 2002] M. Sugi, A. Noda, and N. SATO. Influence of the global warming on tropical cyclone climatology: An experiment with the JMA global model. *Journal of the Meteorological Society of Japan. Ser. II*, 80(2):249–272, 2002.

[Sugi *et al.*, 2009] M. Sugi, H. Murakami, and J. Yoshimura. A reduction in global tropical cyclone frequency due to global warming. *SOLA*, 2009.

[Tang *et al.*, 2010] J. Tang, S. Song, and J Wu. Impacts of the spectral nudging technique on simulation of the East Asian summer monsoon. *Theor. Appl. Climatol.*, 101:41–51, 2010.

[Trenberth and Shea, 2006] K. E. Trenberth and D. J. Shea. Atlantic hurricanes and natural variability in 2005. *Geophys. Res. Lett.*, 33(12):L12704–, June 2006.

[Tsutsui, 2002] J Tsutsui. Implications of anthropogenic climate change for tropical cyclone activity: A case study with the NCAR CCM2. *Journal of the Meteorological Society of Japan. Ser. II*, 80(1):45–65, 2002.

[Tu *et al.*, 2009] J-Y Tu, C Chou, and P-S. Chu. The abrupt shift of typhoon activity in the vicinity of Taiwan and its association with western North Pacific-East Asian climate change. *J. Clim.*, 22:3617–3628, 2009.

[Vanvyve *et al.*, 2008] E. Vanvyve, M.J. Hall, S. Messager, C. Leroux, and J.P. van Ypersele. Internal variability in a regional climate model over West Africa. *Climate Dynamics*, 30:191–202, 2008.

[Velden *et al.*, 2006] C. Velden, B. Harper, F. Wells, J. L. Beven, R. Zehr, T. Olander, M. Mayfield, C. Guard, M. Lander, R. Edson, L. Avila, A. Burton, M. Turk, A. Kikuchi, A. Christian, P. Caroff, and P. McCrone. The Dvorak tropical cyclone intensity estimation technique: A satellite-based method that has endured for over 30 years. *Bull. Amer. Meteor. Soc.*, 87(9):S6–S9, September 2006.

[von Storch and Zwiers, 1999] H. von Storch and F. W. Zwiers. *Statistical analysis in climate research.* Cambridge University Press, 1999.

[von Storch *et al.*, 2000] H. von Storch, H. Langenberg, and Fes. A spectral nudging technique for dynamical downscaling purposes. *Mon. Weather. Rev.*, 128 (10):3664–3673, 2000.

[von Storch, 1999] H. von Storch. *The global and regional climate system. Anthropogenic Climate Change*. Springer-Verlag, 1999.

[Waldron and Horel, 1996] J. Waldron, K. M.and Paegle and J. D. Horel. Sensitivity of a spectrally filtered and nudged limited-area model to outer model options. *Mon. Weather Rev.*, 124:529–47, 1996.

[Walsh and Ryan, 2000] K. Walsh and B. F. Ryan. Tropical cyclone intensity increase near Australia as a result of climate change. *J. Clim.*, 13:3029–3036, 2000.

[Walsh *et al.*, 2004] K. Walsh, K.-C. Nguyen, and J. L. McGregor. Fine-resolution regional climate model simulations of the impact of climate change on tropical cyclones near Australia. *Climate Dynamics*, 22:47–56, 2004.

[Walsh, 2004] K. Walsh. Tropical cyclones and climate change: unresolved issues. *Climate Research*, 27:77–83, 2004.

[Wang and Chan, 2002] B. Wang and J.C.L Chan. How strong ENSO events affect tropical storm activity over the western North Pacific. *J. Clim.*, 15,13:1643–1658, 2002.

[Wang *et al.*, 2004] Y. Wang, L.R Leung, J.L. McGregor, D.-K. Lee, Y. Wang, W.-C.and Ding, and F. Kimura. Regional climate modeling: Progress, challenges, and prospects. *Meteor. Soc. Japan*, 82 (6):1599–1628, 2004.

[Webster *et al.*, 2005] P. J. Webster, G. J. Holland, J. A. Curry, and H.-R. Chang. Changes in tropical cyclone number, duration, and intensity in a warming environment. *Science*, 309:1844, 2005.

[Weisse and Feser, 2003] R. Weisse and F. Feser. Evaluation of a method to reduce uncertainty in wind hindcasts performed with regional atmosphere models. *Coast. Eng.*, 48:211–25, 2003.

[Wu *et al.*, 2005] M.-C. Wu, B. Wang, and S. Geng. Growing typhoon influence on East Asia. *Geophys. Res. Lett.*, 32(18):L18703–, September 2005.

[Wu *et al.*, 2006] M.-C. Wu, K.-H. Yeung, and W.-L. Chang. Trends in western north pacific tropical cyclone intensity. *Eos Trans. AGU*, 87(48), 2006.

[Wu *et al.*, 2012] C.-C. Wu, R. Zhan, Y. Lu, and Y. Wang. Internal variability of the dynamically downscaled tropical cyclone activity over the western North Pacific by the IPRC regional atmospheric model. *J. Clim.*, 25:2104–2121, 2012.

[Yhang and Hong, 2011] Y. B. Yhang and S. Y. Hong. A study on large-scale nudging effects in regional climate model simulation. *Asia-Pacific J. Atmos. Sci.*, 47 235–43, 2011.

[Yoshimura and Sugi, 2005] J. Yoshimura and M. Sugi. Tropical cyclone climatology in a high-resolution AGCM. impacts of SST warming and CO2 increase. *SOLA*, 1:133–136, 2005.

[Yu *et al.*, 2007] H. Yu, C. Hu, and L. Jiang. Comparison of three tropical cyclone intensity datasets. *Acta Meteorologica Sinica*, 1:121–128, 2007.

[Zhang *et al.*, 2006a] H.-M. Zhang, J.J. Bates, and R.W. Reynolds. Assessment of composite global sampling: Sea surface wind speed. *Res. Lett.*, 33:L17714, 2006.

[Zhang *et al.*, 2006b] H.-M. Zhang, W Reynolds, R, and J. J. Bates. Blended and gridded high resolution global sea surface wind speed and climatology from multiple satellites: 1987–present. preprints, 14th Conf. on Satellite Meteorology and Oceanography, Atlanta, GA, Amer. Meteor. Soc., p2.23. [available online at http://ams.confex.com/ ams/annual2006/techprogram/paper_100004.htm.]. In *Preprints, 14th Conf. on Satellite Meteorology and Oceanography, Atlanta, GA, Amer. Meteor. Soc., P2.23. [Available online at http://ams.confex.com/ ams/Annual2006/techprogram/paper_100004.htm.]*, 2006.

[Zhang *et al.*, 2007] X. Zhang, T Li, F. Weng, C.-C. Wu, and L. Xu. Reanalysis of western Pacific typhoons in 2004 with multi-satellite observations. *Meteor. Atmos. Phys.*, 97:3–18, 2007.

Erklärung

Hiermit erkläre ich an Eides statt, dass ich die vorliegende Dissertationsschrift selbst verfasst und keine anderen als die angegebenen Quellen und Hilfsmittel benutzt habe.

_____ _____

Ort, Datum Unterschrift